

WRDC-TR-90-2083

AD-A231 353

AN EXPERIMENTAL STUDY OF EXIT FLOW PATTERNS IN
A MULTISTAGE COMPRESSOR IN ROTATING STALL



Steven E. Gorrell
Compressor Test Group
Technology Branch
Turbine Engine Division

November 1990

Final Report for Period June 89 - May 90

DTIC
ELECTE
JAN 30 1991
S E D

Approved for public release; distribution unlimited

AERO PROPULSION AND POWER LABORATORY
WRIGHT RESEARCH AND DEVELOPMENT CENTER
AIR FORCE SYSTEMS COMMAND
WRIGHT-PATTERSON AIR FORCE BASE, OHIO 45433-6563

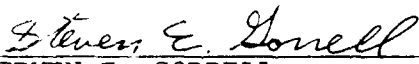
91 1 29 074

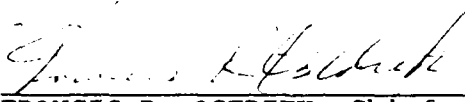
NOTICE

When Government drawings, specifications, or other data are used for any purpose other than in connection with a definitely Government-related procurement, the United States Government incurs no responsibility or any obligation whatsoever. The fact that the government may have formulated or in any way supplied the said drawings, specifications, or other data, is not to be regarded by implication, or otherwise in any manner construed, as licensing the holder, or any other person or corporation; or as conveying any rights or permission to manufacture, use, or sell any patented invention that in any way related thereto.


This report is releasable to the National Technical Information Service (NTIS). At NTIS, it will be available to the general public, including foreign nations.

This technical report has been reviewed and is approved for publication.


STEVEN E. GORRELL
Aerospace Engineer
Compressor Test Group


FRANCIS R. OSTDIEK, Chief
Technology Branch
Turbine Engine Division

FOR THE COMMANDER


THOMAS J. SIMS, Director
Turbine Engine Division
Aero Propulsion and Power Laboratory

If your address has changed, if you wish to be removed from our mailing list, or if the addressee is no longer employed by your organization please notify WRDC/POTX, WPAFB, OH 45433-6563 to help us maintain a current mailing list.

Copies of this report should not be returned unless return is required by security considerations, contractual obligations, or notice on a specific document.

Unclassified

SECURITY CLASSIFICATION OF THIS PAGE

REPORT DOCUMENTATION PAGE

Form Approved
OMB No. 0704-0188

REPORT SECURITY CLASSIFICATION Unclassified		1b. RESTRICTIVE MARKINGS N/A	
SECURITY CLASSIFICATION AUTHORITY N/A		3. DISTRIBUTION / AVAILABILITY OF REPORT Approved for public release; distribution unlimited	
DECLASSIFICATION / DOWNGRADING SCHEDULE N/A			
PERFORMING ORGANIZATION REPORT NUMBER(S) WRDC-TR-90-2083		5. MONITORING ORGANIZATION REPORT NUMBER(S)	
NAME OF PERFORMING ORGANIZATION Aero Propulsion and Power Lab WRDC/AFSC		6b. OFFICE SYMBOL (If applicable) WRDC/POTX	7a. NAME OF MONITORING ORGANIZATION
ADDRESS (City, State, and ZIP Code) Wright-Patterson AFB, OH 45433-6563		7b. ADDRESS (City, State, and ZIP Code)	
NAME OF FUNDING / SPONSORING ORGANIZATION		8b. OFFICE SYMBOL (If applicable)	9. PROCUREMENT INSTRUMENT IDENTIFICATION NUMBER
ADDRESS (City, State, and ZIP Code)		10. SOURCE OF FUNDING NUMBERS	
		PROGRAM ELEMENT NO. 62203F	PROJECT NO. 3066
		TASK NO. 17	WORK UNIT ACCESSION NO. 54
TITLE (Include Security Classification)			
An Experimental Study of Exit Flow Patterns in a Multistage Compressor in Rotating Stall			
PERSONAL AUTHOR(S) Steven E. Gorrell			
a. TYPE OF REPORT Final	13b. TIME COVERED FROM Jun 89 to May 90	14. DATE OF REPORT (Year, Month, Day) Nov 90	15. PAGE COUNT 144
SUPPLEMENTARY NOTATION N/A			
COSATI CODES		18. SUBJECT TERMS (Continue on reverse if necessary and identify by block number)	
FIELD	GROUP	SUB-GROUP	
			Axial Compressor Rotating Stall
			Gas Turbine Stalling Performance
			Aircraft Turbine Engine Stage Performance Characteristics
ABSTRACT (Continue on reverse if necessary and identify by block number)			
High-response pressure measurements of a high-speed, 10-stage, axial-flow compressor operating in rotating stall are analyzed. Procedures used to digitize analog voltages and calibrate pressure transducers are presented. From total and static pressures measured at the exit of the test compressor, stall cell Mach number distributions are calculated and used to study the effects of discharge throttle levels and variable vane changes on the 10th-stage rotating stall cells. Results indicate that significant transition zones exist between the reverse flow and peak Mach number of the stall cell cycle. Since the axial Mach numbers of the stall cell cycle are constantly changing, the amount of leading and trailing edge transition zones and fully unstalled flow zones are not easily defined. A method is devised to approximate the different flow zone ranges and correlate them to in-stall pressure characteristic behavior of the 10th stage of the test compressor. Changes in the time-averaged			
DISTRIBUTION / AVAILABILITY OF ABSTRACT <input checked="" type="checkbox"/> UNCLASSIFIED/UNLIMITED <input type="checkbox"/> SAME AS RPT <input type="checkbox"/> DTIC USERS		21. ABSTRACT SECURITY CLASSIFICATION Unclassified	
NAME OF RESPONSIBLE INDIVIDUAL Steven E. Gorrell		22b. TELEPHONE (Include Area Code) (513) 25504141	22c. OFFICE SYMBOL WRDC/POTX

(continued from Block 19)

pressure characteristics are found to correlate with changes in the rotating stall flow zones. A lower pressure coefficient appears to correspond to an increase in the ratio of trailing to leading edge transition zone size and the average transition zone size. Results also suggest that recovery hysteresis in the test compressor is characterized by reverse flow in the rotating stall cell.

Accession For	
NTIS GRA&I	<input checked="checked" type="checkbox"/>
DTIC TAB	<input type="checkbox"/>
Unannounced	<input type="checkbox"/>
Justification	
By _____	
Distribution/	
Availability Codes	
Dist	Avail and/or Special
A-1	

TABLE OF CONTENTS

	<u>Page</u>
I. INTRODUCTION.....	1
Background.....	1
Off-Design Operation.....	2
Surge and Rotating Stall.....	4
Recoverability.....	7
Purpose of this Research Effort.....	10
Plan of Development.....	10
II. LITERATURE REVIEW.....	12
Mechanism of Rotating Stall.....	12
Low-Speed Test Compressors.....	14
Stall cell details from early experiments.	14
Parallel compressor theory.....	15
Parallel stall cell model.....	15
More stall cell details.....	16
Control volume model.....	18
High-Speed Test Compressors.....	20
Interaction effects.....	20
3-stage compressor.....	22
10-stage E ³ compressor.....	23
CRF 10-stage compressor.....	24
Extended starting theory.....	25
Summary.....	27

III. TEST ARTICLE DESCRIPTION.....	30
CRF Compressor.....	30
IV. COMPRESSOR INSTRUMENTATION.....	34
Stage 10 Instrumentation.....	34
Discharge Instrumentation.....	36
Flow Instrumentation.....	39
V. TIME-AVERAGED DATA REVIEW.....	41
In-Stall Pressure Characteristics.....	41
Test Article Variables.....	43
60-Percent Speed Data.....	44
Pressure Characteristic Changes.....	44
VI. HIGH-RESPONSE DATA REDUCTION AND CALIBRATION.....	47
Data Reduction.....	47
Pressure Calibration.....	49
VII. PRESENTATION OF RESULTS.....	51
Mach Probe High-Response Pressure Calibration..	51
Calibration Errors.....	54
Ensemble Averaging.....	55
High-Response Pressures.....	55
High-Response Axial Mach Numbers.....	57
Reverse flow.....	58
Mach number plots.....	59
Annular Representation of Axial Mach Numbers...	59
VIII. DISCUSSION OF RESULTS.....	77
Characteristic Regions and Rotating Stall Flow Zones.....	77

Nominal In-Stall Pressure Characteristic.....	78
+7 VV In-Stall Pressure Characteristic.....	83
Comparison of Nominal and +7 VV In-Stall Pressure Characteristics.....	85
Transition Zone Ratio and Transition Zone Size.	86
Application of Results to the Extended Starting Theory and Recovery.....	91
IX. SUMMARY AND CONCLUSIONS.....	93
X. RECOMMENDATIONS.....	97
REFERENCES.....	99
APPENDIX A. COMPRESSOR RESEARCH FACILITY DESCRIPTION.....	102
APPENDIX B. DATA ACQUISITION METHODS.....	106
High-Response Pressure Measurements.....	107
Time-Averaged Pressure Measurements.....	110
Measurement Uncertainty.....	111
Steady and Quasi-Steady Performance Mapping...	112
Time-Resolved Performance Data.....	112
APPENDIX C. TEST COMPRESSOR PRESSURE CHARACTERISTIC LEAST-SQUARE CURVE FITS.....	114
APPENDIX D. TEST COMPRESSOR HIGH-RESPONSE PRESSURE MEASUREMENTS.....	125

LIST OF FIGURES

<u>Figure</u>	<u>Page</u>
1. Compressor Map.....	3
2. Compressor Surge Operation.....	5
3. Compressor Rotating Stall Operation.....	6
4. Stall Margin.....	8
5. Mechanism of Rotating Stall.....	13
6. Overall Pressure Rise as Defined in [11]...	17
7. Control Volumes as Defined in [13].....	19
8. Compressor Pressure Characteristics Used by Benser [15].....	21
9. 10th-Stage Pressure Characteristic Presented by Copenhaver [3].....	26
10. Extended Starting Region.....	28
11. Test Article.....	31
12. 10-Stage Test Compressor.....	32
13. Test Compressor Exit.....	35
14. Stator 10 Instrumentation.....	37
15. Exit Instrumentation.....	38
16. Mach Probe.....	40
17. Pressure Coefficient Differences Between Nominal and +7 VV Settings.....	45
18. Digitized Operating Points.....	48
19. Labeled Operating Points.....	52
20. High-Response Pressure Calibration Standards.....	53

21.	High-Response Pressure Measurements, Data Point 1193.....	56
22.	Rotating Stall Mach Numbers, Data Point 1267.....	61
23.	Rotating Stall Mach Numbers, Data Point 1195.....	62
24.	Rotating Stall Mach Numbers, Data Point 1193.....	63
25.	Rotating Stall Mach Numbers, Data Point 1259.....	64
26.	Rotating Stall Mach Numbers, Data Point 1227.....	65
27.	Rotating Stall Mach Numbers, Data Point 166.....	66
28.	Rotating Stall Mach Numbers, Data Point 162.....	67
29.	Rotating Stall Mach Numbers, Data Point 160.....	68
30.	Rotating Stall Mach Numbers, Data Point 135.....	69
31.	Rotating Stall Mach Numbers, Data Point 148.....	70
32.	Station 3.0 Axial Mach Number Distributions, Data Point 1227.....	71
33.	Station 3.0 Axial Mach Number Distributions, Data Points 1259 and 1193..	72
34.	Station 3.0 Axial Mach Number Distributions, Data Points 1195 and 1267..	73
35.	Station 3.0 Axial Mach Number Distributions, Data Point 148.....	74
36.	Station 3.0 Axial Mach Number Distributions, Data Points 135 and 160....	75
37.	Station 3.0 Axial Mach Number Distributions, Data Points 162 and 166. .	76

38.	10th-Stage Pressure Characteristic Regions	79
39.	Nominal Pressure Characteristic Mach Number Distributions.....	80
40.	+7 VV Pressure Characteristic Mach Number Distributions.....	84
A-1.	Compressor Research Facility.....	104
A-2.	CRF Test Chamber.....	105
B-1.	High-Response Data Acquisition System....	108
C-1.	10th-Stage Pressure Characteristic Least- Square Curve Fits.....	115
C-2.	9th-Stage Pressure Characteristic Least- Square Curve Fits.....	116
C-3.	8th-Stage Pressure Characteristic Least- Square Curve Fits.....	117
C-4.	7th-Stage Pressure Characteristic Least- Square Curve Fits.....	118
C-5.	6th-Stage Pressure Characteristic Least- Square Curve Fits.....	119
C-6.	5th-Stage Pressure Characteristic Least- Square Curve Fits.....	120
C-7.	4th-Stage Pressure Characteristic Least- Square Curve Fits.....	121
C-8.	3rd-Stage Pressure Characteristic Least- Square Curve Fits.....	122
C-9.	2nd-Stage Pressure Characteristic Least- Square Curve Fits.....	123
C-10.	1st-Stage Pressure Characteristic Least- Square Curve Fits.....	124
D-1.	High-Response Pressure Measurements, Data Point 1267.....	126
D-2.	High-Response Pressure Measurements, Data Point 1195.....	127

D-3.	High-Response Pressure Measurements, Data Point 1193.....	128
D-4.	High-Response Pressure Measurements, Data Point 1259.....	129
D-5.	High-Response Pressure Measurements, Data Point 1227.....	130
D-6.	High-Response Pressure Measurements, Data Point 166.....	131
D-7.	High-Response Pressure Measurements, Data Point 162.....	132
D-8.	High-Response Pressure Measurements, Data Point 160.....	133
D-9.	High-Response Pressure Measurements, Data Point 135.....	134
D-10.	High-Response Pressure Measurements, Data Point 148.....	135

LIST OF TABLES

<u>Table</u>	<u>Page</u>
1. Flow Zone Percentages.....	82
2. T_{TE}/T_{LE} and T_{avg} for Nominal and +7 VV Operating Points.....	88

I. INTRODUCTION

Background

At present, the majority of knowledge regarding rotating stall cells, as well as models used to predict rotating stall operation, has been obtained from low-speed, low-pressure-rise, 1-to-5-stage compressor experimental data. Only since 1986 have data been acquired from high-speed, high-pressure-ratio, multistage compressors operating in rotating stall. During the time of February through May 1987, a 10-stage, high-speed, axial-flow compressor test program was accomplished in the Wright-Patterson Air Force Base, Aero Propulsion and Power Laboratory, Compressor Research Facility (CRF). The CRF has the ability to accurately measure and record steady-state and transient experimental data from full scale, multistage fans and compressors.

Details of the CRF test program, test results, and data analysis were presented by Copenhaver [1]. The CRF test has provided a large experimental data base from which much is being learned about high-speed, multistage compressors operating in rotating stall. The purpose of this research effort is to follow up and analyze in greater detail some of the results and theories presented by Copenhaver.

Off-Design Operation

Compressors are designed to operate at a design point specified by a mass flow, pressure ratio, and efficiency. However, there are many instances when the compressor must operate at conditions other than those set as the design point. Engine starting, idling, reduced power, maximum power, acceleration and deceleration are a few examples [2]. With the introduction of thrust vectoring and the ability of military aircraft to perform high-angle-of-attack maneuvers, the amount and severity of off-design operation encountered by compressors is greatly increasing. For this reason, the ability to understand and predict the off-design performance associated with axial-flow compressors has become a key factor in the research and development of modern-day and next-generation aircraft gas turbine engines.

The operating region of a compressor is bounded on the high-flow end by blade passage choking and on the low-flow end by blade and/or endwall stalling. Figure 1 shows this operating region on a typical compressor map. When a compressor is operating in this region the flow is essentially steady and axisymmetric on the scale of the circumference. If for a given rotational speed the flow is reduced below that defined by the stall line, the flow becomes unsteady and may also be non-axisymmetric.

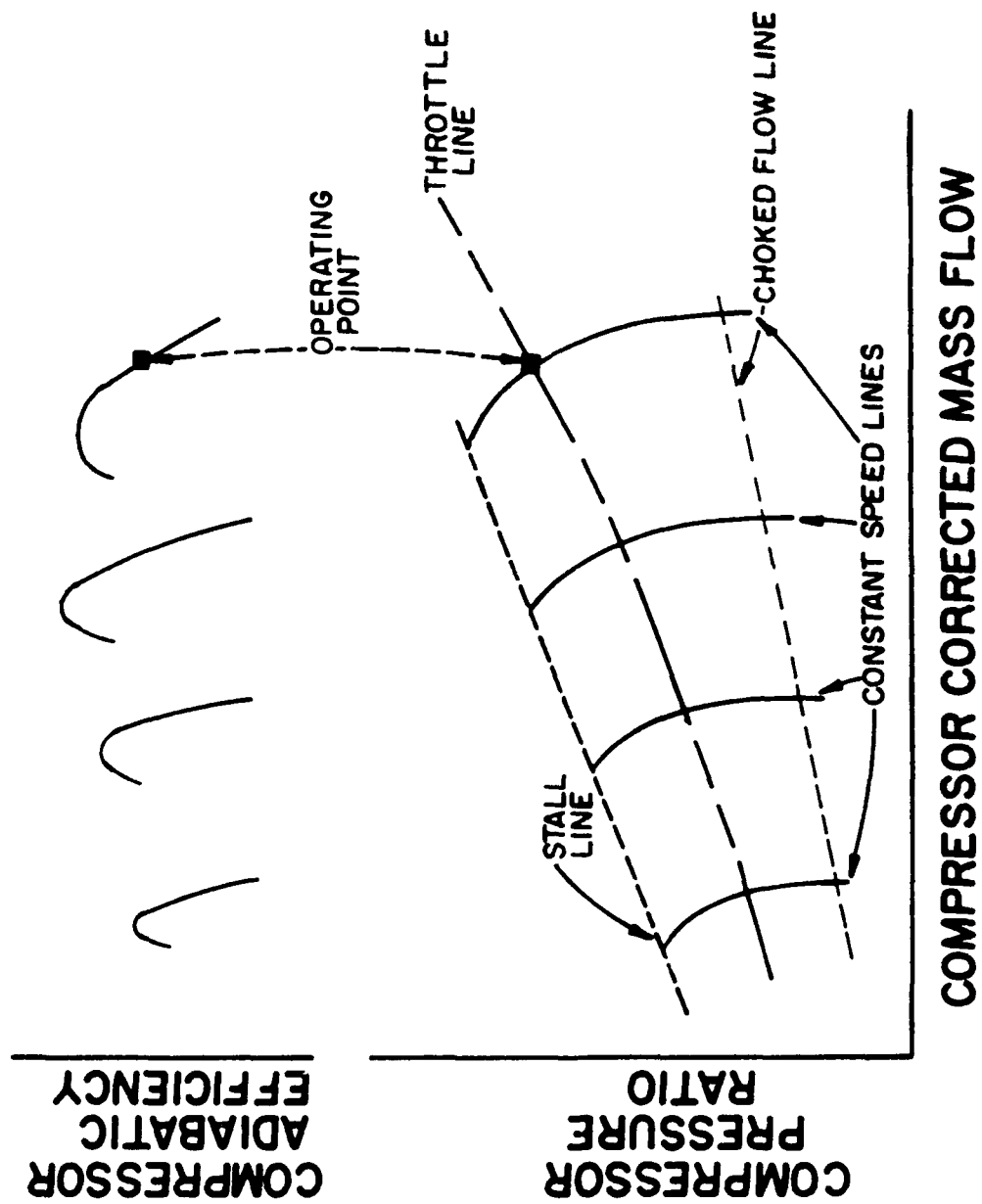


Figure 1. Compressor Map

Surge and Rotating Stall

When the flow rate for a compressor drops below the stall line, two types of flow instability may occur: surge and rotating stall. Surge usually occurs at higher speeds and is characterized by large amplitude planar oscillations in mass flow and pressure rise. Surge is cyclic in nature and may be accompanied by reverse flow. During surge cycles, the compressor transiently operates near the unstalled, in-stall, and possibly the reverse flow characteristics as shown in Fig. 2.

Rotating stall results from stall in blade passages and is characterized by zones of stalled flow propagating in the direction of compressor rotation. These zones are referred to as rotating stall cells, and may vary in number and in size radially from root to tip (part span or full span stall) and circumferentially around the compressor annulus. Reverse flow may also be present within the stall cell. After rotating stall inception, the compressor operates along a quasi-steady in-stall characteristic as explained in Fig. 3. Because blade passages are stalled, the pressure rise through the compressor is significantly reduced. In many cases, the reduced performance conditions are not sufficient to produce self-sustained engine operation.

Both surge and rotating stall are undesirable from the standpoint of engine operation and engine fatigue. These

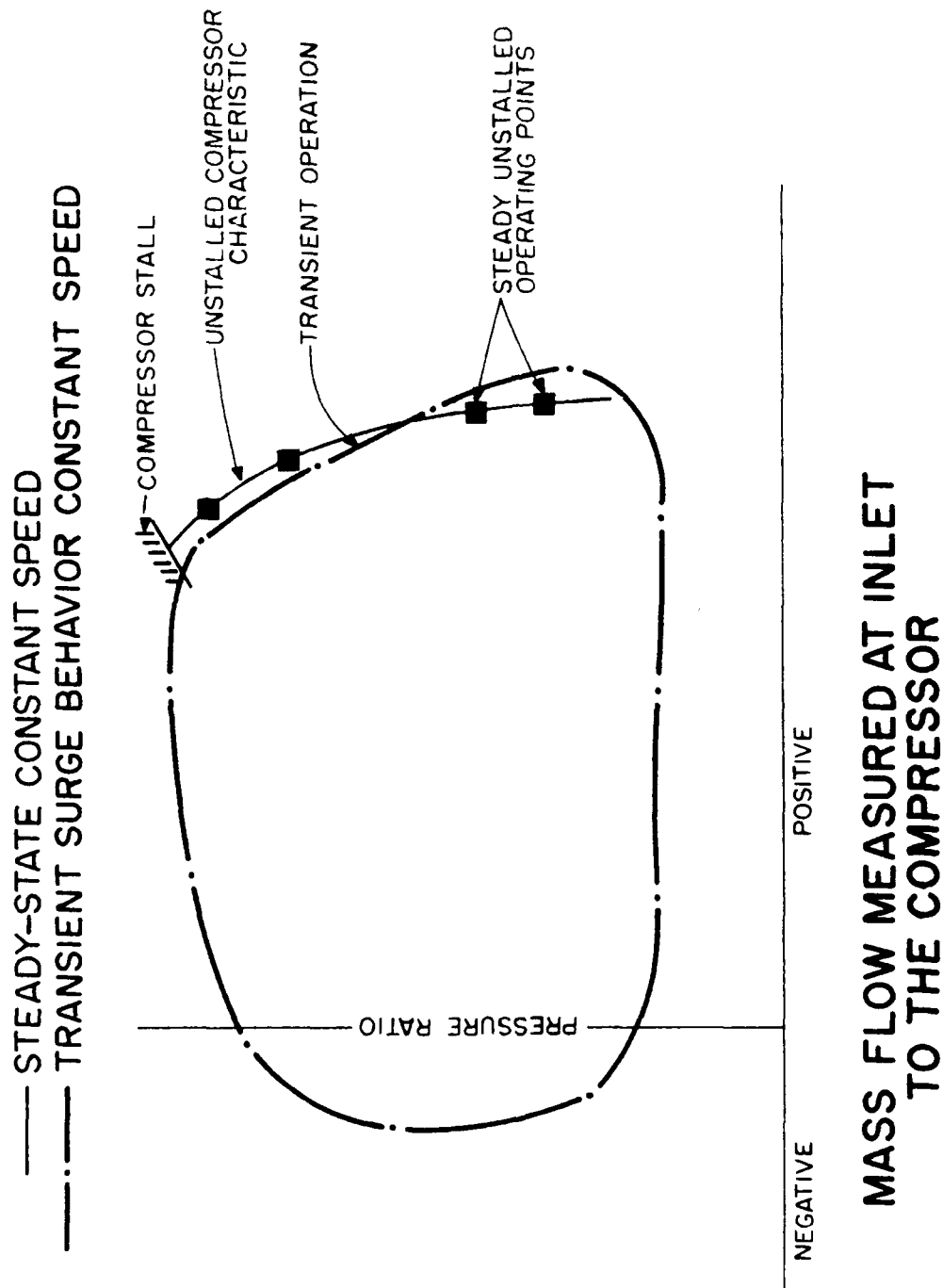


Figure 2. Compressor Surge Operation

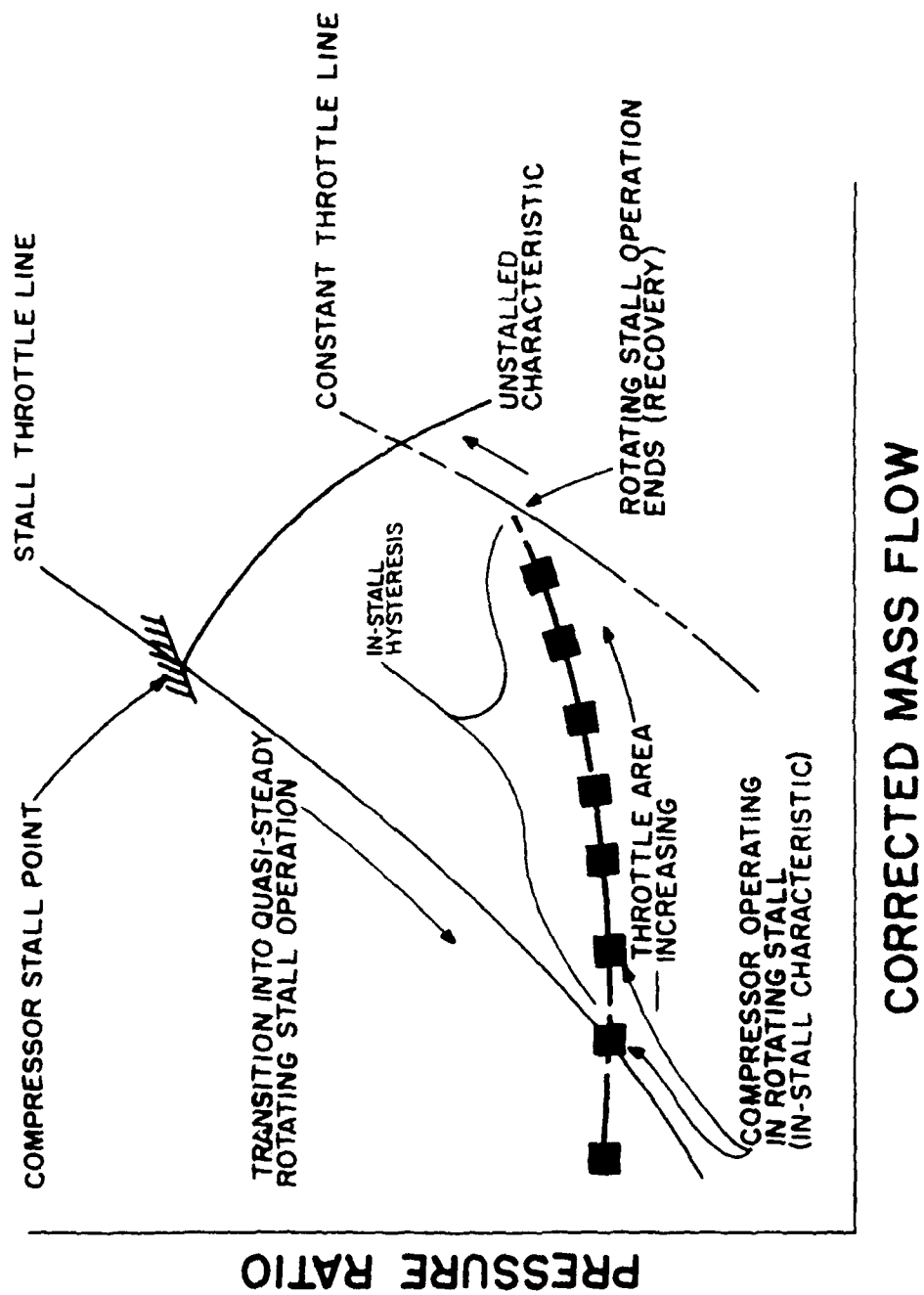


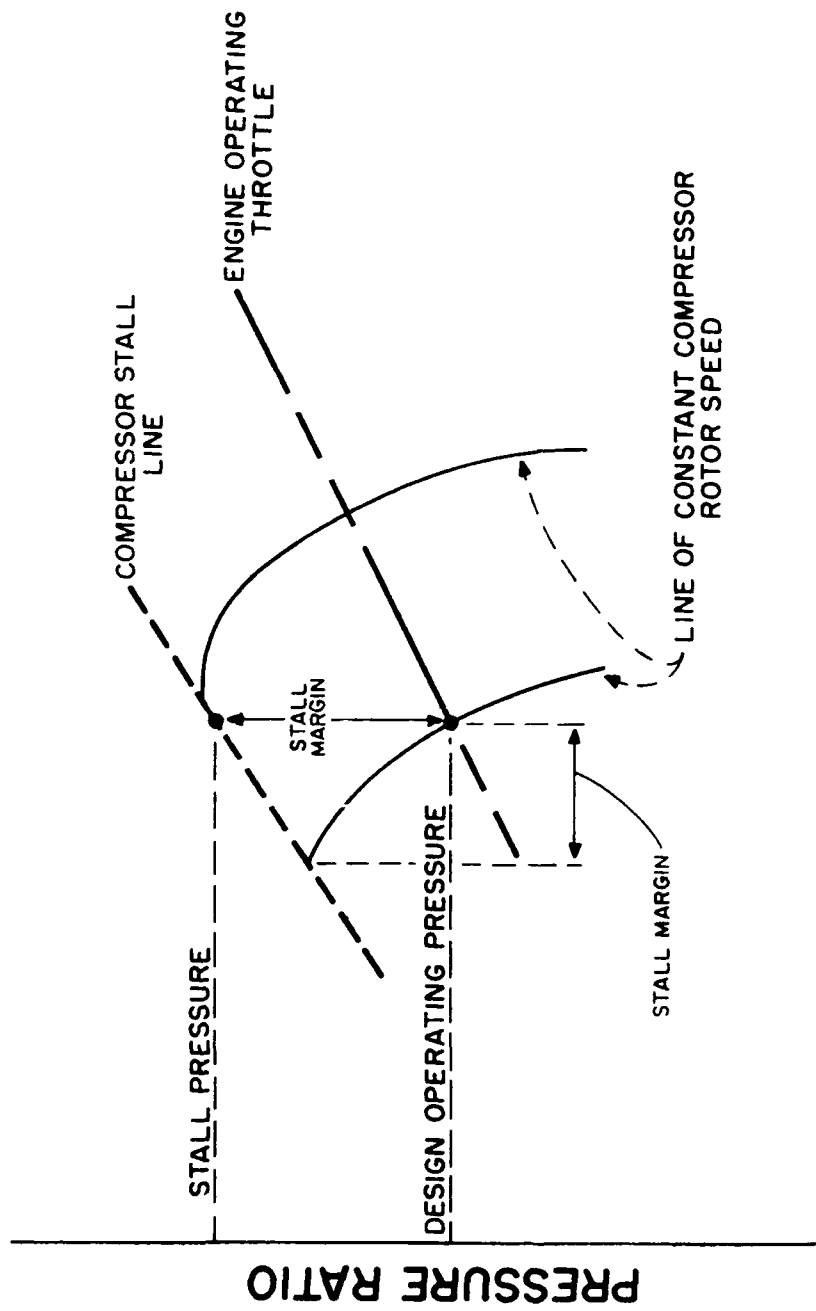
Figure 3. Compressor Rotating Stall Operation

instabilities result in a reduced flow rate and pressure rise, a drop in efficiency, low engine thrust, elevated turbine temperatures, and high blade stress levels.

When operating at or very near the stall line, a small flow perturbation may result in the inception of rotating stall or surge. Since the effects of rotating stall and surge can lead to a severe performance reduction of the entire engine, a margin must be established between the design operating point and the stall line. Stall margin is the measure of the operating range between the design point and the stall point. This stall margin increases the operating range by allowing the compressor to react to moderate inlet distortions and flow instabilities without progressing into rotating stall or surge. For a given compressor, the tradeoffs for increased stall margin, as seen from Fig. 4, include lower operating line conditions and ultimately a decrease in thrust and specific fuel consumption. Due to these factors, there is a limit to how much stall margin a compressor can have.

Recoverability

Even with a today's moderate stall margins of 15 to 25 percent, off-design operation in a high performance compressor will at times produce surge or rotating stall. The ability to recover from these instabilities, once encountered, is critical. Recoverability is the ability of the compressor to



CORRECTED MASS FLOW

Figure 4. Stall Margin

return to steady-state unstalled operation after the instability-causing mechanism is removed.

During part of a surge cycle, the compressor operates transiently along its unstalled characteristic (see Fig. 2). Consequently, if the cause of surge is removed during the cycle, the compressor will recover. From a recoverability criteria, surge is desired over rotating stall.

When a compressor is experiencing rotating stall, it operates on its in-stall quasi-steady characteristic. Once the rotating-stall-causing perturbation is removed, the compressor will still operate and must recover along its in-stall characteristic. Recovery from rotating stall may be characterized by in-stall hysteresis; that is, recovery may require a greater mass flow than that value at stall inception. In extreme cases, engine throttle response is insufficient to cause recovery. For this condition, rotating stall is also known as "nonrecoverable", "hung", or "stagnation" stall and the engine must be shut down and restarted to clear from rotating stall operation.

As defined by Copenhaver [3] and shown in Fig. 3, in-stall hysteresis is the increase in mass flow coefficient needed to move from the initial in-stall operating point to the near-recovery point. The smaller the hysteresis, the easier and quicker the compressor can recover.

Purpose of This Research Effort

The need to develop engine and compressor models that can simulate off-design operation has directly resulted in the need to understand and predict a compressor's in-stall characteristic. Models that are dependent on stage characteristics to determine blade forces such as those developed by Davis [4], are very useful in the design and analysis of today's compressors [5].

As mentioned at the beginning of this section, the purpose of this research effort is to analyze in detail some of the results and theories presented by Copenhaver in [1]. In particular, this report will offer additional insights into the effects of discharge throttle levels and variable vane changes on rotating stall cells, and correlate these changes to compressor in-stall stage operation.

Through an increased understanding of rotating stall cells, thereby enhancing the prediction capabilities of analytical tools, it will be possible to design compressors/engines that are less susceptible to severe flow instabilities and more recoverable from those instabilities if they are encountered.

Plan of Development

Before data from the CRF compressor test are presented and analyzed, some background information from previous tests and rotating stall theories will be presented in a literature

review. Next, the test facilities and test article used will be described, followed by an in-depth explanation of the CRF compressor instrumentation and data acquisition methods. Finally, after the results of the report have been presented and reviewed, conclusions and suggestions for future investigations will be given.

II. LITERATURE REVIEW

This literature review will describe some of the ideas previously presented in the study of rotating stall phenomena. In particular, it will show the progression of theories and models concerning stall cell and in-stall characteristic behavior.

Mechanism of rotating stall.

The mechanisms of rotating stall inception and propagation were first explained by Emmons [6] in 1955 and may be summarized as follows. Consider a row of compressor blades operating at a high angle of attack as shown in Fig. 5. If a transient disturbance causes an increased angle of attack on blade 2 causing it to stall, flow will separate on the suction side. The result is a decrease in flow area between blades 1 and 2 which increases the angle of attack on blade 1 and decreases the angle of attack on blade 3. The increased angle of attack on blade 1 causes it to stall, and the decreased angle of attack on blade 3 inhibits it from stalling. As the action repeats itself, the stall will propagate along the blade row in the direction shown. If the stall-causing disturbance is strong and persists, the propagation can become a fully developed rotating stall cell.

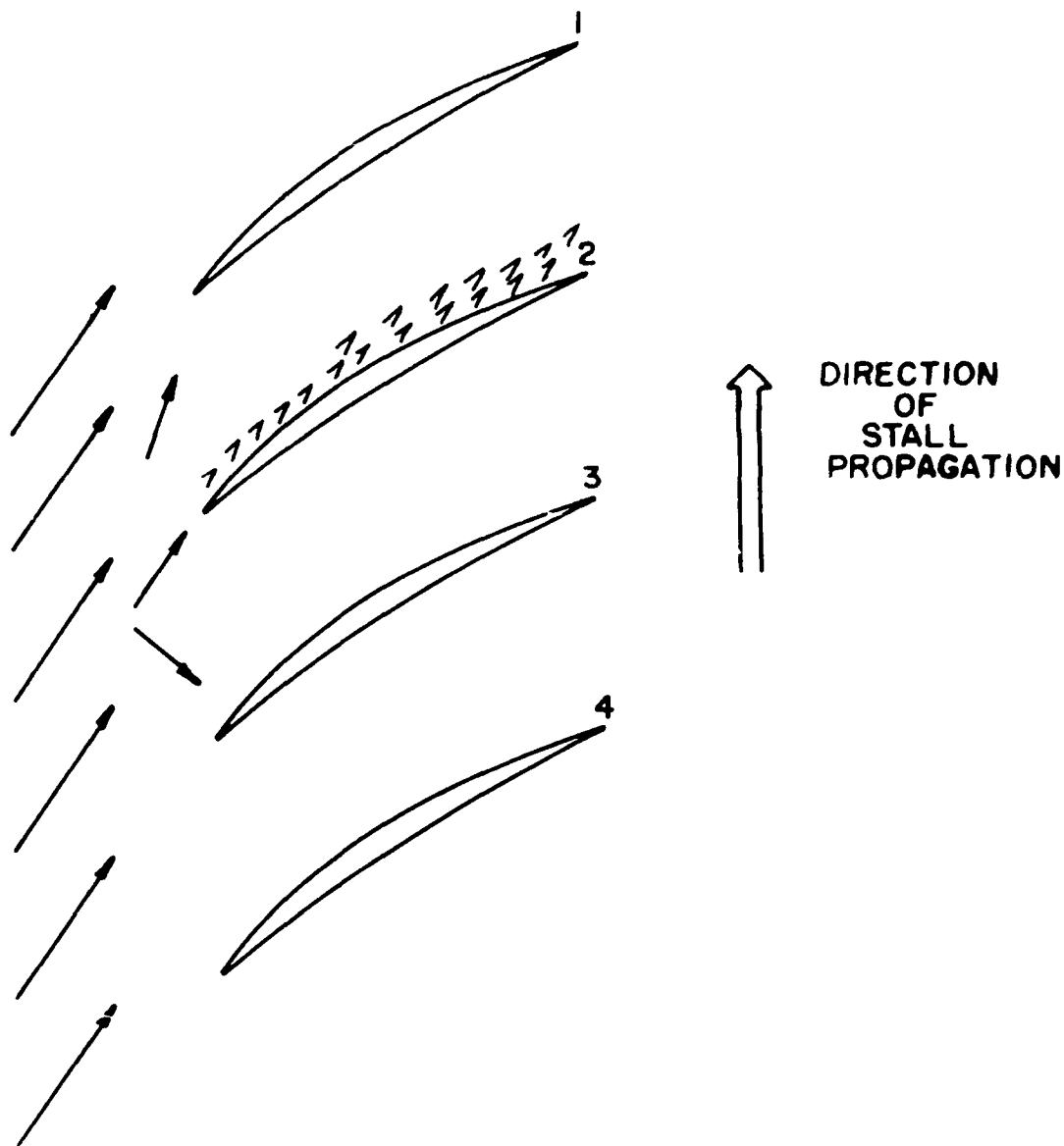


Figure 5. Mechanism of Rotating Stall

Low-Speed Test Compressors

The majority of the tests conducted in the past have used low-speed, low-pressure-rise compressors. This was primarily due to the complexity, expense, and power requirements necessary to test high-speed, multistage compressors.

Stall cell details from early experiments. Until 1977, most research efforts on rotating stall focused on predicting stall inception and propagation speed of rotating stall. This was primarily motivated by blade failures from resonant response to the stall cell propagation frequency. Some efforts were made to model the stall cell by Stenning and Kriebel [7], and Fabri [8]. They modeled the stall cell as a passive region of fluid which extended through the blade row like the wake of a bluff body.

Day and Cumpsty [9] were some of the first to use a high-response instrumentation and data acquisition system to obtain measurements within the stall cell itself. They also used a rig that could test builds from an isolated rotor to 1-4 stages and different aerodynamic designs. Many interesting results were provided by their work; however, only those relevant to this report will be mentioned here.

Day and Cumpsty established that the stall cell extended axially through the compressor and was an active 3-dimensional flow rather than a passive region. From the existence of high

tangential velocities ahead of each rotor throughout the stall cell, Day and Cumpsty proposed that the unstalled flow crossed from one side of the cell to the other. Although small compared to the tangential velocities, both positive and negative axial flows were measured in the stall cell. They also reported that the total-to-static pressure rise per stage was independent of blade design and constant for all the builds tested. This finding would be an assumption used in many models to follow.

Parallel compressor theory. Results from Day and Cumpsty led to the adaption of the parallel compressor theory to rotating stall analysis. Pearson [10] developed the parallel compressor concept in 1963 to model circumferential distortion. His theory divided the distorted compressor into separate sections working in parallel with each other. The theory was based on the following assumptions: all compressor sections discharged to the same static pressure, there was no fluid flow across parallel sections, and each section operated on its own unique point of the performance characteristic.

Parallel stall cell model. In 1978, Day, Greitzer, and Cumpsty [11] developed a model of the stalled flow in axial compressors. Their review of experimental data showed that both the stalled and unstalled flow exited at the same average static pressure. Following the parallel compressor theory, Day, Greitzer, and Cumpsty modeled the compressor as two

separate compressors: one stalled and one unstalled. Based on results from [9], they assumed that the total-to-static pressure rise was the same in the stall cell and the unstalled region. From their experiments, Day, Greitzer, and Cumpsty found that the pressure rise in the stall cell was close to the overall total-to-static pressure rise of the compressor at the shut-off throttle setting. Based on this observation, it was concluded that the compressor shut-off pressure rise determined the overall pressure rise delivered by the compressor during rotating stall operation as shown in Fig. 6.

Further observation showed that the circumferential extent of the stall cell (blockage) was an important parameter when correlating in-stall performance and recovery. In doing some recovery studies, Day, Greitzer, and Cumpsty found that increasing the design flow coefficient and/or the number of stages increased the amount of hysteresis.

More stall cell details. Additional studies were done by Das and Jaing [12] in 1983 on a 3-stage, low-speed compressor equipped with 3-hole cylindrical pressure probes. They showed that the high tangential velocities were present in the stalled area ahead of the rotor except near the stall cell edges. Behind the rotor, the tangential velocities were much lower in the center of the stall cell and actually could be in the opposite direction from the flow ahead of the rotors. The results of Das and Jaing did not support the ideas presented

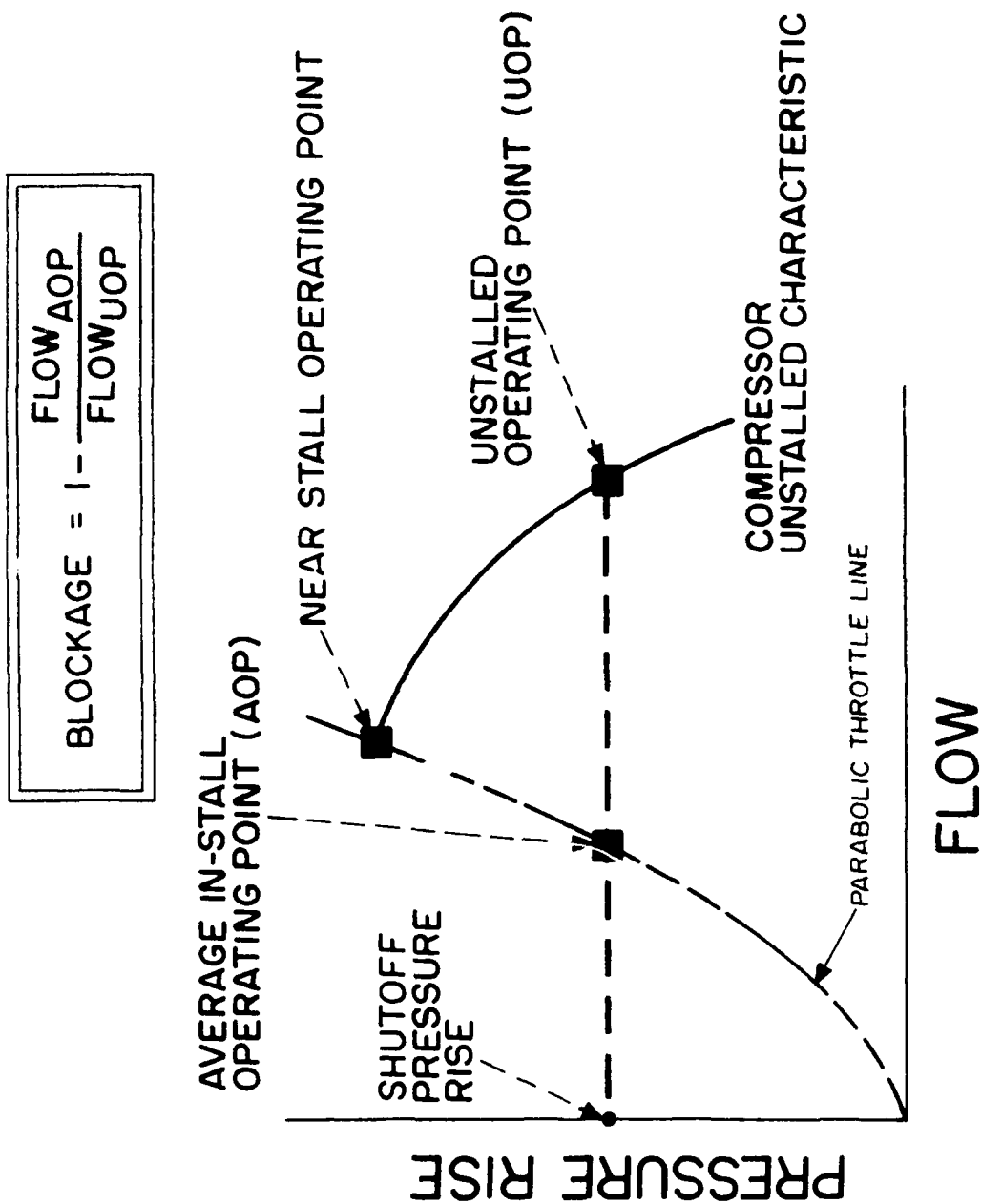
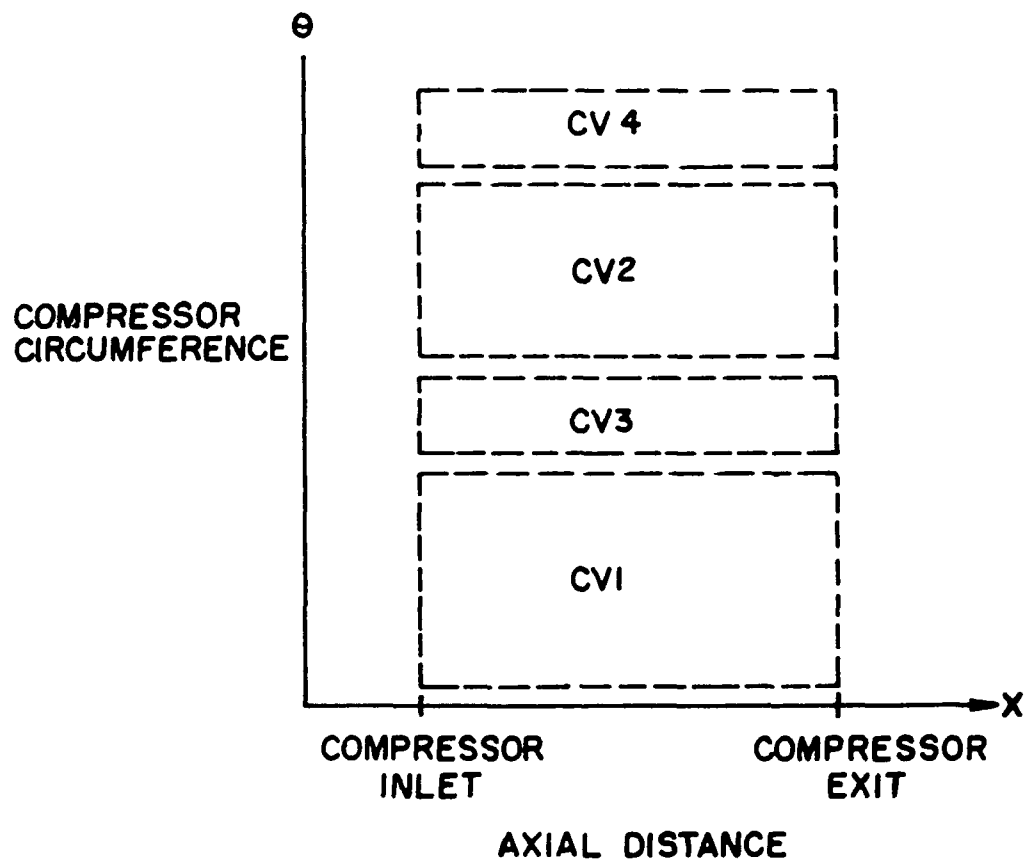


Figure 6. Overall Pressure Rise as Defined in [11]

in [9] that the unstalled flow tangentially crossed the stall cell, but did show the existence of some mass transport at the stall cell boundaries which they attributed to centrifugal effects. Also the existence of the stall cell did have an effect on the unstalled flow. These two findings did not support the assumption made in the parallel compressor theory that there was no fluid flow across parallel sections.

Another important observation made was that although the stalled flow was similar in nature in each stage, there were axial variations in flow velocities and pressures. This resulted in a more active stall cell from the front to rear stages of the compressor. The in-stall pressure characteristics measured by Das and Jaing were nearly constant (a slight positive slope) which was consistent with the other works reviewed previously.

Control volume model. One of the most recent and complex rotating stall models was the control volume approach developed by Koff, Davis, and Greitzer [13] in 1987. This was an extension of the parallel compressor theory using four sections (control volumes) instead of two. Figure 7 shows the four control volumes as fully stalled flow, fully unstalled flow, a leading edge transition zone, and a trailing edge transition zone. Koff, Davis, and Greitzer based their transition zones on axial velocity profiles obtained from references 9, 12, and 14. From these data, they proposed that



CV1 = CONSTANT UNSTALLED FLOW REGION

CV2 = CONSTANT STALLED FLOW REGION

**CV3 = TRANSITION ZONE AT LEADING EDGE OF
STALL CELL**

**CV4 = TRANSITION ZONE AT TRAILING EDGE OF
STALL CELL**

Figure 7. Control volumes as Defined in [13]

the large change in axial flow between the stalled and unstalled regions was concentrated in the two transition zones.

After developing and validating their model, Koff, Davis, and Greitzer found that the transition regions were important in determining the pressure rise of the compressor during rotating stall operation. This conclusion was very significant because it was previously believed that the average pressure rise of the stalled and unstalled sections set the performance of the compressor. The authors found that the slope and magnitude of the in-stall characteristic varied with the ratio of trailing to leading edge transition zone size and the average transition zone size. Studies on recovery showed that a higher pressure rise and positively sloped in-stall characteristic lead to a more recoverable compressor.

High-Speed Test Compressors

Interaction effects. In 1965 Benser [15] reported some qualitative studies made from a hypothetical 12-stage compressor. Benser used a stage-stacking model with stage performance characteristics assumed to be those obtained from single stage compressors. One set of characteristics used is shown in Fig. 8 which also shows the nature of progressive and abrupt rotating stall inception. The purpose of his study was to evaluate stage interaction effects by modifying the assumed

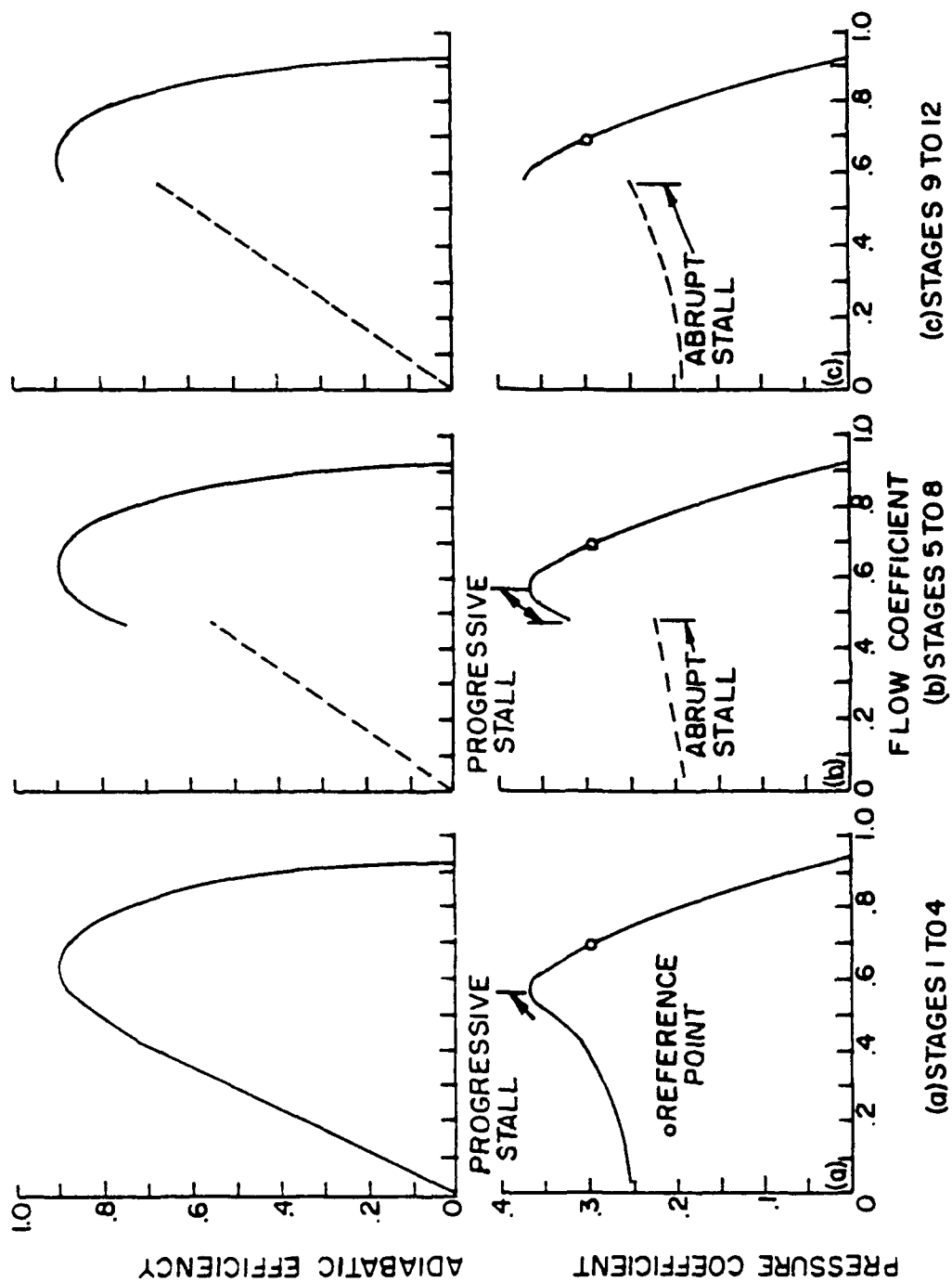


Figure 8. Compressor Pressure Characteristics Used by Benser [15]

performance curves. Benser attributed these effects to two main sources: radial maldistribution of flow due to off-design performance, and circumferential maldistribution of flow or unsteady flow due to rotating stall.

Benser concluded that unsteady flow resulting from part or full-span rotating stall in the inlet stages was partly responsible for multi-valued overall performance curves and low part-speed efficiencies found in multistage compressors. A multi-value characteristic means that for a given flow coefficient, the compressor can operate at one pressure rise if it was stalled, or another pressure rise if it was unstalled. Benser also stated that stages with continuous progressive stall characteristics at their stall point (see Fig. 8) resulted in higher part-speed efficiencies and less susceptibility to full-span rotating stall. Benser stated that the qualitative nature of his analysis was necessary because of the difficulty of obtaining experimental stage characteristics for his model. Now that the technology exists to obtain those characteristics, many of his ideas are gaining further support.

3-stage compressor. One of the early experimental studies of in-stall characteristics on high speed machines was done in 1985 by Small and Lewis [14] on a 3-stage, axial-flow research rig. They reported large throttle hysteresis and reverse flow during rotating stall operation as had been

observed in low-speed machines. Small and Lewis showed that the overall-in-stall characteristics were flat but varied with the speed of the compressor. The variation of in-stall characteristics had not been observed in the low-speed machines.

10-stage E³ compressor. In 1986 Hosny and Steenken [16] presented results from a high-speed, high-pressure-ratio, 10-stage test article known as the Energy Efficient Engine (E³) Compressor. One result of this effort was the affirmation that there are many differences between the in-stall operation of low-speed, low-pressure-rise, and high-speed, high-pressure-rise compressors. The E³ compressor's overall in-stall characteristics were flat at lower speeds and increased in slope at higher speeds. Contrary to models based on low-speed machines, Hosny and Steenken showed that the pressure rise in the unstalled and stalled portions of the compressor were not equal.

Another observation not found in previous tests was that the stall cell did not extend through all ten stages but was confined to the rear of the compressor. They found that for a given speed, the stall cell size varied with the flow coefficient. The IGV's and first four stators of the E³ compressor were variable. A change in the vane schedule did not affect the overall in-stall pressure characteristic or the recovery point.

CRF 10-stage compressor. An even more detailed research effort was presented by Copenhaver [3] in 1989. He offered results from a high-speed, 10-stage compressor tested extensively in stall. Similar to the E³ compressor, Copenhaver found that the overall in-stall pressure rise varied with shaft speed and the stall cell was located in the rear half of the compressor. High in-stall hysteresis levels were reported for the CRF compressor and recovery blockage levels were found to be as low as 17 percent of compressor annulus area compared to 30 percent observed in the other low and high-speed compressors presented in this review.

What was unique about Copenhaver's effort was the acquisition of inlet, exit, and all ten stage characteristics for a variety of speeds and variable geometry settings. A stage by stage analysis by Copenhaver showed that with the exception of stages 2 and 3, the in-stall pressure characteristics plotted as pressure coefficient versus flow coefficient did not vary with shaft speed. Opening the IGV's and stators one and two changed the overall characteristic only slightly and did not effect the in-stall characteristics of stages four through eight. However, stage nine and especially stage ten's in-stall characteristic dropped to a lower pressure level as a result of opening the variable geometry vanes and stators. The 10th-stage pressure

characteristic presented by Copenhaver is shown in Fig. 9 and will be extensively studied in the sections that follow.

Copenhaver further showed that the 10th-stage in-stall pressure coefficient was at a negative level for all speeds and operating points, something not observed in previous high or low-speed machines. Copenhaver has proposed that at certain speeds while the overall compressor was in rotating stall, low pressure rise in the front and middle stages and high temperatures due to the stalled flow resulted in low density air entering the rear stages which in turn produced choked flow conditions. It was this choked flow that prolonged the recovery of the compressor as the flow needed to unchoke before the compressor could recover. From this Copenhaver concluded that the compressor operating in stall is very similar to conditions found when starting multistage, high-speed compressors.

Extended starting theory. Recently, O'Brien and Boyer [17] developed the extended starting theory of compression system recovery hysteresis from a combination of the stage interaction ideas of Benser [15], the experimental data of Copenhaver [1], and a compressor system model developed by Davis [4]. O'Brien and Boyer proposed that the flow patterns found during rotating stall at mid-range (50 to 80 percent design corrected) speeds were similar to those of a failed compressor start, namely, stalled front stages, choked rear

TENTH STAGE PRESSURE CHARACTERISTIC VARIABLE GEOMETRY EFFECTS, 75% SPEED

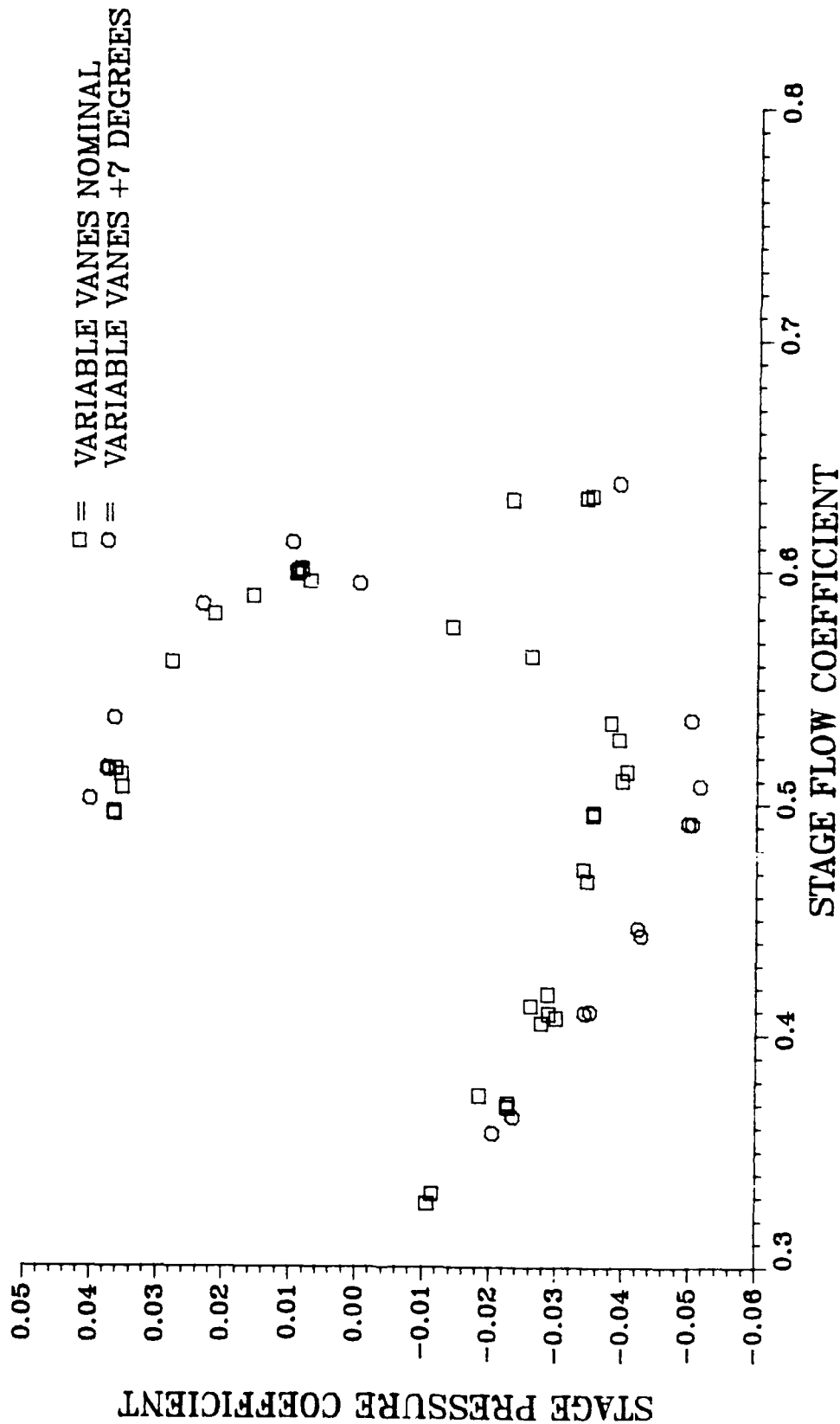


Figure 9. 10th-Stage Pressure Characteristics Used by Copenhagen [3]

stages, and recovery hysteresis. The extended starting region, shown in Fig. 10, implies non-recoverable stall problems at speeds within the compressor's normal operating range.

The significance of the extended starting explanation of compressor recovery hysteresis was realized when means of improving recovery behavior were examined. O'Brien and Boyer proposed that a compressor operating in an extended starting state (stagnation stall) should experience improved recovery behavior through measures which encouraged starting. By applying a stage-by-stage mathematical model to the CRF 10-stage compressor [5], O'Brien and Boyer showed that properly applied bleed flows and variable geometry did improve the recoverability of the compressor. They also concluded that stability and in-stall compressor operation were related to the details of stage design and matching, as well as overall turbine engine system considerations.

Summary

The literature reviewed has shown that there are significant differences between the in-stall operation of low-speed, low-pressure-rise compressors, and high-speed, high-pressure-rise, multistage compressors. Since current stall cell and in-stall characteristic models are based on low-speed, low-pressure-rise compressor experimental data, caution

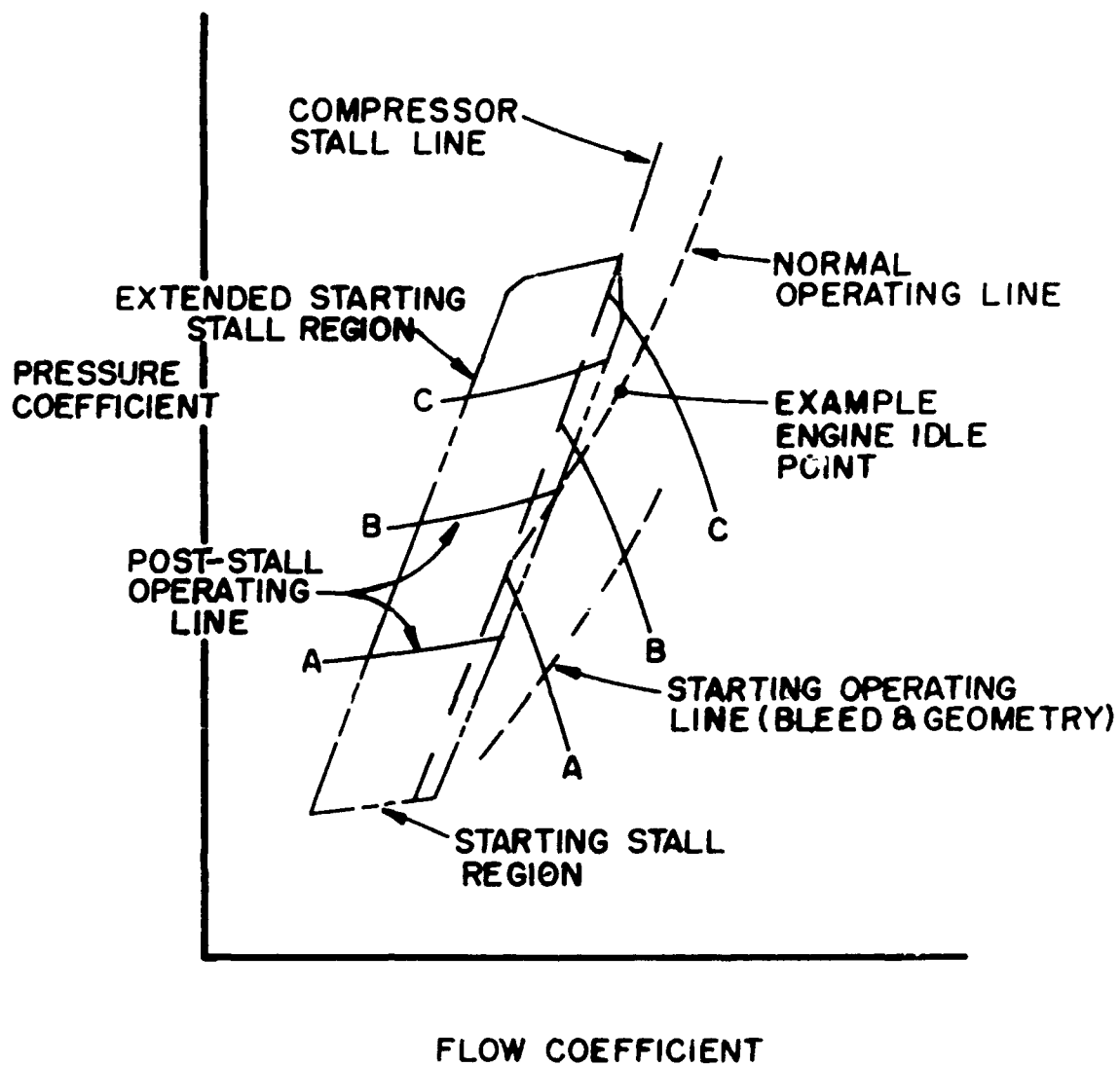


Figure 10. Extended Starting Region

should be used when applying these models to high-speed, multistage compressors.

In order to develop models that apply to high-speed, multistage compressors, a better understanding of rotating stall cells and in-stall characteristics are needed. The CRF compressor test provided such a opportunity. This report will focus on increasing the understanding of stall cells and in-stall characteristics at the 10th stage of the CRF test compressor and how they were effected by discharge throttle levels and variable vanes. In addition, the results obtained from this effort will be compared with the most advanced theories developed by Koff, Davis, and Greitzer [13] and O'Brien and Boyer [17]. As more is learned about rotating stall in high-speed, multistage compressors, models can then be developed to predict in-stall compressor behavior.

III. TEST ARTICLE DESCRIPTION

CRF Compressor

The data analyzed in this work were obtained during testing of a refurbished compressor taken from a modern aircraft gas turbine engine removed from service. The test compressor was a 10-stage, axial-flow compressor with a design pressure ratio of 8.3, a design corrected speed of 10,913 rpm, and a design corrected mass flow of 54.44 lbm/s (24.69 kg/s). The overall test article as shown in Fig. 11, consisted of the inlet case, the high-pressure compressor, the diffuser, and the combustor section from the engine.

The stages of the compressor were defined in a stator-rotor combination rather than the conventional rotor-stator definition. This was done because the total temperature, total pressure, and the majority of the static pressure instrumentation was located at the stator leading edge. Figure 12 shows the inlet guide vane (IGV), rotor, and stator layout of the CRF compressor.

The compressor had variable geometry devices in stages 1, 2, and 3. The IGV's and stators 1 and 2 were connected to sync-ring assemblies to allow for variation in vane stagger angle. The position of the IGV's and stators were measured by potentiometers and could be varied independently of each other.

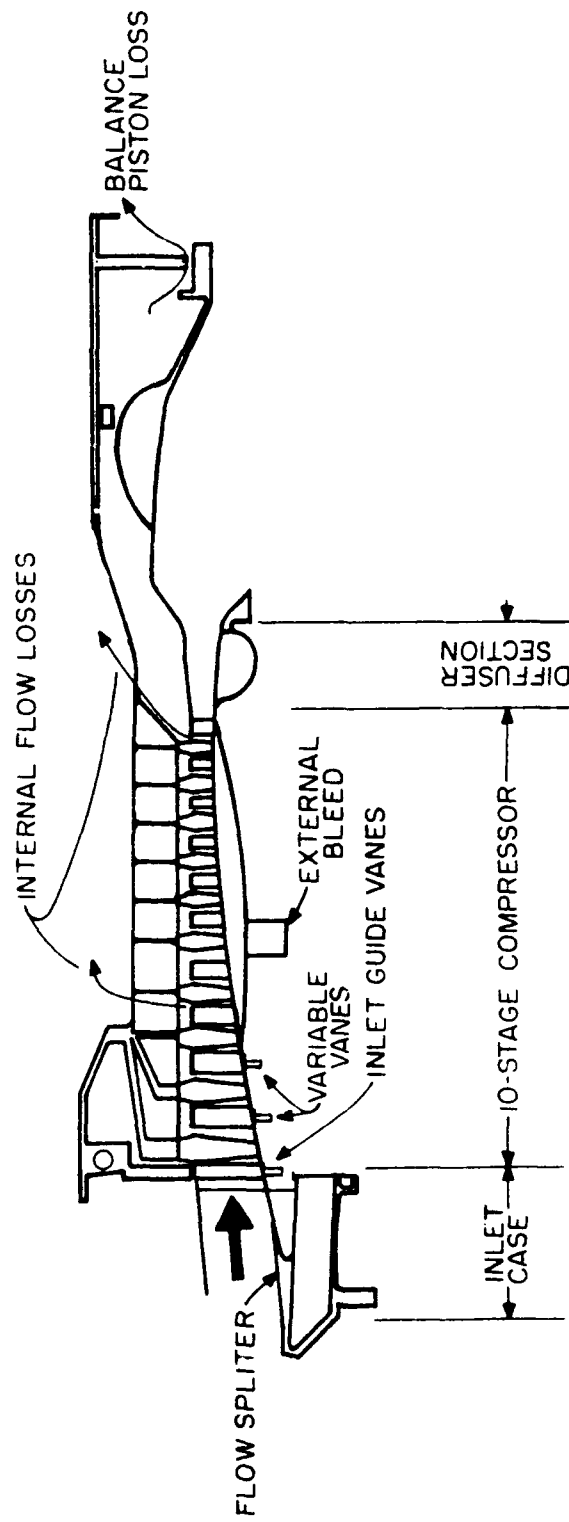


Figure 11. Test Article

R=ROTOR
S=STATOR
STG=STAGE

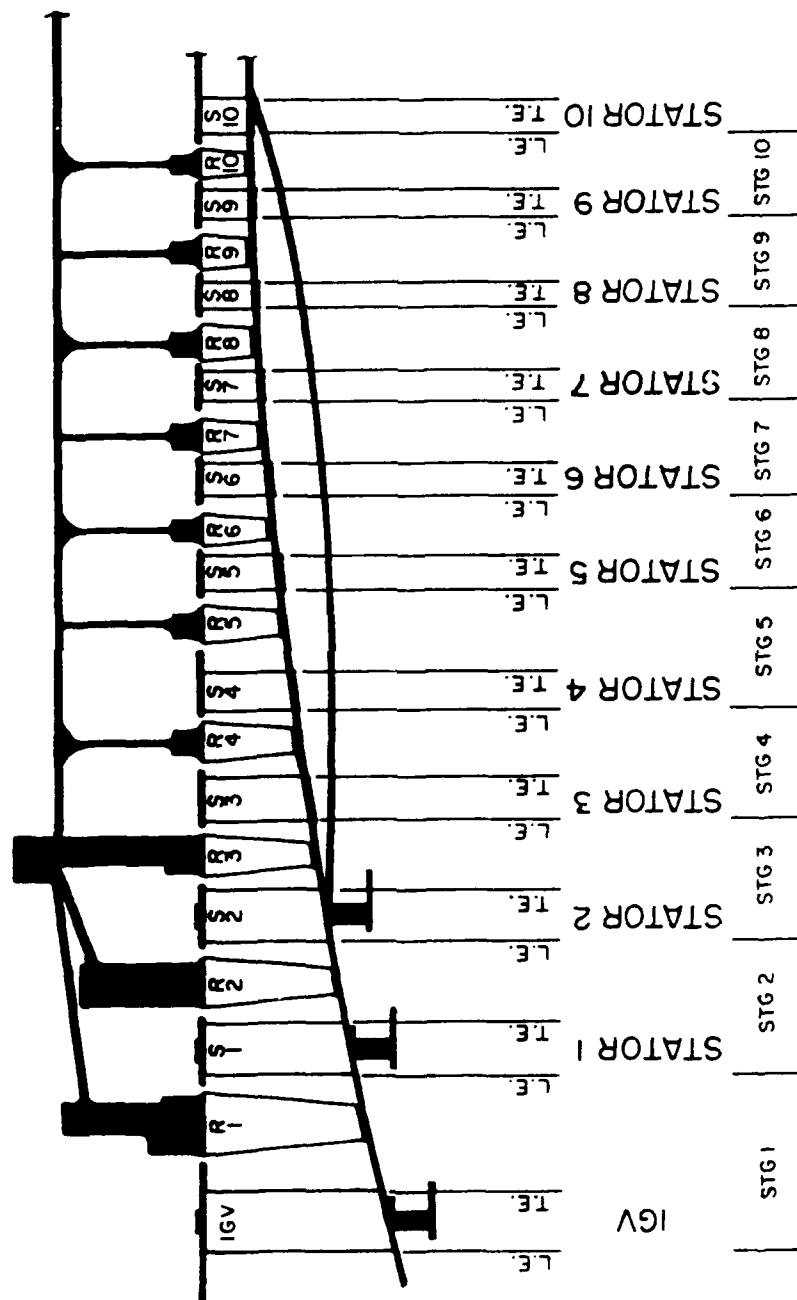


Figure 12. 10-Stage Test Compressor

A description of the buildings, rooms, and computer systems comprising the CRF is provided in Appendix A.

IV. COMPRESSOR INSTRUMENTATION

To measure the performance of the CRF compressor, total pressure, static pressure, and total temperature instrumentation were positioned at inlet, interstage, and exit locations. Since this report deals with phenomena observed at the tenth stage and exit of the compressor, only instrumentation at those positions is detailed in this section. For a complete description of all the instrumentation, reference 1 should be consulted.

Pressure measurements for the CRF test were acquired with frequency responses of 200 Hz (high-response), 70 Hz (close-coupled), or 0.5 Hz (time-averaged). Temperature measurements were acquired at 5 Hz (high-response) and 0.5 Hz (time-averaged). High-response measurements were used to analyze unsteady pressure variations observed during compressor in-stall operation. Time-averaged measurements were used to characterize the steady unstalled and quasi-steady, in-stall compressor performance. Details of the data acquisition methods used to measure the pressures presented in this report are provided in Appendix B. The type and location of the instrumentation is presented below.

Stage 10 Instrumentation

Figure 13 shows stages 8 and 9 and the discharge section of the test compressor. Time-averaged total pressures were

R = ROTOR
S = STATOR
STG = STAGE

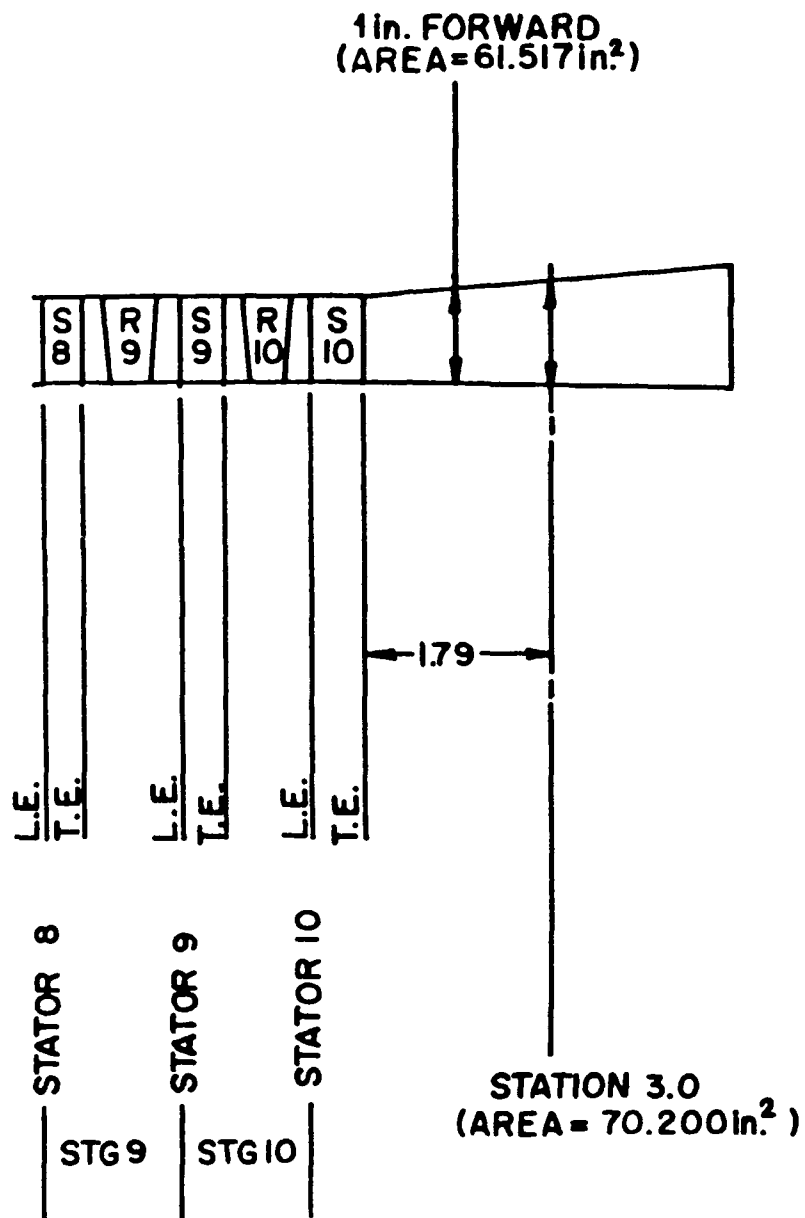


Figure 13. Test Compressor Exit

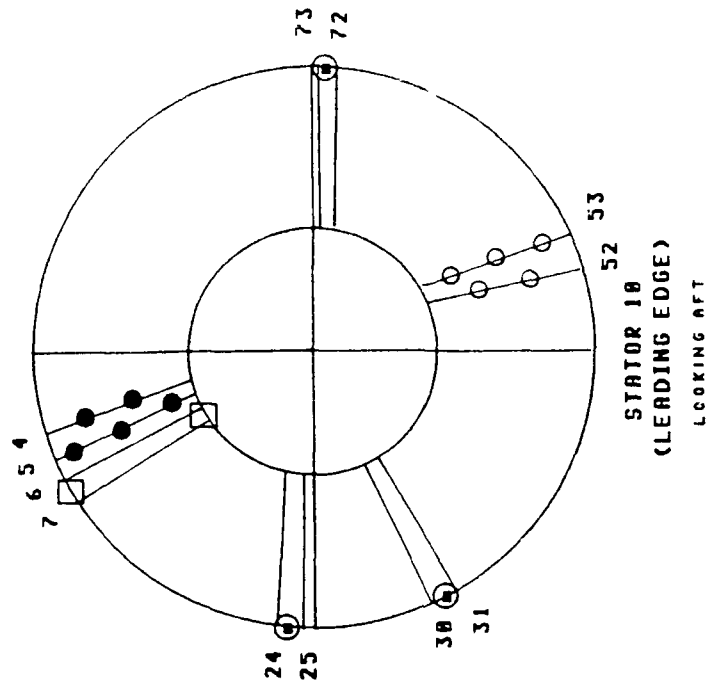
measured at each stage from kiel head probes located at five different radial centers of equal annulus area. The probes were located on the leading edge of the stators: three on one blade and two on the adjacent blade in stage 10 as shown in Fig. 14.

Both time-averaged and high-response static pressures were obtained from outside diameter wall taps at stator leading edges. As shown in Fig. 14, the 10th stator leading edge had three high-response and two time-averaged static pressure taps at different circumferential locations. The 10th-stage trailing edge also had one inside annulus time-averaged static pressure tap.

Time-averaged total temperatures were measured at each stage with the layout of thermocouples similar to that of the total pressure probes (see Fig. 14).

Discharge Instrumentation

Instrumentation at the exit of the compressor was positioned at two axial locations as shown in Fig. 13. Circumferential locations of the exit instrumentation are given in Fig. 15. The time-averaged and high-response static pressure taps were located at the annulus inner and outer wall 1 inch forward of station 3.0. Time-averaged total pressure and total temperature measurements were taken at station 3.0 and were once again positioned at five radial centers of equal annulus area (see Fig. 15).



LEGEND

- PRESSURE, STATIC
- PRESSURE, TOTAL
- TEMPERATURE, TOTAL
- ⊙ PRESSURE, STATIC, HIGH RESPONSE
- PRESSURE, TOTAL, HIGH RESPONSE, RADIAL RAKE
- ⊗ TEMPERATURE, TOTAL, CLOSE COUPLED
- ◻ STALL DETECTION

Figure 14. Stator 10 Instrumentation

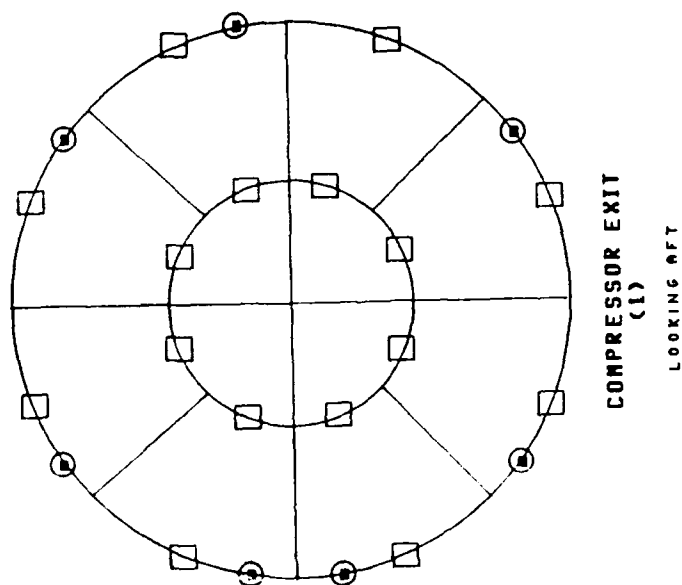
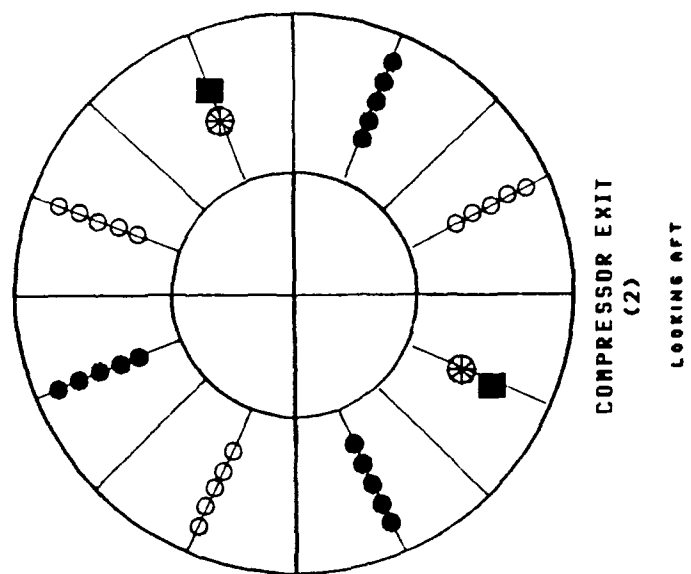


Figure 15. Exit Instrumentation

High-response total pressure and close-coupled total temperature measurements were made from a device called a Mach probe shown in Fig. 16. The Mach probe was located at station 3.0. Each Mach probe measured one upstream pressure, one downstream pressure, and one total temperature. The location of these probes is shown in Fig. 15.

Flow Instrumentation

Compressor discharge flow rates were measured by a calibrated 19-inch throat diameter flow venturi located approximately 100 ft (25 pipe diameters) downstream of the compressor exit.

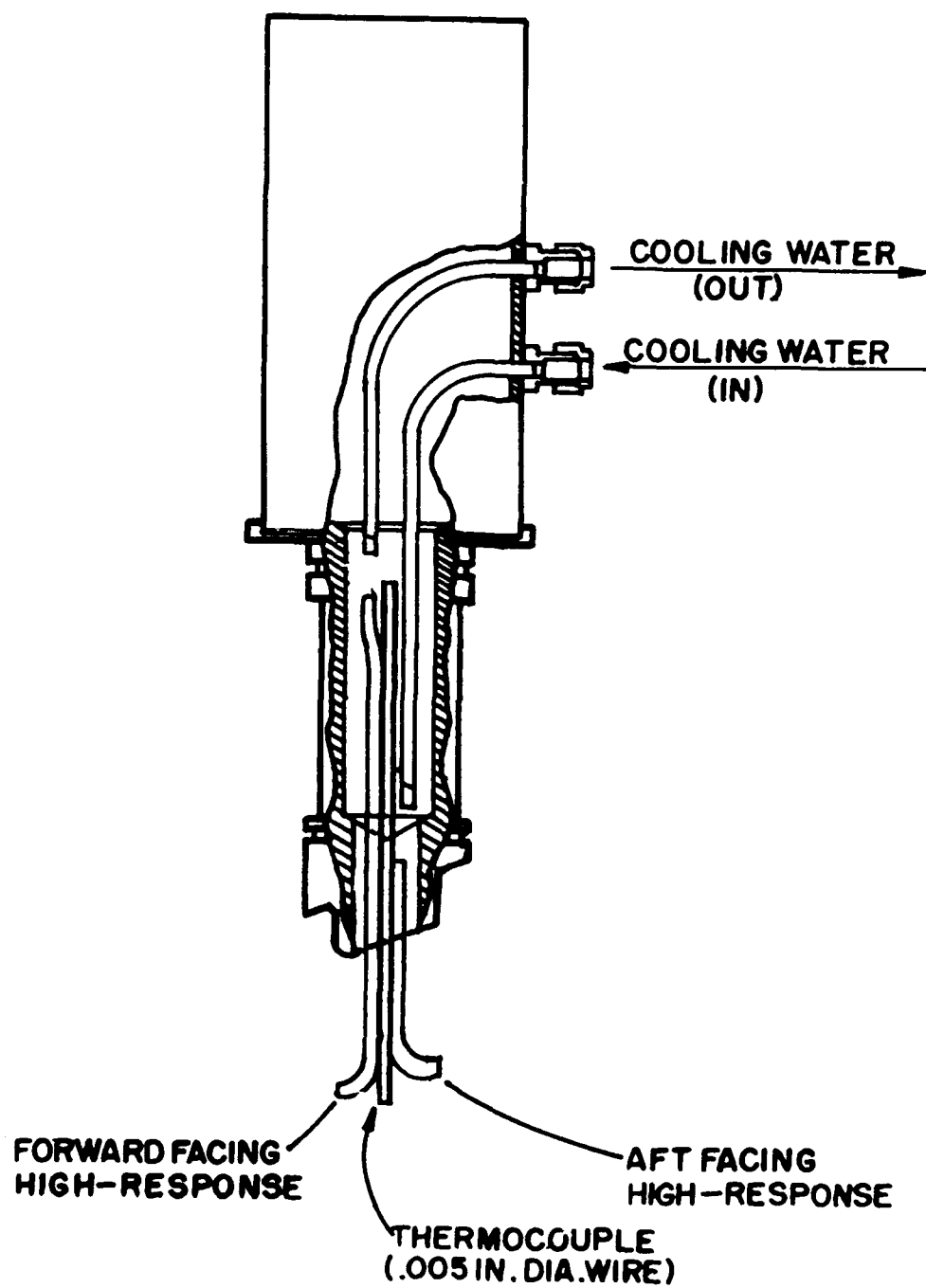


Figure 16. Mach Probe

V. TIME-AVERAGED DATA REVIEW

This section will present efforts made to validate and quantify the differences observed in the test compressor's stage, time-averaged, in-stall pressure characteristics. This was done to define stage characteristic changes that required further detailed high-response stall cell investigations.

In-Stall Pressure Characteristics

The pressure characteristics of the test compressor were a plot of the nondimensional pressure and flow coefficients at constant rotational speeds. The pressure coefficient (Ψ) and the flow coefficient (Φ) used in plotting, analyzing, and modeling the compressor data were defined as [4]

$$\Psi = \left[PR^{\frac{\gamma-1}{\gamma}} - 1 \right] \left[\frac{(N/\sqrt{\theta})_{design}}{(N/\sqrt{\theta})_{actual}} \right]^2 \quad (1)$$

$$\Phi = \frac{\left[\frac{w\sqrt{T_t}}{P_t A} \right] \left[\frac{(N/\sqrt{\theta})_{design}}{(N/\sqrt{\theta})_{actual}} \right]}{0.5318} \quad (2)$$

where

$$\theta = T_t/T_{ref}$$

PR = pressure ratio,

γ = ratio of specific heats,

N = rotor speed,

T_t = total temperature,

T_{ref} = standard day reference temperature,

W = mass flow,

A = area.

Performance characteristics may be defined for a single, compressor stage, a group of stages, or for the overall compressor. Performance characteristics relate the pressure ratio, temperature ratio, and efficiency to the flow through the stage or compressor. The coefficients that make up a characteristic may be defined in different ways [2]. A stage pressure characteristic plotted from equations 1 and 2 is a single curve for a given aerodynamic design and is theoretically independent of compressor speed effects. The pressure characteristics of the data showed how each stage operated for different mass flows. If the aerodynamic design of the stage was changed by variable geometry, the pressure characteristic would be expected to change also. However, the 10th-stage in-stall pressure characteristic varied without a change in the geometry of the stage as reported by Copenhaver [3]. This requires an explanation.

During rotating stall operation, the stage of a compressor is subject to segments of stalled and unstalled flow. Each of these flows is assumed to have a unique pressure characteristic, as in parallel compressor theories. The in-stall pressure characteristic of the CRF compressor was actually based on time-averaged measurements of the pressure rise generated in the stalled and unstalled segments of the stage as it operated in rotating stall. Thus, in accordance with the above assumption, to say that the 10th-stage in-stall pressure characteristic changed means that the time-averaged pressure rise representing the stalled and unstalled pressure characteristic was different, not the pressure characteristics themselves.

Test Article Variables

During the CRF test, some changes were made to the test article to observe effects on compressor operation. Changes included variable geometry, combustor volume, and start bleed. The CRF record of test variables at the 75-percent speed data points showed the combustor volume to be "nominal" (nominal was defined as the design condition for any test variable) and the start bleed to be closed for both variable geometry settings of nominal and +7°. A setting of +7° represented a 7° opening in IGV, stator 1 and stator 2 stagger angle. Thus, changes observed by Copenhaver [3] for the 75-percent speed

in-stall pressure characteristics could only be attributed to changes in the variable vanes.

60-Percent Speed Data

Variable geometry effects were also analyzed at 60-percent speed with the combustor volume and start bleed held constant as described above. Pressure characteristic plots showed that the 9th and 10th-stage in-stall pressure characteristics did vary when the variable vanes in stages 1 through 3 were changed from nominal to +7° stagger in the same manner as observed at 75-percent speed.

Pressure Characteristic Changes

To further quantify the changes in the in-stall stage characteristic as a result of stagger angle changes in stages 1, 2, and 3, least-square curve fits were applied to the in-stall, time-averaged quasi-steady operating points taken during the CRF test. Plots of these curve fits are given in Appendix C as Figs. C-1 to C-10. Using the curve fit equations, the pressure coefficients for nominal and +7° stagger on IGV's and stators 1 and 2 (designated hereafter as +7 variable vane or +7VV) settings were calculated over each stage flow coefficient range and compared. Figure 17 shows the absolute difference between the nominal and +7VV in-stall pressure coefficients ($\Psi_{\text{NOM}} - \Psi_{+7\text{VV}}$) for all stages.

A look at the magnitude of absolute pressure coefficient difference in the variable geometry stages was helpful in

VARIABLE GEOMETRY EFFECTS ON IN-STALL CHARACTERISTIC SPEED = 75%

ABSOLUTE DIFFERENCE IN PRESSURE COEFFICIENT

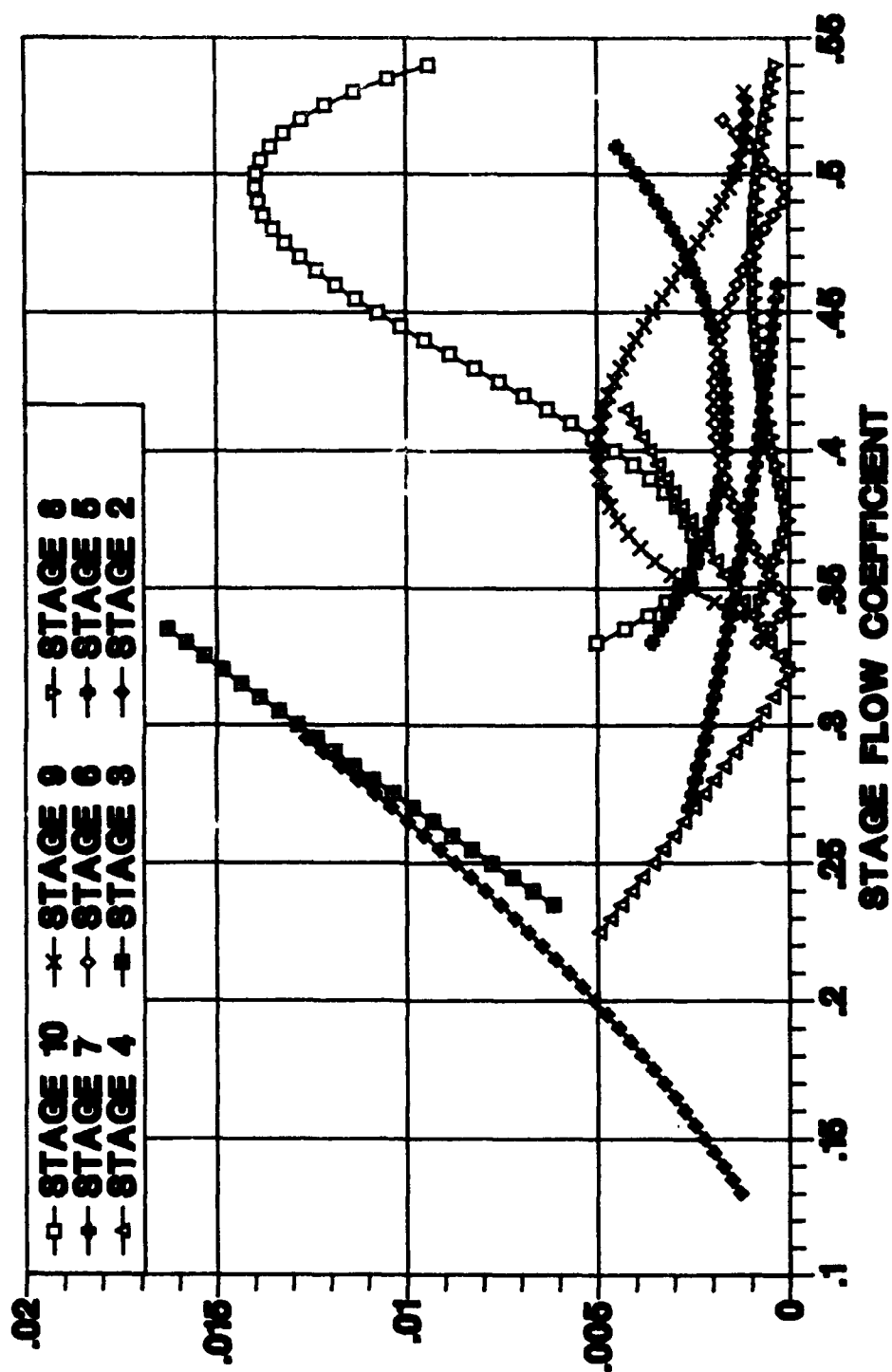


Figure 17. Pressure Coefficient Differences Between Nominal and +7 VV Settings

determining the significance of measured changes in stages 4 through 10. From Fig. 17, stages 2 and 3 had a maximum difference of 0.0127 and 0.0163 respectively. The maximum difference for stages 4 through 9 was 0.005 or less. The maximum difference for stage 10 was 0.0140, which was of the same magnitude as the changes observed in stages 2 and 3. This indicated a significant change in the 10th-stage in-stall characteristic due to stagger angle changes in stages 1 through 3. These results added additional support for further investigations into the 10th-stage, time-resolved, in-stall performance to help explain the observed changes in characteristics.

VI. HIGH-RESPONSE DATA REDUCTION AND CALIBRATION

In order to analyze the high-response pressures recorded during the CRF test, the measured voltages were digitized and converted to engineering units. This was accomplished in two steps as outlined below.

Data Reduction

During the CRF test, numbers were assigned to every steady and quasi-steady operating point (or data point). Along with these data, high-response pressures were recorded. Time-averaged data points were acquired for each steady and quasi-steady operating condition during the CRF test. Figure 18 shows operating points plotted as pressure coefficient verses flow coefficient in the 10th stage. Nine in-stall quasi-steady operating points and three unstalled steady operating points were digitized from the high-response data.

The frequencies on the 28-channel FM tapes were converted to digital voltages and placed on 9-track digital tapes at the NASA Langley Research Center Central Data Transcription Facility (CDTF). Since the analog tapes were continuously recording high-response pressure data during the CRF test, time intervals were defined to be digitized corresponding to the absolute time that the time-averaged data points were obtained. At the CDTF, anti-aliasing filters were set at 200 Hz, the sampling rate was adjusted to 1000 samples per second,

TENTH STAGE PRESSURE CHARACTERISTIC VARIABLE GEOMETRY EFFECTS, 75% SPEED

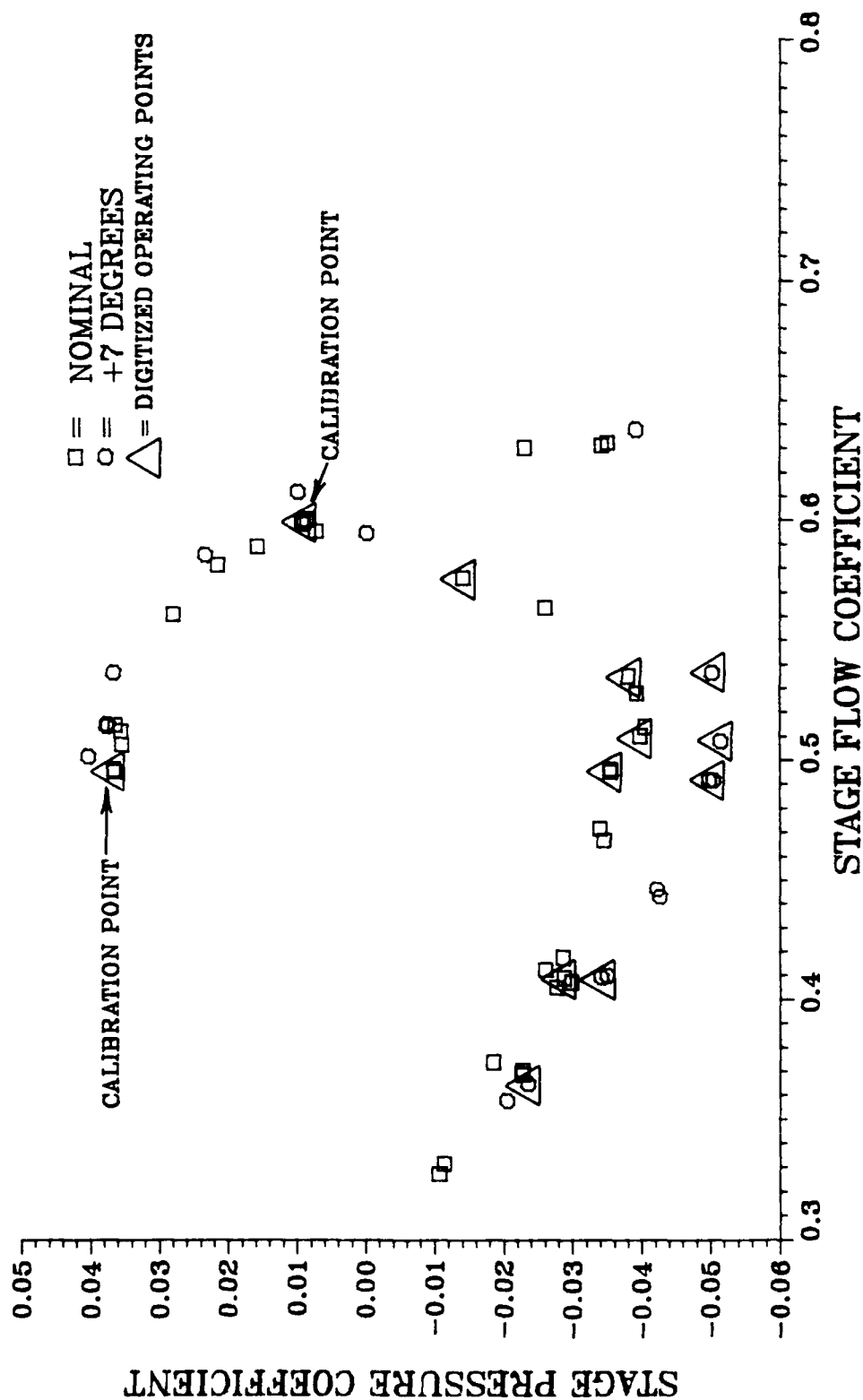


Figure 18. Digitized Operating Points

and the start and stop times of the digitization were recorded at an accuracy of 0.1 msec.

The format of the CDTF tapes was then modified to a CRF Standard Format Tape (SFT). This organized the data in a way that allowed plotting and other post-processing software available at the CRF to be used when analyzing the data.

Pressure Calibration

The next step was to calculate time-resolved pressures from the digitized voltages. This was accomplished by obtaining a calibration equation relating high-response pressure channel voltages to corresponding time-averaged pressure measurements acquired during the CRF test. Figure 18 shows the pre-stall and recovery steady operating points used for the calibration. Two steady operating points were used rather than three because no appreciable increase in accuracy was gained with a quadratic equation due to the linear nature of the high-response pressure transducers.

To obtain the calibration voltages, 30 scans of the desired high-response channel were averaged. The standard deviation was also calculated and any scans outside the average plus or minus two standard deviations (95-percent confidence level) were discarded. The standard deviations for the channels calibrated were between 0.18 and 0.43 percent of the mean voltage.

The high-response pressures were calibrated to time-averaged pressures measured during steady-state operating conditions at the same radial immersion and as close circumferentially and axially as available. Details of the channel calibrations are given in Section VII.

Knowing the two pressures and their corresponding voltages, coefficients A and B of the linear equation

$$\text{Pressure} = A + B(\text{Volts}) \quad (3)$$

were calculated. This equation was then used to calculate the in-stall, high-response pressures.

VII. PRESENTATION OF RESULTS

High-response total pressure, static pressure, and Mach number were calculated at station 3.0 of the test compressor for each of the in-stall, quasi-steady operation points shown in Fig. 19. This section will present these data and define the principles used to obtain them.

Mach Probe High-Response Pressure Calibration

The data presented in this section were obtained by calibrating the high-response pressures measured by the station 3.0 Mach probe as outlined in Section VI. The calibrations were made against standards defined as steady-state measurements obtained at steady operating conditions, following the procedure defined in Section VI. This type of calibration was required to minimize the sensitivity and offset drift effects of the high-response transducers.

The forward-facing pressure probe measured a total pressure and was calibrated to a time-averaged total pressure at the same radial and axial location, and the nearest circumferential measurement station. The locations of the time-averaged pressures used for the calibrations are shown in Fig. 20. When the axial flow past the Mach probe was in the positive direction, the rear-facing probe measured the pressure in the wake of the Mach probe. This pressure was calibrated to a time-averaged static pressure. Since the wall

TENTH-STAGE PRESSURE CHARACTERISTIC

VARIABLE GEOMETRY EFFECTS

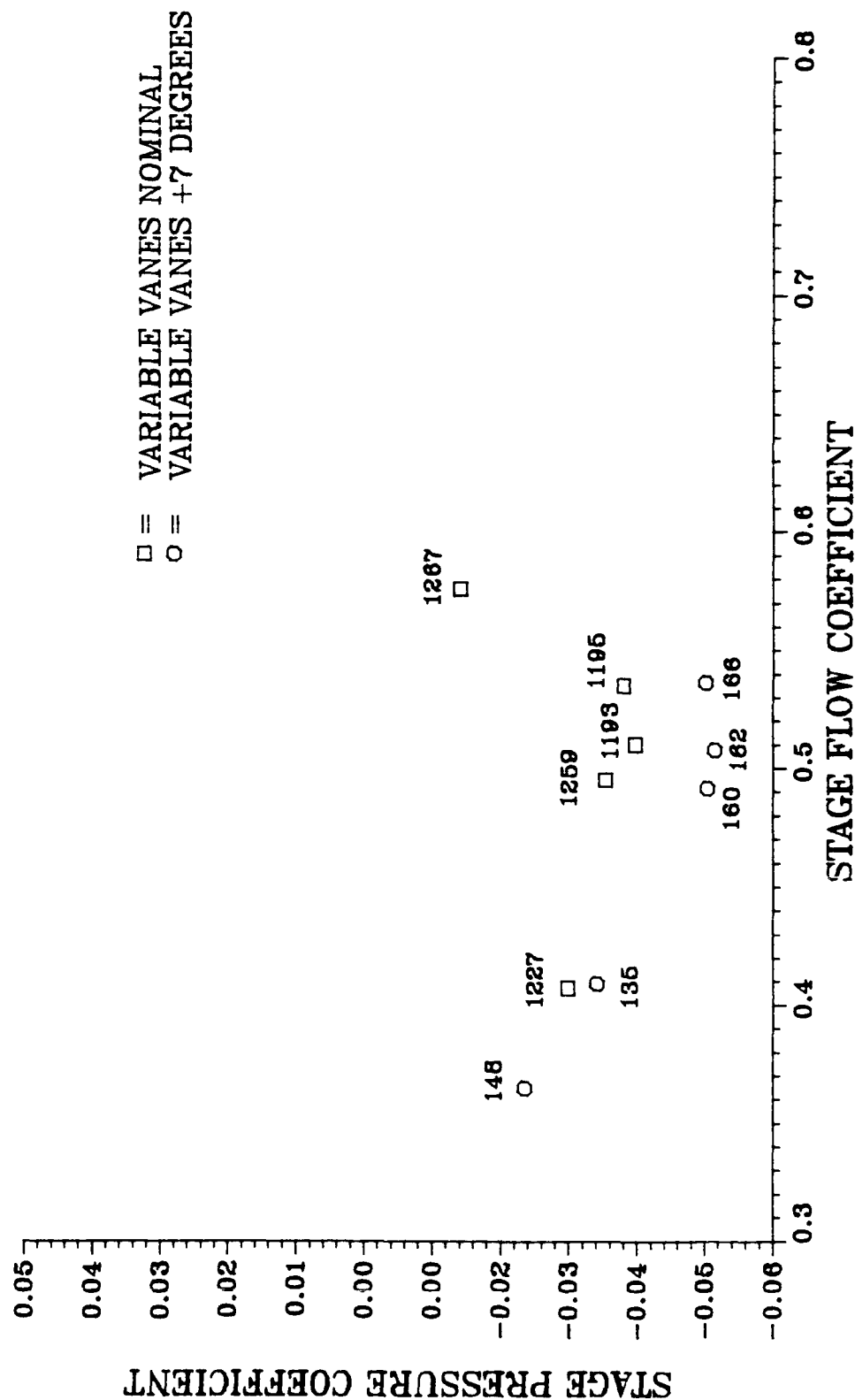


Figure 19. Labeled Operating Points

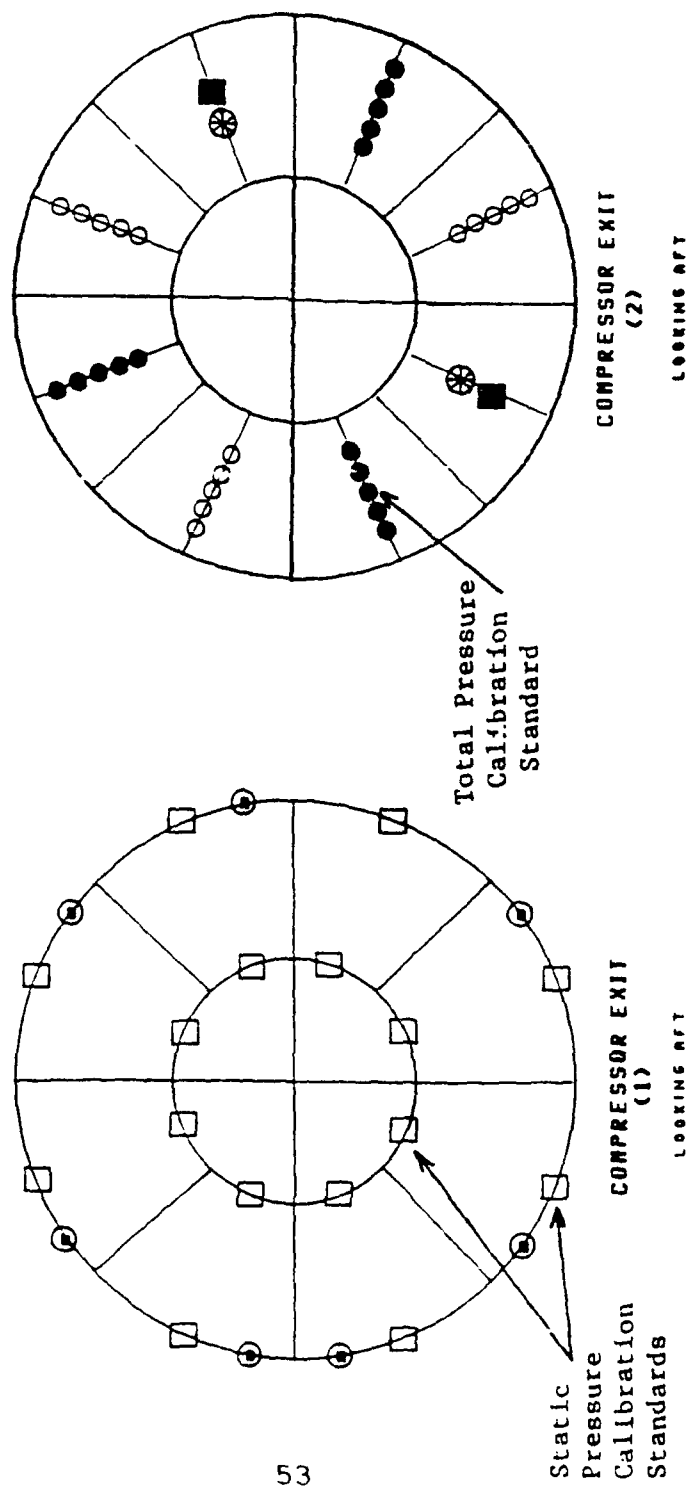


Figure 20. High-Response Pressure Calibration Standards

static pressures were measured 1 in. forward of station 3.0 (see Fig. 13), the time-averaged static pressures at station 3.0 were determined assuming an isentropic expansion of the flow from the wall static location to station 3.0.

Calibration Errors

Because the steady-state compressor total and static pressure measurements were used as a calibration standard, their associated uncertainties were added as bias error to the high-response measurements. The bias errors of the steady-state measurements (± 0.5 psi) were higher than would be desired for a calibration standard. They were deemed acceptable as an alternative to utilizing bench calibrations of the high-response transducers, and not knowing how much drift in offset and sensitivity occurred after installation of the transducer. Comparison of the bench calibration to those obtained from steady-state measurements indicated a drift occurred after installation. This drift was approximately 1 psia for the total pressures and 0.3 psia for the static pressures in the range of pressures measured.

Regardless, the errors associated to bias were not a major concern, as the primary emphasis of this report was to determine relative changes in the stall cell characteristic to throttle and stator vane stagger angle changes. Precision errors for the high-response pressure transducers and associated electronic equipment were determined from a review

of multiple bench calibrations, manufacturer's specifications, and multiple scans of data during steady operating conditions. This review indicated approximate expected error in precision of ± 0.15 psia in the range of measurements obtained.

Ensemble Averaging

An ensemble averaging method was used to remove randomness from the high-response pressure measurements. Reference 18 explains the principles and applications of ensemble averaging. A single time history representing a random phenomena is defined as a sample function (or a sample record when observed over a finite time interval). The collection of sample functions which forms a random process is called an ensemble. To obtain an ensemble average, the functions of the sample records are summed and divided by the number of samples. For the high-response pressure measurements, 15 sample records each 0.06 second in duration were collected and averaged together. This averaged time history corresponded to 3 to 3.5 cycles of the periodic pressures measured.

High-Response Pressures

The Mach probe total and static high-response pressures at station 3.0 for data point 1193 are shown in Fig. 21. The pressures for all other data points are presented in Appendix D as Figs. D-1 to D-10. Because of the format of the CRF data and the ensemble averaging method used, all plots of ensemble

HIGH RESPONSE PRESSURE MEASUREMENTS ENSEMBLE AVERAGE OF DATA POINT 1193

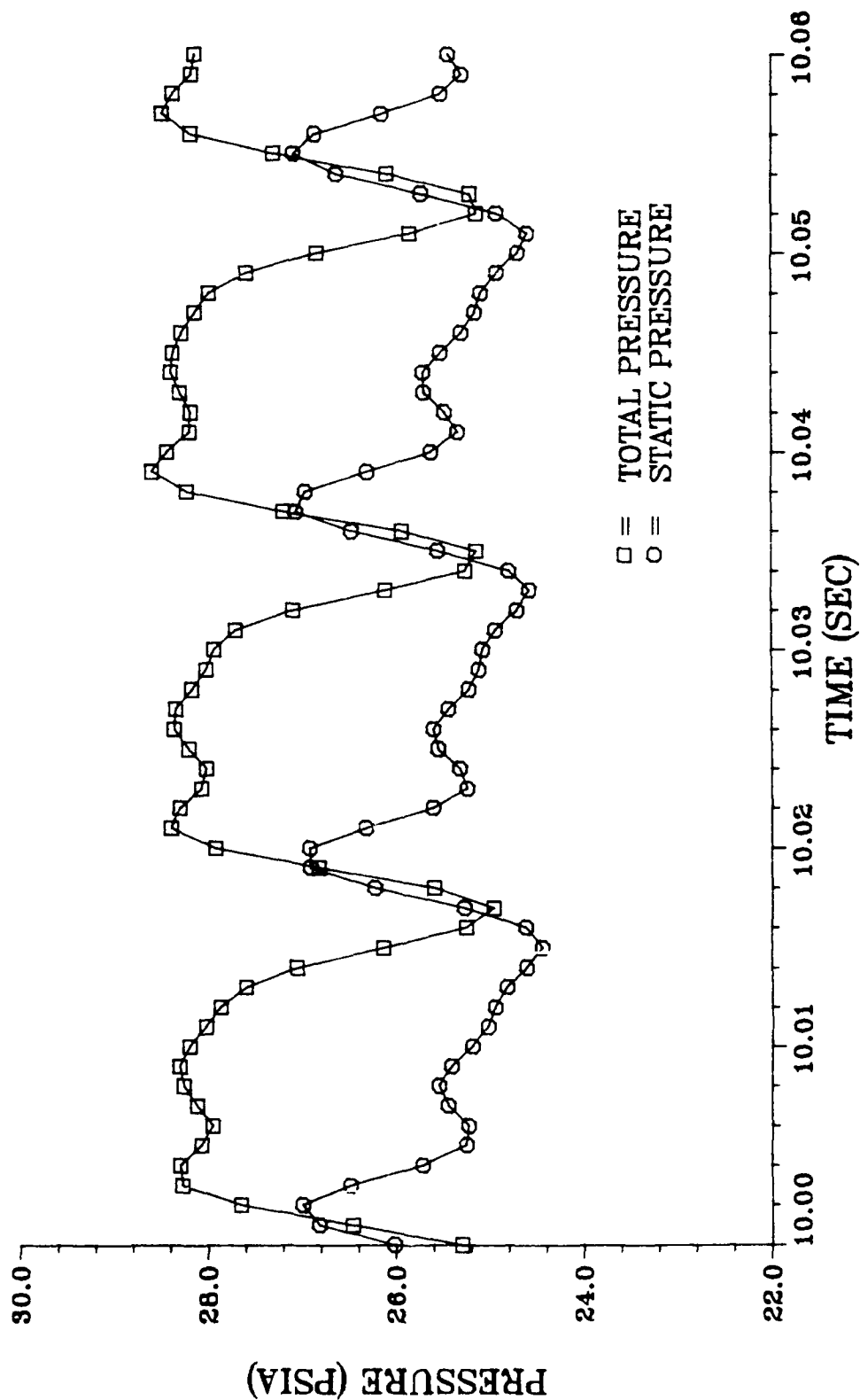


Figure 21. High-Response Pressure Measurements, Data Point 1193

averages were normalized with a time axis from 10.00 to 10.06 sec. Phase relationship between total and static pressures for a given quasi-steady operating point was maintained.

The high-response pressure plots showed the cyclic nature of the stall cell and the magnitude of the total and static pressure variation at station 3.0 in the CRF compressor while operating in rotating stall.

High-Response Axial Mach Numbers

Axial Mach number time histories were determined utilizing the ensemble averaged high-response total and static pressures from the equation

$$M = \left\{ \left[\left(\frac{P_t}{P} \right)^{\frac{\gamma-1}{\gamma}} \right] \frac{2}{\gamma-1} \right\}^{\frac{1}{2}} \quad (4)$$

where

M = Mach number,

P_t = total pressure,

P = static pressure,

γ = ratio of specific heats.

For this calculation, the ratio of specific heats was assumed to be a constant determined from the time-averaged total temperature. For air temperatures below 1800°R (1000°K), γ has

been shown [19] to be a function of static temperature. Time-resolved static temperature could not be determined at station 3.0 of the test compressor, therefore γ was estimated from the time-averaged total temperature measured from the thermocouple on the Mach probe. For the flow velocities and time-averaged total temperatures (from 770 to 980°R (427.8 to 544.5°K)) at station 3.0, the difference between the total and static temperature were not enough to change the value of γ enough (less than 25°) to affect the calculation of Mach number.

With regard to the use of a time-averaged temperature, little is known about temperature fluctuations during rotating stall. Na'covska' [20] reported temperature changes in a multistage, axial-flow compressor operating in rotating stall to be ± 1 percent of the mean. However, she also observed that because of the frequency response limitations of her measurement instrumentation, temperature fluctuations could have been higher. For the Mach numbers calculated at the exit of the test compressor, a 200° difference in temperature would result in a 0.30-percent difference in Mach number due to variations in γ . Since temperature variations greater than this magnitude were extremely unlikely, the time-averaged temperature assumption was considered acceptable.

Reverse flow. Reverse flow was represented by a negative Mach number. Reverse flow was assumed to be present when the pressure from the aft-facing probe of the Mach probe was

greater than the forward-facing probe. The magnitude of the Mach number was calculated by substituting the rear-facing probe pressure for P_t and the forward-facing probe pressure for P in equation 4.

Mach number plots. The calculated high-response Mach number plots at station 3.0 for each quasi-steady, in-stall operating point are shown in Figs. 22 to 31. These plots illustrate how the flow through the compressor exit varied as a result of the rotating stall cell. Each plot details the axial Mach numbers of the stalled and unstalled flow and the apparent transition zones from one to the other at each quasi-steady operating point.

Annular Representation of Axial Mach Numbers

The high-response Mach number plots presented in Figs. 22 through 31 showed there was a definite region of transition (for details see Fig. 31) between negative axial Mach numbers (stalled flow) to the maximum axial Mach number (unstalled flow). They also showed that this transition region's circumferential extent varied for different quasi-steady operating points (compare 148 and 162). To show how the Mach numbers varied circumferentially in the compressor annulus at station 3.0 for a given instant of time at each quasi-steady point, an annular representation was devised.

Since the high-response axial Mach number curves were generated from stationary pressure probes, one cycle

represented 360° of the compressor annulus. Therefore, figures were generated of axial Mach number ranges as a function of the test compressor circumference at station 3.0. Figures 32 to 37 present an annular view of the axial Mach numbers for all quasi-steady operation points. These figures were made by taking one cycle from each high-response Mach number plot and dividing it into ranges of reverse flow, 0 to 49 percent, 50 to 69 percent, 70 to 79 percent, 80 to 89 percent, and 90 to 100 percent of the peak Mach number calculated at station 3.0 for that cycle.

HIGH RESPONSE MACH NUMBER CALCULATIONS
STATION 3.0, DATA POINT 1267

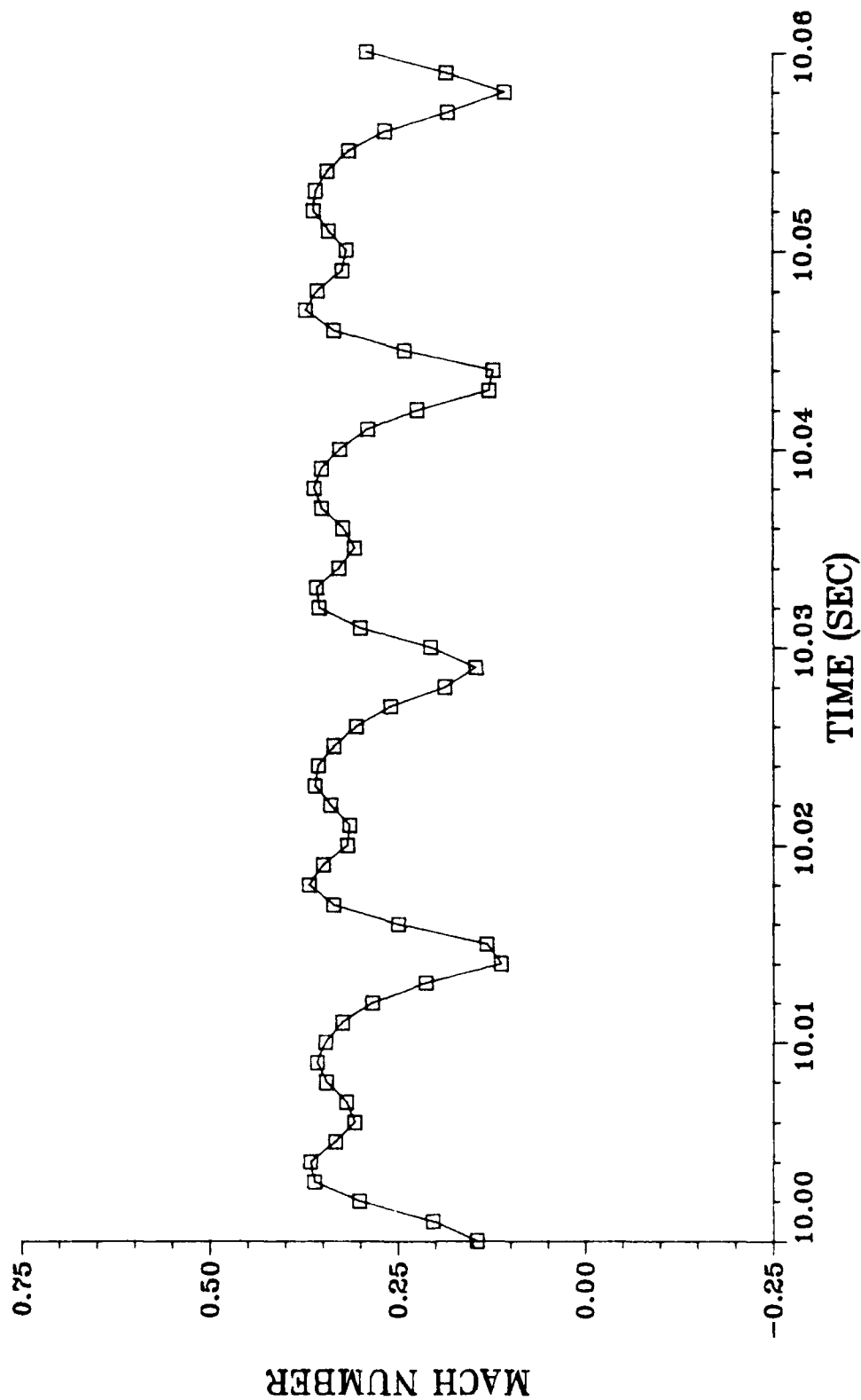


Figure 22. Rotating Stall Mach Numbers, Data Point 1267

HIGH RESPONSE MACH NUMBER CALCULATIONS STATION 3.0, DATA POINT 1195

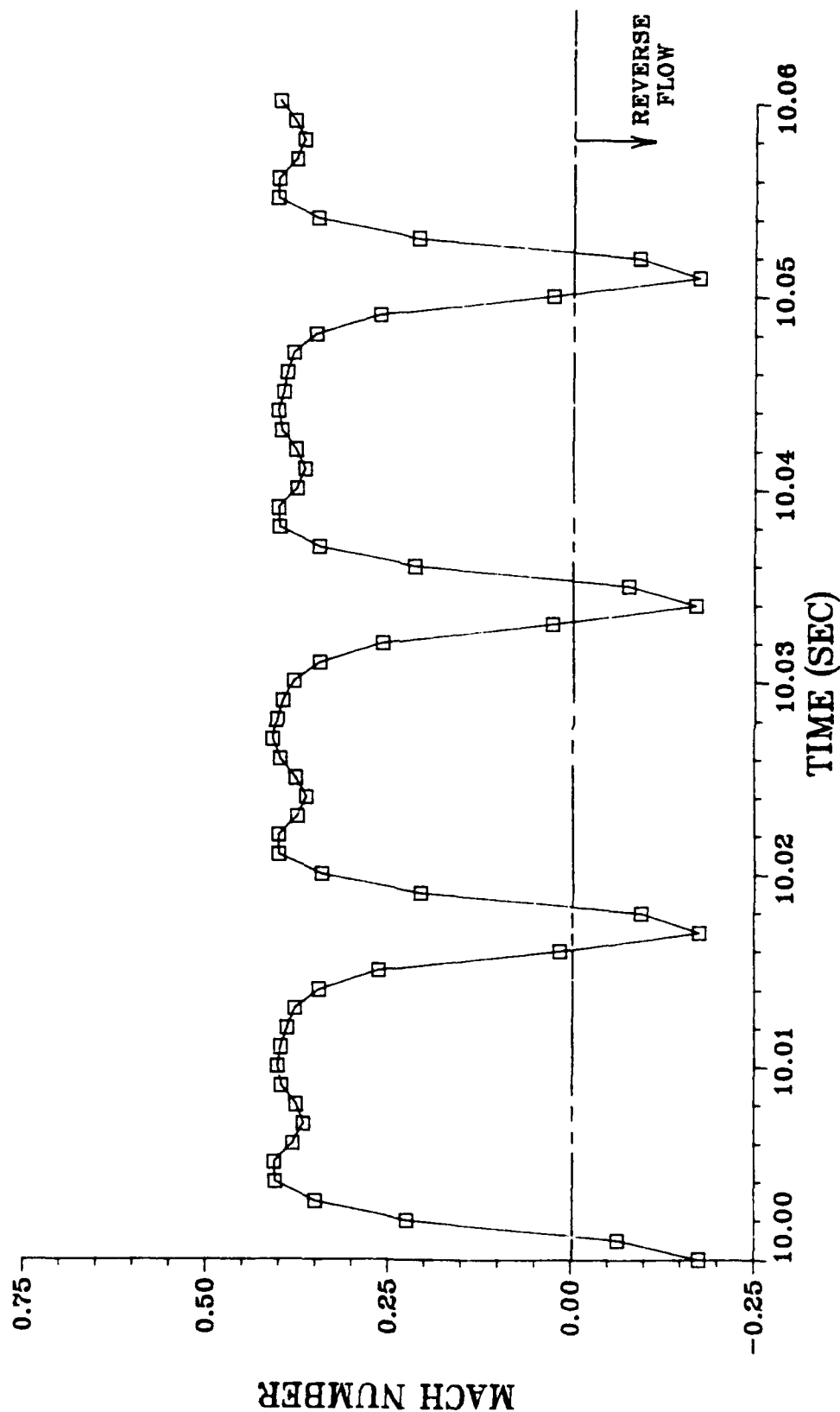


Figure 23. Rotating Stall Mach Numbers, Data Point 1195

HIGH RESPONSE MACH NUMBER CALCULATIONS STATION 3.0, DATA POINT 1193

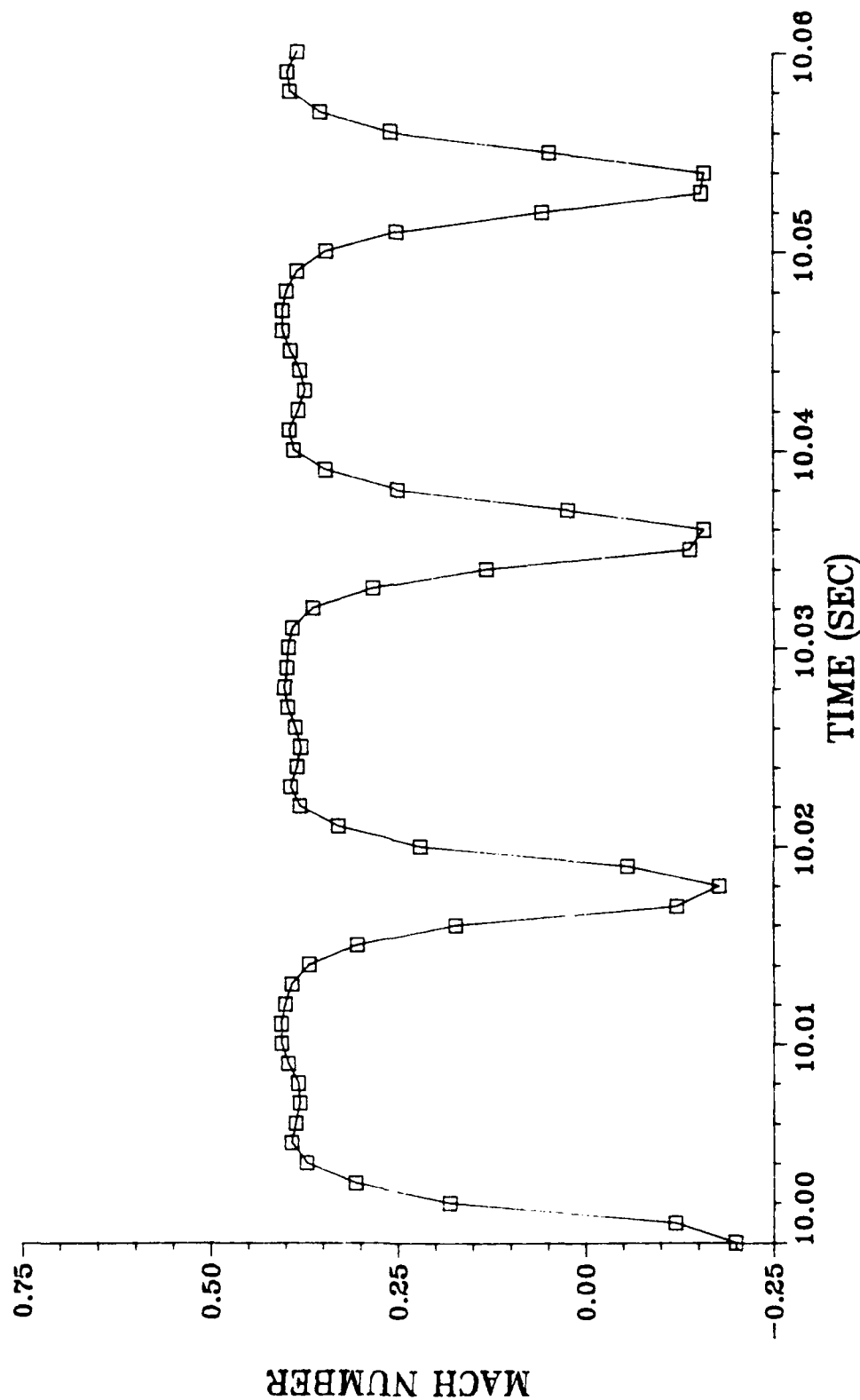


Figure 24. Rotating Stall Mach Numbers, Data Point 1193

HIGH RESPONSE MACH NUMBER CALCULATIONS STATION 3.0, DATA POINT 1259

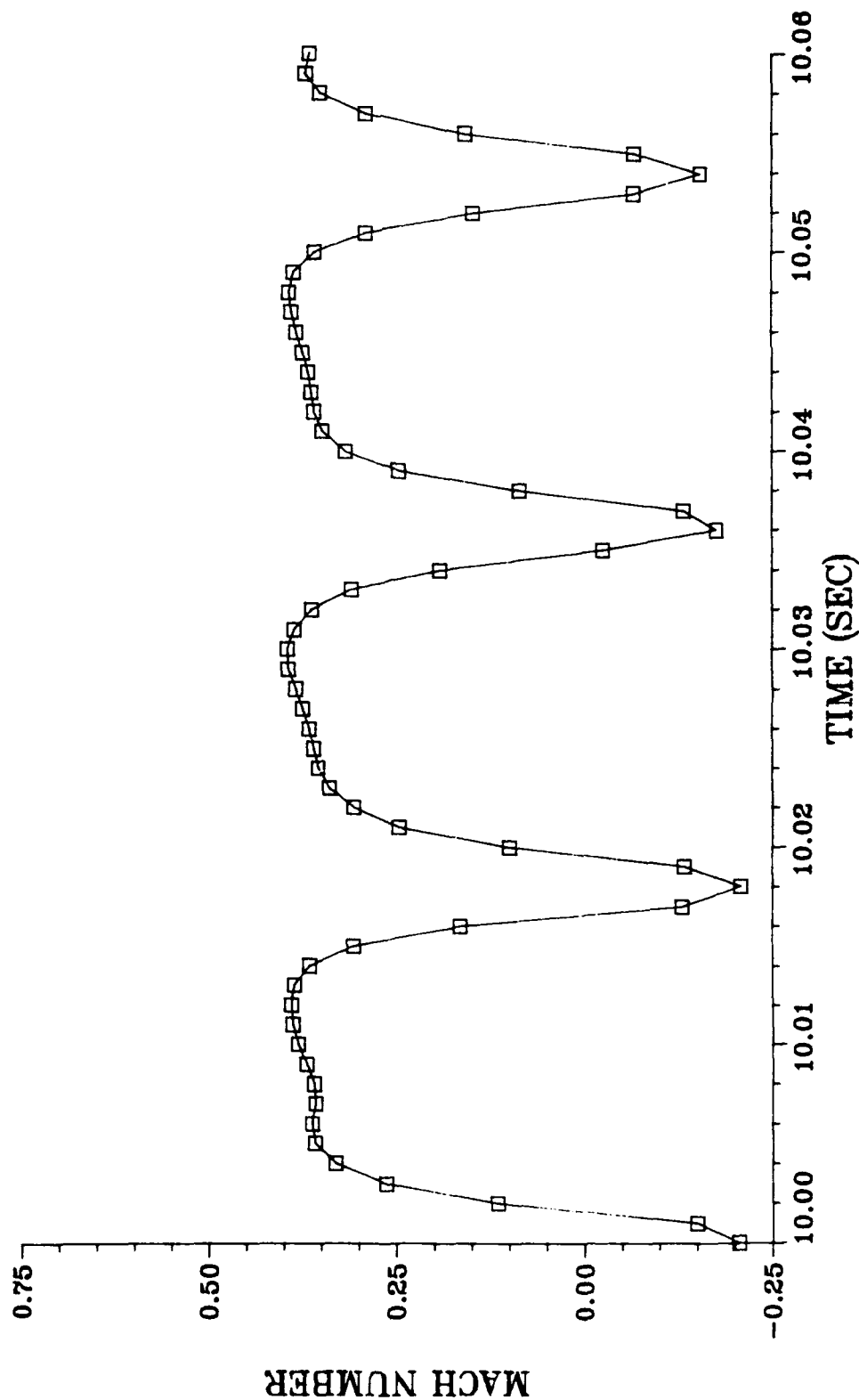


Figure 25. Rotating Stall Mach Numbers, Data Point 1259

HIGH RESPONSE MACH NUMBER CALCULATIONS
STATION 3.0, DATA POINT 1227

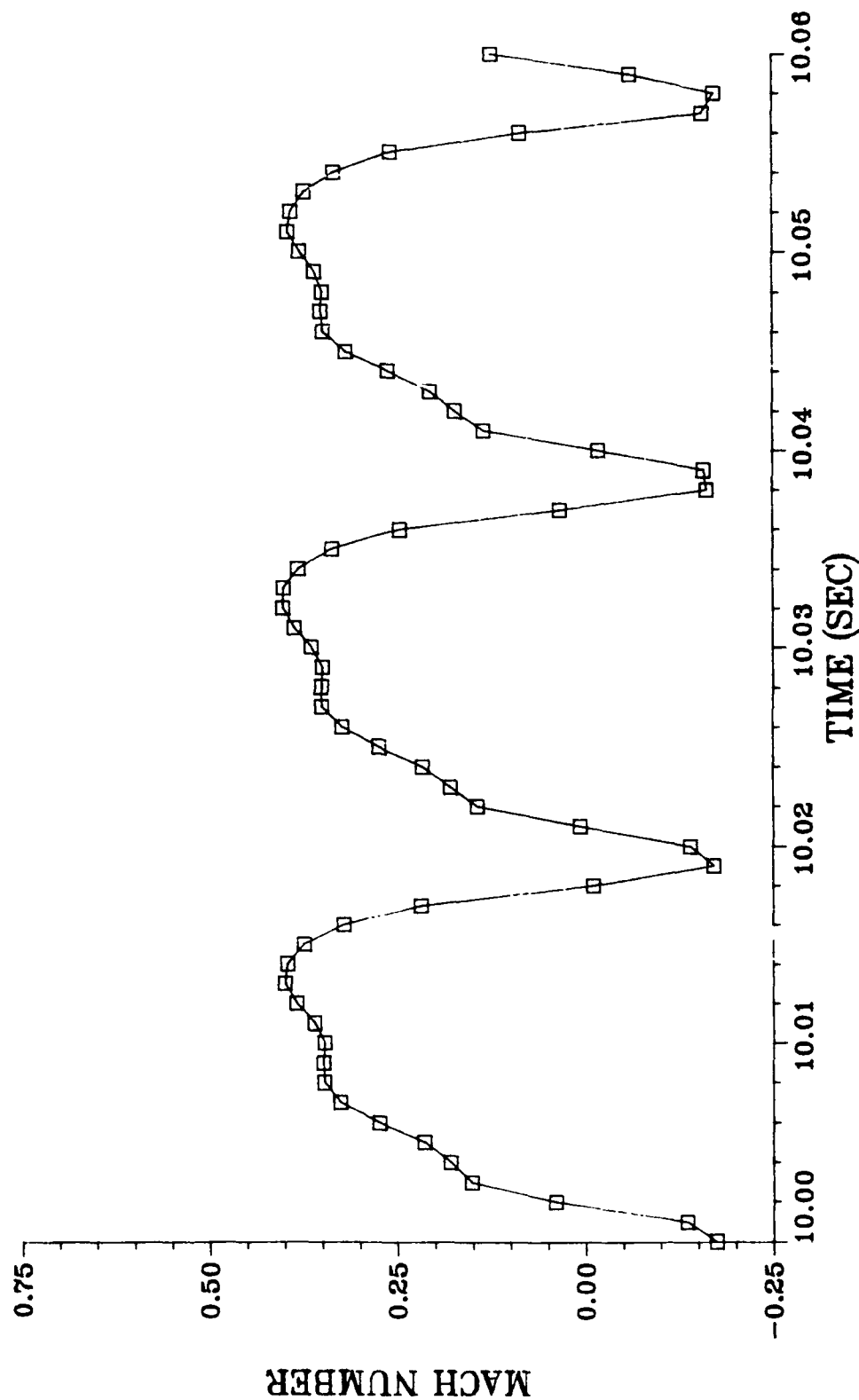
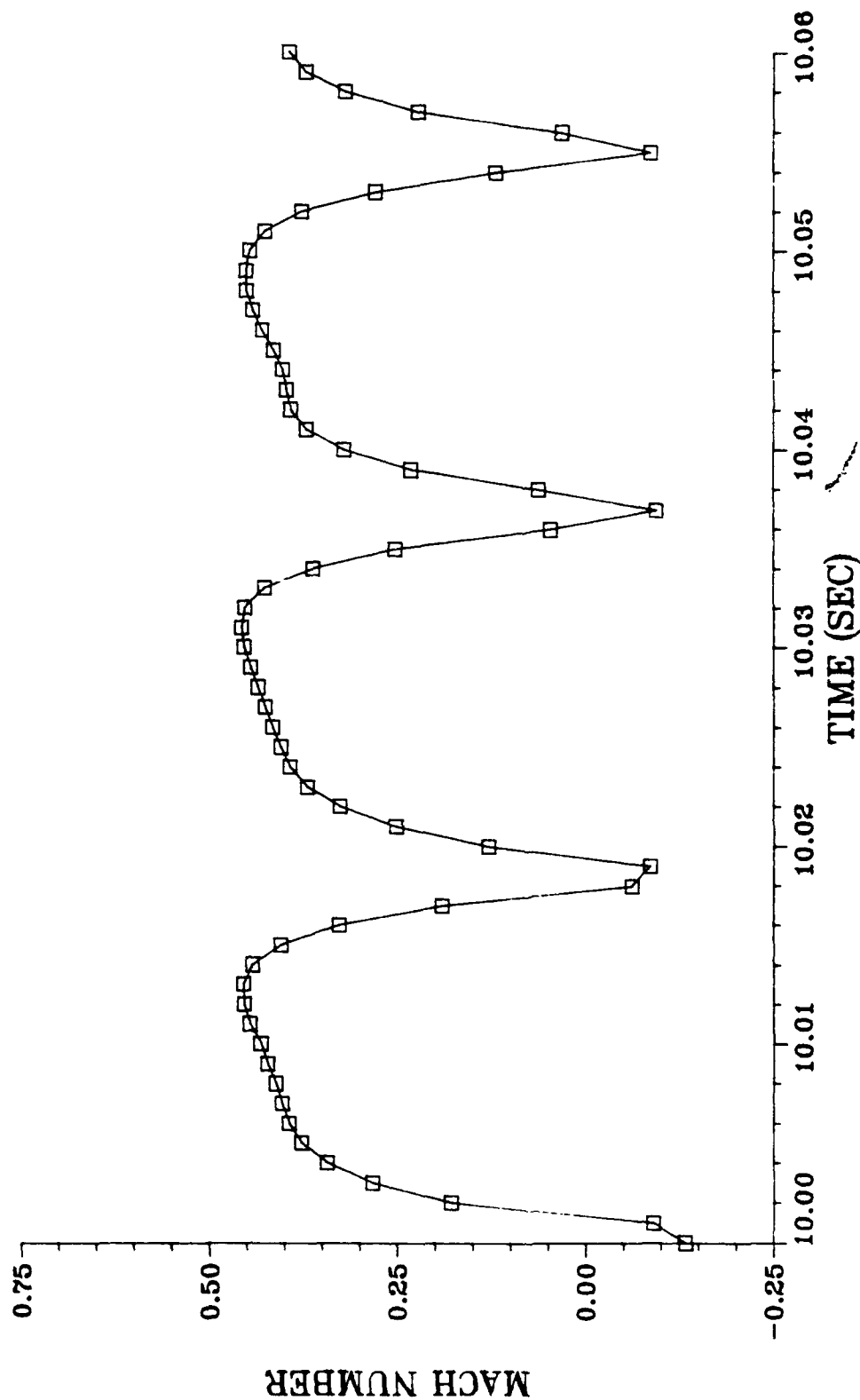


Figure 26. Rotating Stall Mach Numbers, Data Point 1227

HIGH RESPONSE MACH NUMBER CALCULATIONS STATION 3.0, DATA POINT 166



HIGH RESPONSE MACH NUMBER CALCULATIONS STATION 3.0, DATA POINT 162

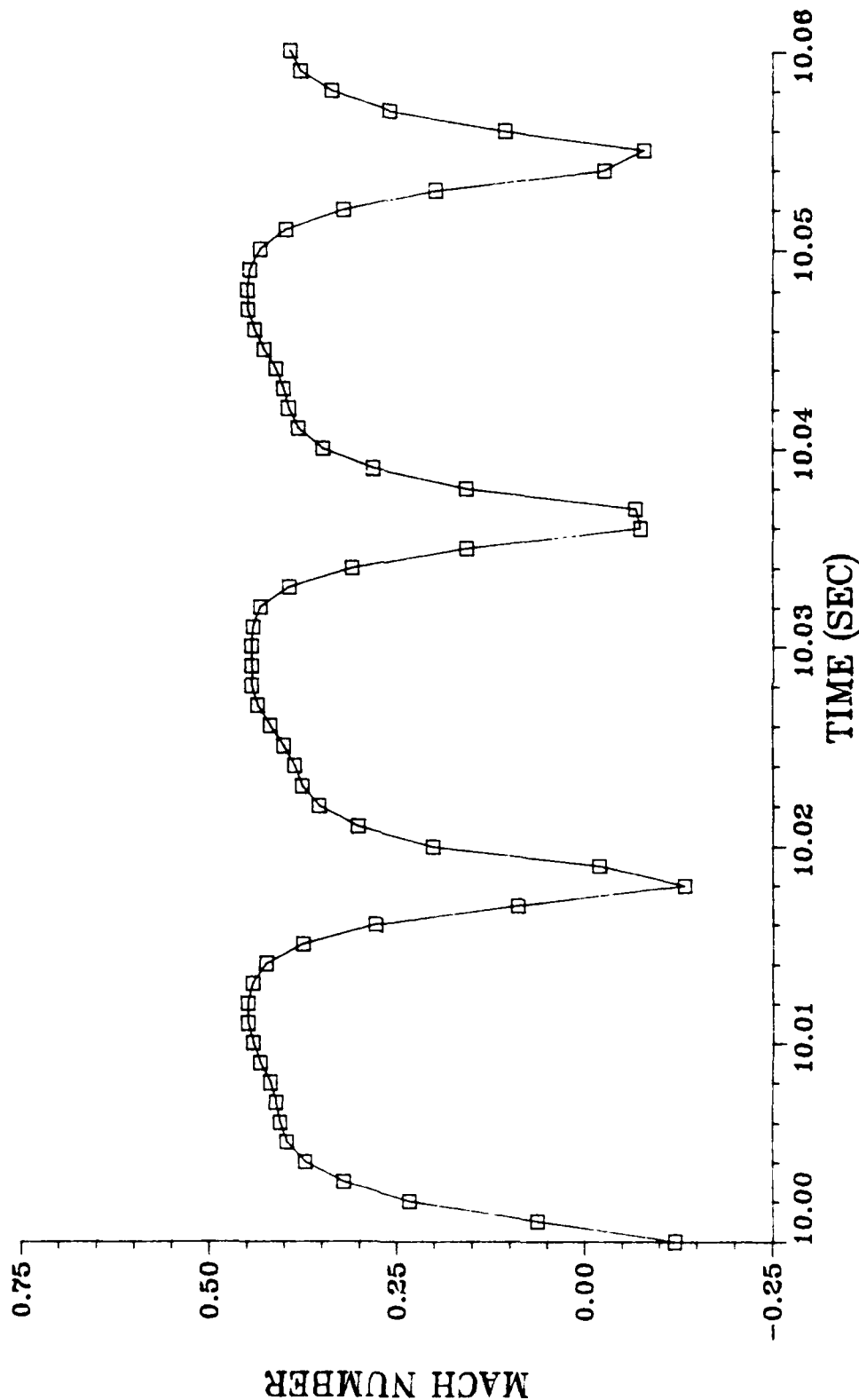


Figure 28. Rotating Stall Mach Numbers, Data Point 162

HIGH RESPONSE MACH NUMBER CALCULATIONS STATION 3.0, DATA POINT 160

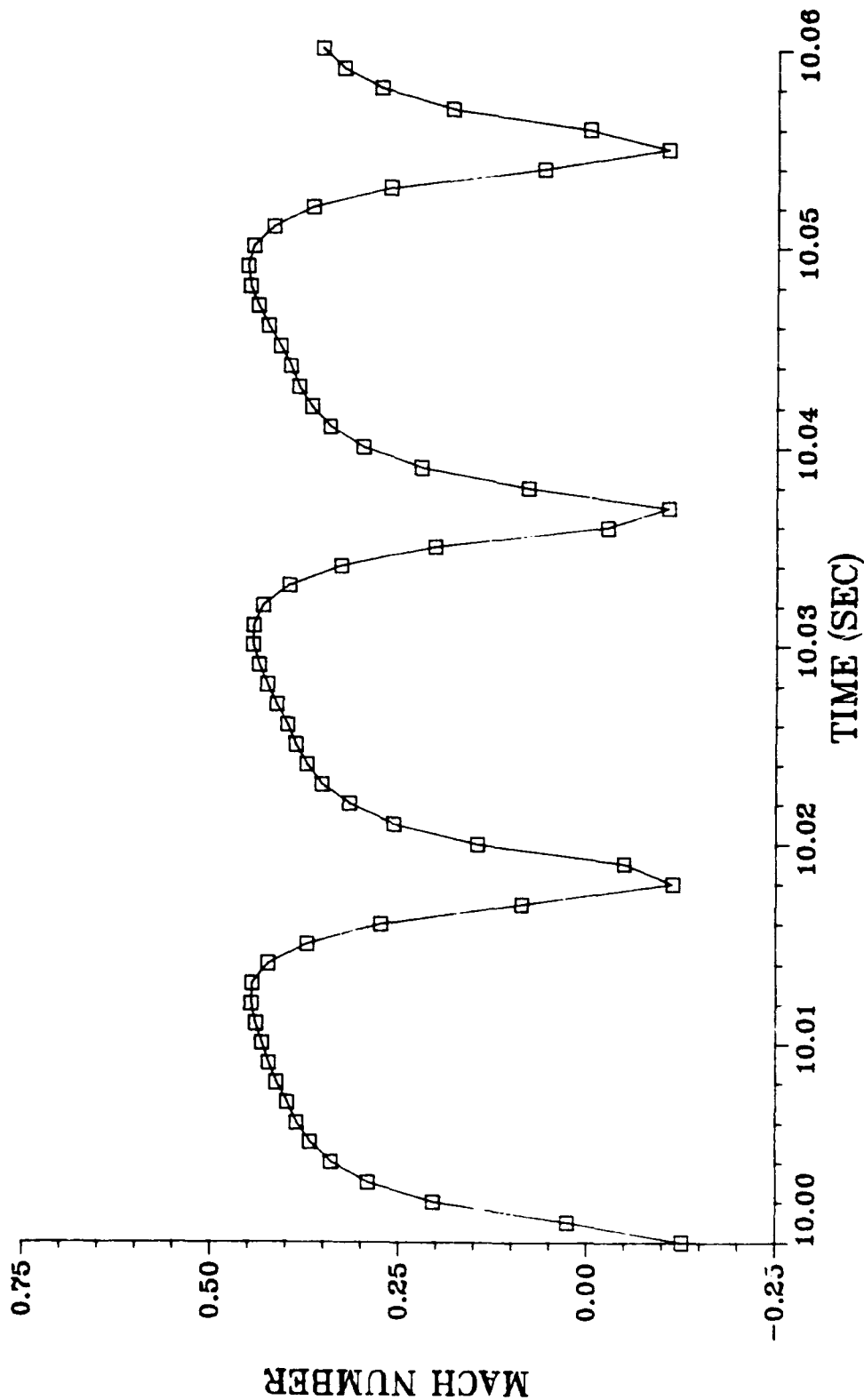


Figure 29. Rotating Stall Mach Numbers, Data Point 160

HIGH RESPONSE MACH NUMBER CALCULATIONS STATION 3.0, DATA POINT 135

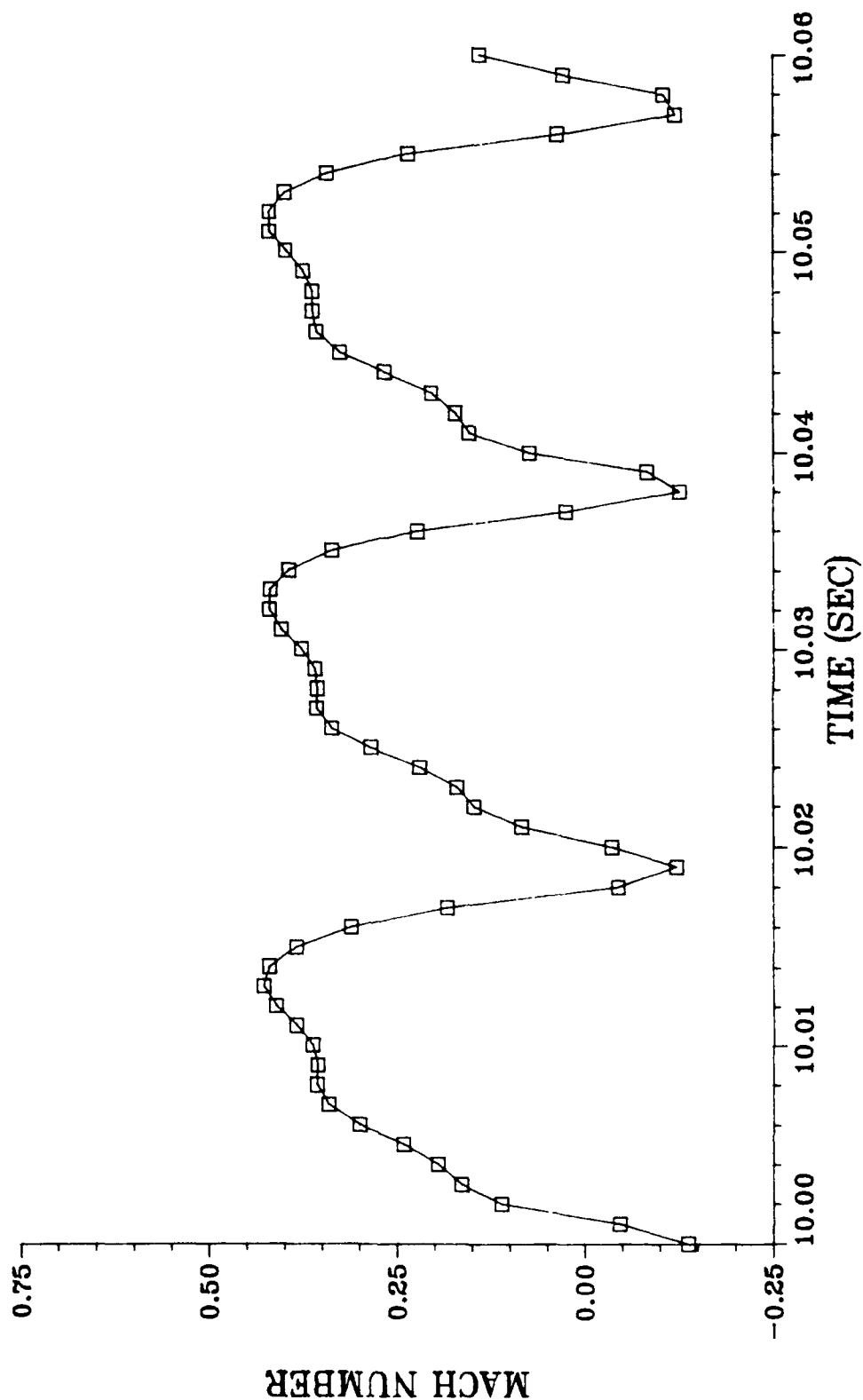


Figure 30. Rotating Stall Mach Numbers, Data Point 135

HIGH RESPONSE MACH NUMBER CALCULATIONS

STATION 3.0, DATA POINT 148

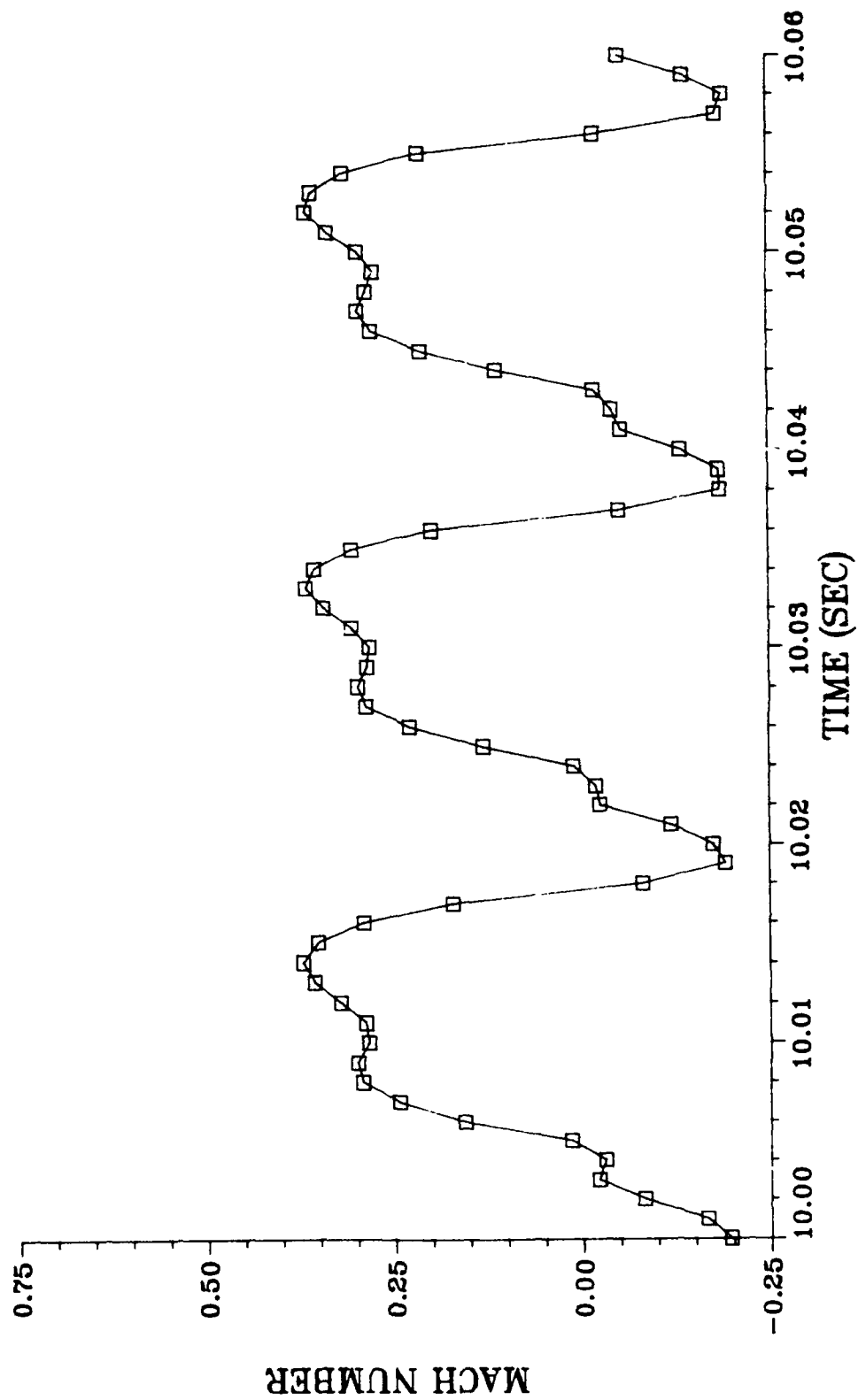


Figure 31. Rotating Stall Mach Numbers, Data Point 148

AXIAL MACH NUMBER DISTRIBUTION STATION 3.0, VARIABLE VANES NOMINAL

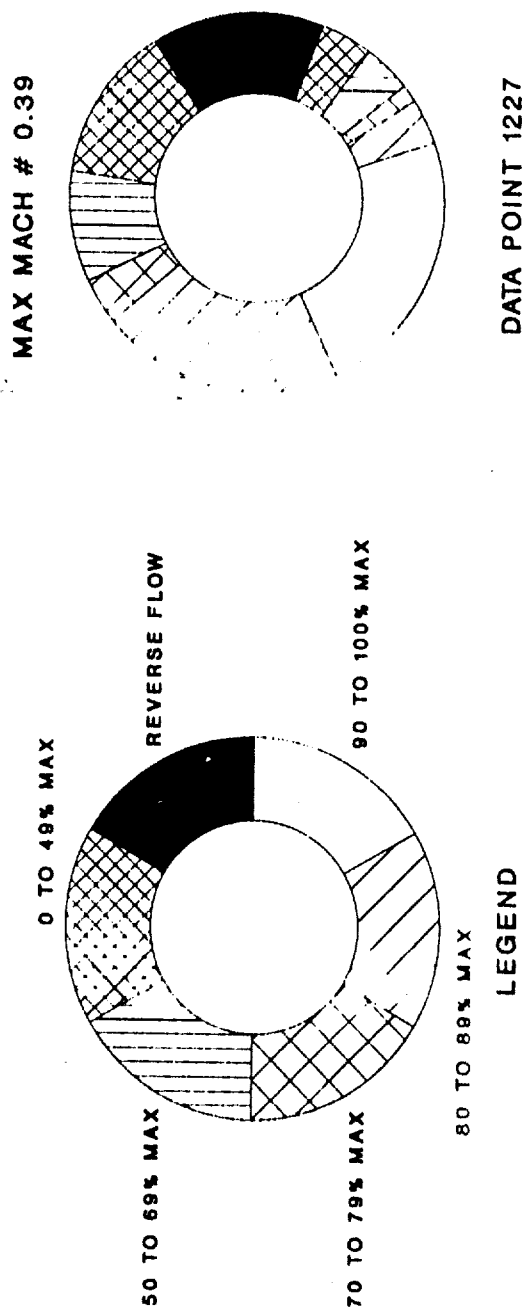


Figure 32. Station 3.0 Axial Mach Number Distributions, Data Point 1227

AXIAL MACH NUMBER DISTRIBUTION STATION 3.0, VARIABLE VANES NOMINAL

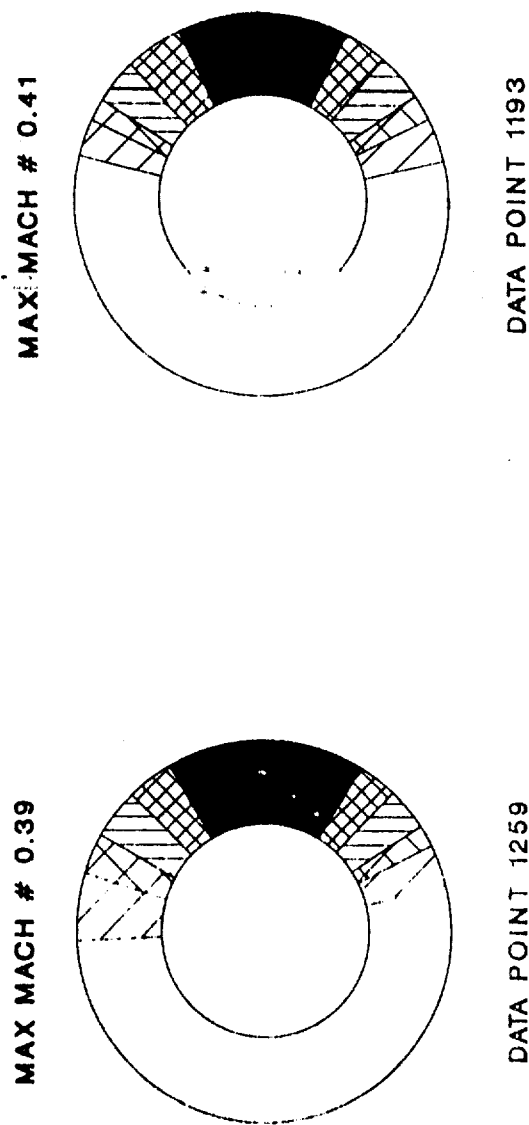
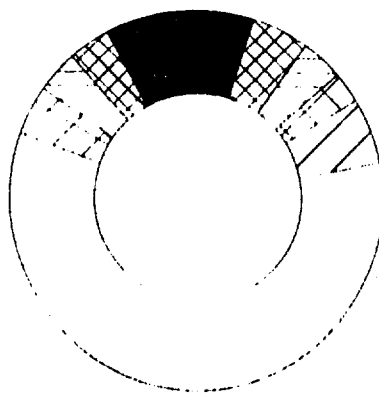


Figure 33. Station 3.0 Axial Mach Number Distributions, Data Points 1259 and 1193

AXIAL MACH NUMBER DISTRIBUTION

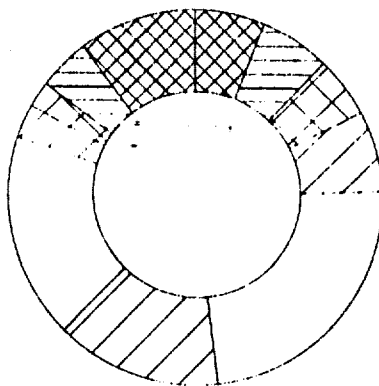
STATION 3.0, VARIABLE VANES NOMINAL

MAX MACH # 0.41



DATA POINT 1195

MAX MACH # 0.37



DATA POINT 1267

Figure 34. Station 3.0 Axial Mach Number Distributions, Data Points 1195 and 1267

AXIAL MACH NUMBER DISTRIBUTION STATION 3.0, VARIABLE VANES +7 DEGREES

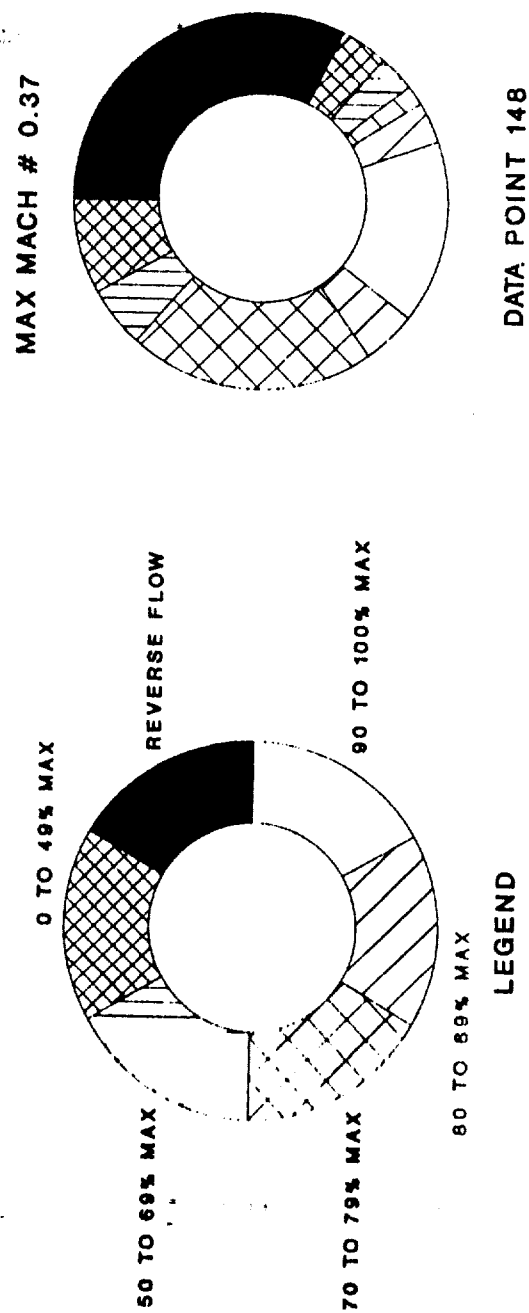
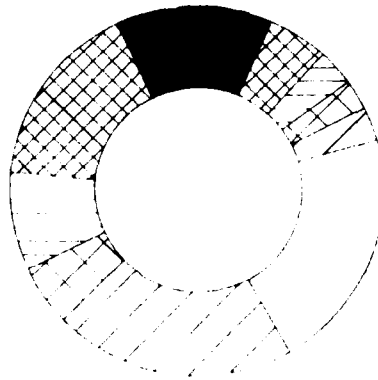


Figure 35. Station 3.0 Axial Mach Number Distributions, Data Point 148

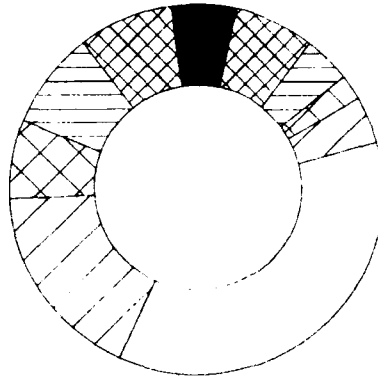
AXIAL MACH NUMBER DISTRIBUTION
STATION 3.0, VARIABLE VANES +7 DEGREES

MAX MACH # 0.43



DATA POINT 135

MAX MACH # 0.46

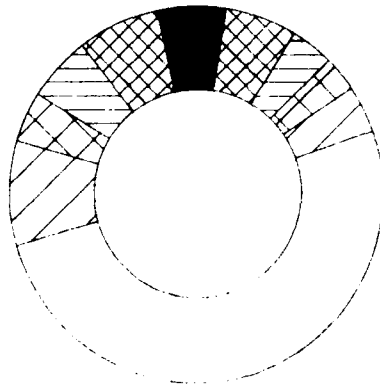


DATA POINT 160

Figure 36. Station 3.0 Axial Mach Number Distributions, Data Points 135 and 160

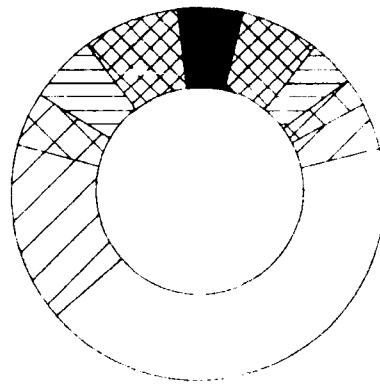
AXIAL MACH NUMBER DISTRIBUTION STATION 3.0, VARIABLE VANES +7 DEGREES

MAX MACH # .49



DATA POINT 162

MAX MACH # .45



DATA POINT 166

Figure 37. Station 3.0 Axial Mach Number Distributions, Data Points 162 and 166

VIII. DISCUSSION OF RESULTS

Analysis of the figures showing the axial Mach number distribution while operating in quasi-steady rotating stall provided many interesting insights into the rotating stall behavior of the test compressor. These figures detailed how the rotating stall cell at the compressor exit changed as a function of throttle and variable vane stagger angle setting.

Characteristic Regions and Rotating Stall Flow Zones

To organize the results of Figs. 32 to 37 and apply them to the 10th-stage in-stall pressure characteristic, the rotating stall flow was separated into four zones and the in-stall characteristic was divided into three regions.

The four flow zones were defined based on ranges of axial Mach number. Figures 22 to 31 showed that although there was a definite transition between reverse and unstalled flow, clearly defined transition zones did not exist. With the exception of operating points 1195 and 1193, the test data showed continuous changes of the axial Mach number between reverse flow and the maximum Mach number for a cycle. Because of this, rotating stall flow zone definitions based on low-speed observations [13] were not applicable. For this effort, the following arbitrary method was used to define the different rotating stall flow zones. Reverse flow was one zone, 90 to 100 percent of the maximum axial Mach number was defined the fully unstalled zone, and the leading and trailing

edge transition zones at the leading and trailing edge of the reverse flow region were made up of the remaining 0 to 89 percent of the maximum axial Mach number.

The 10th-stage in-stall pressure characteristic was divided into three regions as shown in Fig. 38. From the initial in-stall point to the point where the slope of the characteristic changed from negative to positive was defined as the negative-sloped hysteresis region. The positive sloped portion of the in-stall characteristic was defined the positive-sloped recovery region, and the region to the left of the initial in-stall point was defined as the reduced throttle region. Changes in flow zone sizes will be correlated to the specific regions on the 10th-stage characteristic.

A review of Fig. 13 shows that the 10th stage and station 3.0 were separated by the 10th stator and an axial distance with area change. Although the magnitude of Mach numbers will change between the exit of stage 10 and station 3.0, an important assumption made in this report was that the axial Mach number distribution percentages presented in Figs. 32 to 37 were constant between the two locations.

Nominal In-Stall Pressure Characteristic

Figure 39 shows the axial Mach number distribution for quasi-steady operating points 1227, 1259, 1193, 1195, and 1267. Figure 39 also shows the relative position of the operating points to on the in-stall characteristic as

TENTH STAGE PRESSURE CHARACTERISTIC VARIABLE GEOMETRY EFFECTS, 75% SPEED

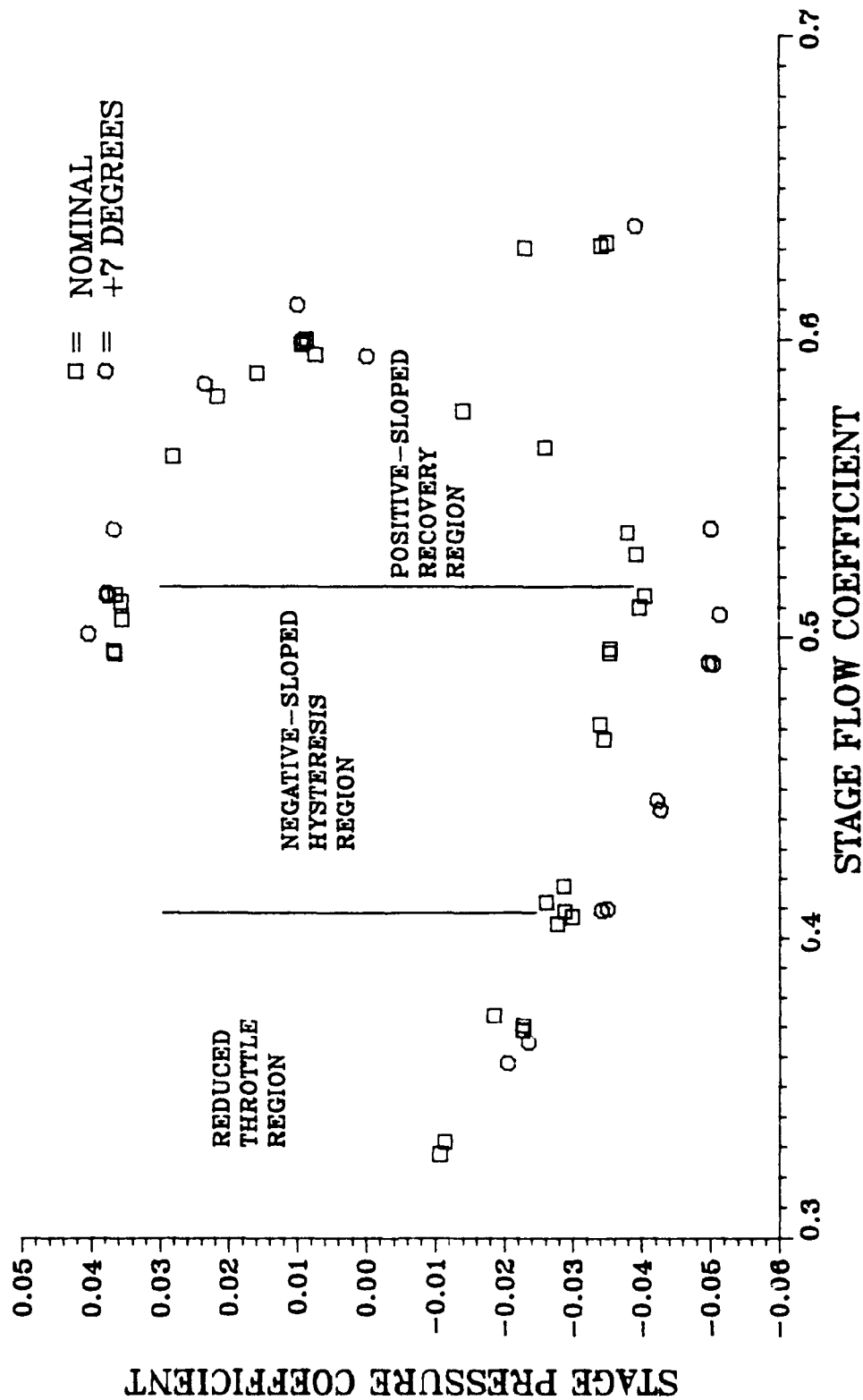


Figure 38. 10th-Stage Pressure Characteristic Regions

IN-STALL EXIT MACH DISTRIBUTION NOMINAL CONFIGURATION

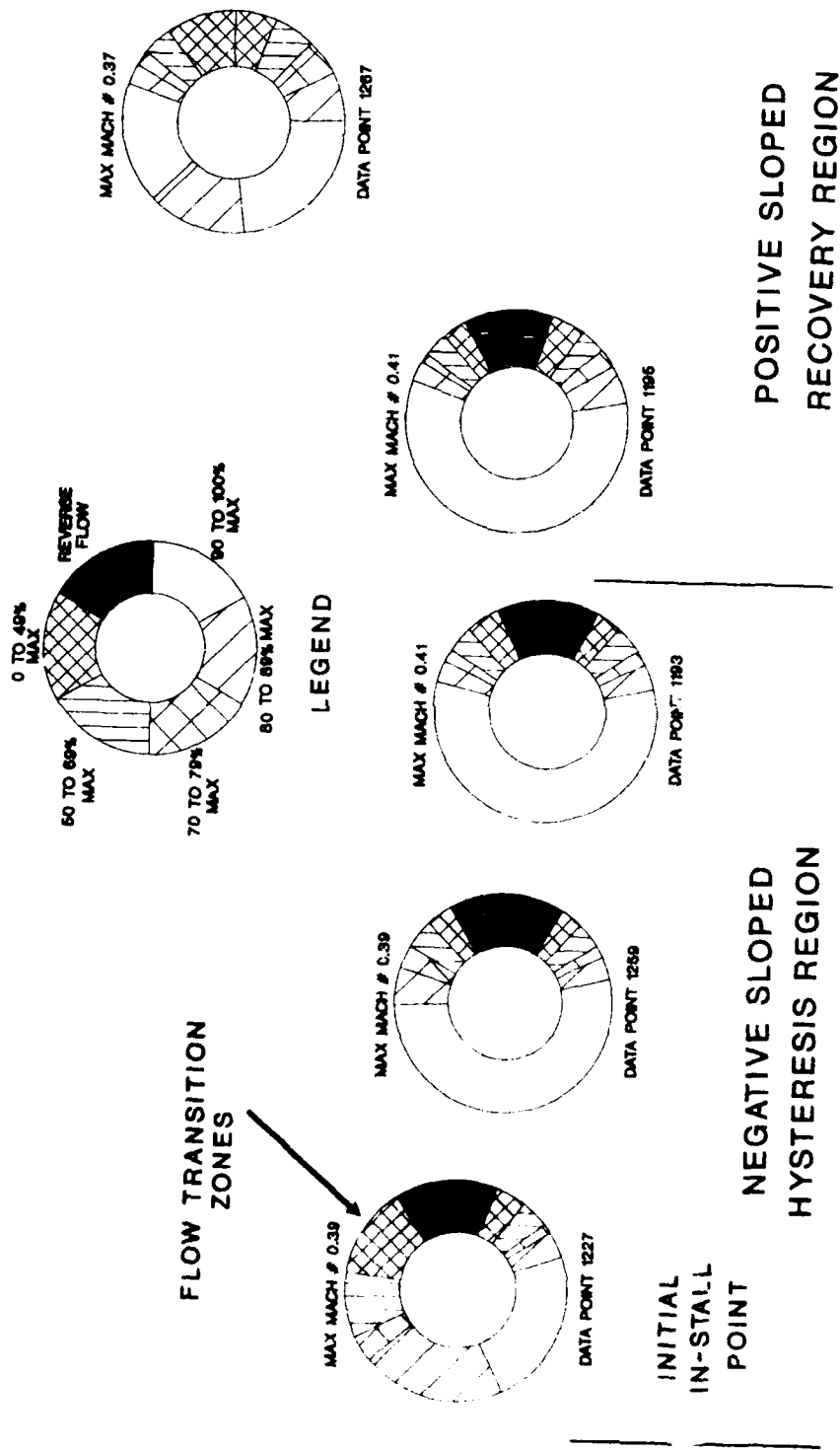


Figure 39. Nominal Pressure Characteristic Mach Number Distributions

presented in Fig. 38. These data points detail the in-stall characteristic from the initial in-stall point to the near recovery point for the variable vanes set at their nominal value.

This figure suggests that for the axial Mach number distribution in the negative-sloped hysteresis region of the in-stall characteristic, the reverse flow and leading edge transition zones were nearly constant. Table 1 shows the zone sizes for all quasi-steady operating points. The reverse flow zone in this region of the characteristic ranged from 13 to 15 percent of the compressor station 3.0 annulus. The leading edge transition zone varied from 12 to 14 percent of the compressor annulus. The trailing edge transition zone changed significantly. It ranged from a maximum value of 48 percent at the initial in-stall operating point to a minimum of 14 percent at operating point 1193. From these data, it can be concluded that changes in throttle primarily resulted in changes in the stall cell trailing edge transition zone size.

For operation in the positive-sloped recovery region of the in-stall pressure characteristic, the leading edge transition zone increased to 24 percent and the reverse flow zone disappeared. This suggested that these zones did not change until the test compressor was operating in the positive-sloped recovery region. It would appear that the

Table 1. Flow Zone Percentages

<u>OPERATING POINT</u>	<u>REVERSE FLOW ZONE</u>	<u>FULLY UNSTALLED ZONE</u>	<u>LEADING EDGE TRANSITION ZONE</u>	<u>TRAILING EDGE TRANSITION ZONE</u>
1227	15	23	13	48
1259	17	53	12	17
1193	15	58	14	14
1195	13	42	12	18
1267	0	42	20	24
148	32	16	13	39
135	13	21	14	51
160	5	36	17	41
162	5	51	17	26
166	6	43	17	35

reverse flow zone diminished along the positive sloped in-stall pressure characteristic until it no longer existed.

+7 VV In-Stall Pressure Characteristic

The axial Mach number distribution for all the +7 VV quasi-steady, in-stall operating points are presented in Fig. 40 which also shows their relative position to each other on the in-stall characteristic as presented in Fig. 38. Quasi-steady data points 135, 160, and 162, were in the negative-sloped hysteresis region. Table 1 shows the different zone sizes for the +7 VV characteristic. For operating points 160 and 162, the reverse flow zone and leading edge transition zone were constant with values of 5 and 17 percent of the CRF compressor annulus respectively. However, the initial in-stall operating point had a larger reverse flow zone of 13 percent and a slightly smaller leading edge transition zone of 14 percent. Figure 40 indicates that while operating in the negative-sloped hysteresis region of the characteristic, the trailing edge transition zone decreased in size. As the throttle was opened, this transition zone varied in size from 51 percent at data point 135 to 26 percent at data point 162.

The primary feature of the axial Mach number distribution in the reduced throttle region was a large increase in the size of the reverse flow zone from 13 percent to 32 percent of the CRF compressor annulus. The leading edge transition zone appeared to remain constant as was nearly the case for all

IN-STALL EXIT MACH DISTRIBUTION +7VV CONFIGURATION

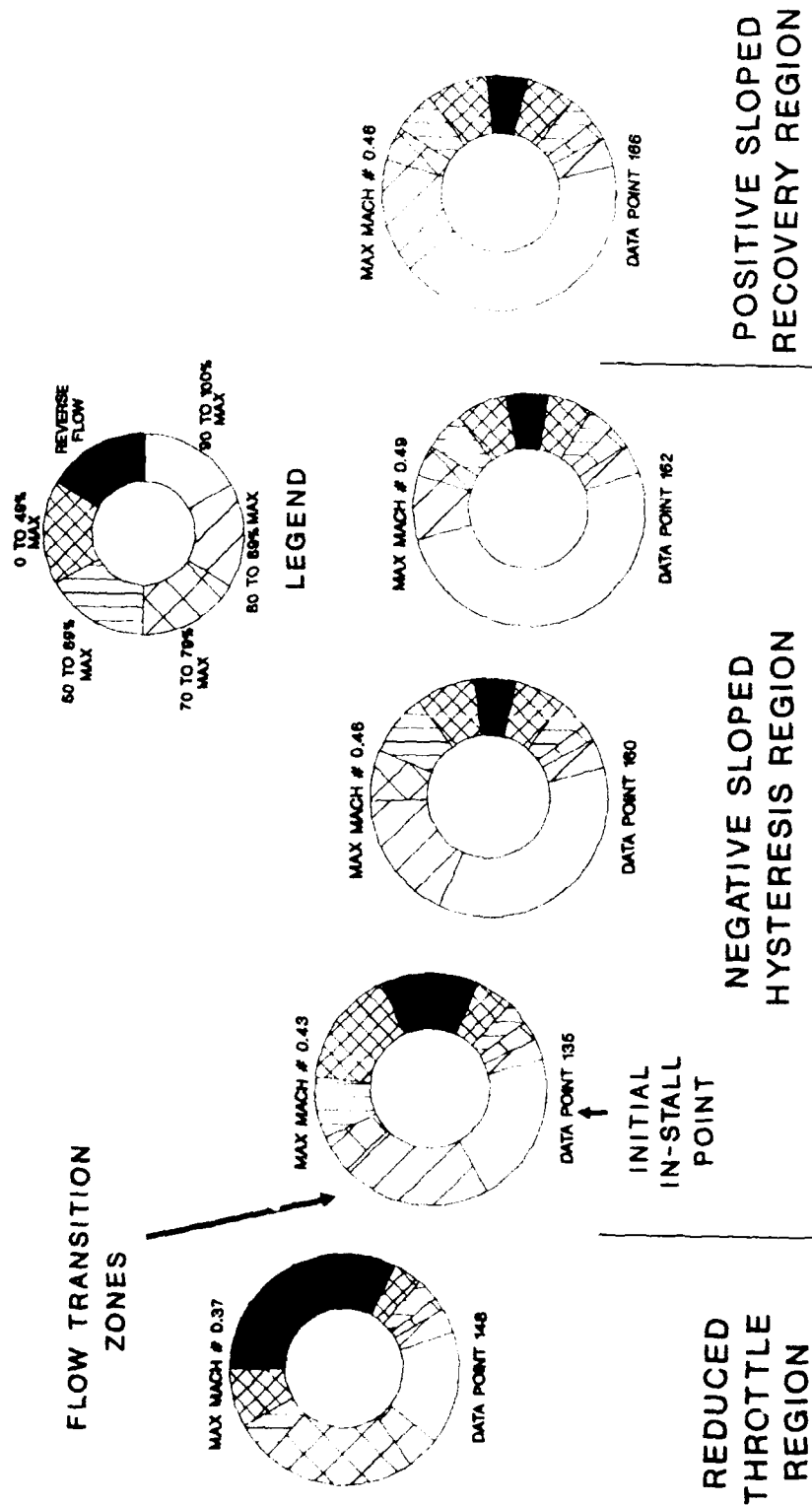


Figure 40. +7 VV Pressure Characteristic Mach Number Distributions

quasi-steady in-stall operating points. The trailing edge transition zone size decreased in the reduced throttle region from 51 percent to 39 percent.

Comparison of Nominal and +7 VV In-Install Pressure Characteristics

One purpose of this report was to understand more about the differences observed between the nominal and +7 VV 10th-stage, in-stall pressure characteristics of the CRF compressor. To help accomplish this, pairs of operating points - one nominal and one +7 VV - were digitized based on similar flow coefficients. The data chosen for comparison were in the negative-sloped hysteresis region of the in-stall pressure characteristics. It was in this region that the changes between the nominal and +7 VV characteristics were noted. As shown in Fig. 38, the pressure characteristics differed very little in the reduced throttle region.

The axial Mach number distribution for data obtained at the initial in-stall location for nominal and +7 VV configurations were nearly identical. Significant changes were not observed in the distribution of axial Mach numbers until the throttle was increased as quasi-steady operating points 1259 and 160 indicate. For operating point pairs 1259 and 160, 1193 and 162, and 1195 and 166, the reverse flow and leading edge transition zones did not vary appreciably with throttle changes but did vary with changes in variable vane

stagger angle setting. The reverse flow zone was smaller and the leading edge transition zone was slightly larger on the +7 VV in-stall pressure characteristic than on the nominal. It appeared that these changes corresponded to the divergence in the +7 VV pressure characteristic from the nominal pressure characteristic as was noted in Fig. 38. This would explain why the flow zones for the initial in-stall operating points 1227 and 135 were similar while the other pairs on the negative-sloped hysteresis region differed. This also suggests that the nominal and +7 VV data Mach number distributions at similar flow coefficients in the reduced throttle region of the in-stall pressure characteristic were alike since the in-stall characteristics were similar.

Transition Zone Ratio and Average Transition Zone Size

The control volume model [13] of Koff, Davis, and Greitzer also presented transition zones and postulated their importance in determining the rotating stall operation of a multistage, low-speed, axial-flow compressor. A few principles and conclusions of the Koff control volume model are presented below and compared to the data presented in this report.

1. The change in axial velocity divided by blade speed (C_x/U) from the fully stalled to unstalled flow was defined to exist in transition zones.

2. Transition zones were assumed constant for a given speed line, and the amount of stalled or unstalled flow changed along the speedline.
3. As the ratio of leading edge to trailing edge transition zone ratio (T_{TE}/T_{LE}) increased, the pressure coefficient decreased for a constant average transition zone size.
4. As the average transition zone size $[(T_{TE} + T_{LE})/2]$ increased, the pressure coefficient increased for a constant T_{TE}/T_{LE} ratio.

Although the model of reference 13 was presented for a multistage compressor, the above principles will be applied to the observed 10th-stage behavior of the test compressor.

When comparing the results of the test compressor with the control volume model, it is important to remember that the transition zones in the test compressor were based on Mach number ranges while those defined in [13] were based on C_x/U . The main difference between these two definitions was that a transition zone based on Mach number does not include the effects of temperature variations in the annulus during rotating stall operation.

The control volume model assumed that T_{TE}/T_{LE} and T_{avg} were constant for a given speed line. The authors of [13] stated that these assumptions were based on very limited data. Data obtained from the test compressor showed that T_{TE}/T_{LE} and T_{avg} defined by Mach number distributions did change along a speed line. Table 2 presents values of T_{TE}/T_{LE} and T_{avg} for all quasi-steady in-stall operating points analyzed in this report. For

Table 2. TTE/TLE and Tavg for Nominal and
+7 VV Operating Points

OPERATING POINT	TTE/TLE	Tavg (%)
1227	3.7	30.5
1259	1.4	14.5
1193	1.0	14.0
1195	0.7	15.0
148	3.0	26.0
135	3.6	32.5
160	2.4	29.0
162	1.5	21.5
166	2.1	26.0

the nominal in-stall pressure characteristic, T_{avg} varied from 30.5 percent to 14 percent of the compressor station 3.0 annulus and T_{TE}/T_{LE} varied from 3.7 to 0.7. On the +7 VV characteristic, T_{avg} ranged from 32.5 percent to 21.5 percent of the compressor annulus and T_{TE}/T_{LE} changed from 3.6 to 1.5.

The control volume model predicted that for a constant T_{avg} , as the ratio T_{TE}/T_{LE} increased, the in-stall pressure characteristic dropped to a lower pressure coefficient level. When T_{TE}/T_{LE} was held constant and T_{avg} decreased, the in-stall pressure characteristic decreased. Since both T_{TE}/T_{LE} and T_{avg} changed between the nominal and +7 VV in-stall pressure characteristics, comparisons of these predictions could not be made. However, if T_{avg} were assumed constant, the trend of a lower pressure characteristic with increases in T_{TE}/T_{LE} would be seen in the data analyzed.

Such differences between the control volume model and the test compressor may be explained in different ways. One possible reason is the difference in transition zone definitions. As explained above, the transition zones of [13] were based on velocities and were clearly discernable. The transition zones of the test compressor were arbitrarily chosen based on axial Mach number ranges due to the continuous changes observed in the rotating stall cell. However, it does not seem that this would cause such large differences as those observed between the test compressor and the control volume

model. A more likely reason was that the test compressor was a high-speed, high-pressure-rise, 10-stage compressor and the control volume model was based on low-speed, low-pressure-rise compressor observations. As discussed in the literature review, many differences have been observed between the two types of compressors.

The quasi-steady, in-stall operating points of the negative-sloped hysteresis region gave some insights into how the pressure coefficient of the nominal and +7 VV in-stall characteristic varied as T_{TE}/T_{LE} and T_{avg} changed. Comparing the initial in-stall operating points (135 and 1227) showed that T_{TE}/T_{LE} and T_{avg} were almost the same for both operating points (see Table 2). This is why the difference in pressure coefficient was small between these two operating points.

Analysis of all other nominal and +7 VV quasi-steady, in-stall operating points in the negative-sloped hysteresis region showed that differences in T_{TE}/T_{LE} and T_{avg} resulted in different values of pressure coefficient for a similar flow coefficient. Table 2 shows that T_{TE}/T_{LE} and T_{avg} were greater for the +7 VV in-stall characteristic compared to the nominal characteristic at similar flow coefficients.

These results indicated that the lower in-stall pressure coefficients of the +7 VV characteristic corresponded to increased values of T_{TE}/T_{LE} and T_{avg} . Although the assumptions and predictions of the Koff control volume appear not to agree

with the 10th-stage test compressor data, the idea that transition zones are an important part of determining the pressure coefficient was observed and is very significant.

Application of Results to the Extended Starting Theory and Recovery

In the extended starting theory [17] presented in Section II, O'Brien and Boyer stated that rotating stall flow patterns in the extended starting region (see Fig. 10) were characterized by stalled front stages, choked or otherwise blocked rear stages, and recovery hysteresis. From the results of this report, it appears that the negative-sloped hysteresis region shown in Figs. 39 and 40 can describe the rotating stall flow associated with recovery hysteresis in the extended starting region. Figures 39 and 40 suggest that recovery hysteresis and reverse flow in the stall cell are related. The positive-sloped recovery region described in this section shows that as the amount of reverse flow in the compressor annulus is reduced, the stage will begin to recover. From a recovery viewpoint, the smaller the negative sloped hysteresis region of the compressor, the easier the compressor will recover.

Studies on compressor recovery [13] have shown that install characteristics with higher pressure coefficients and a positive slope improve the recoverability of a compressor. For this test compressor, increasing the variable vane stagger

angle 7° resulted in a lower in-stall 10th-stage pressure characteristic which hindered recovery. It would be very beneficial to observe the in-stall pressure characteristic response to decreasing the variable vane stagger angle. Unfortunately, due to time constraints, this was not done during the CRF test.

IX. SUMMARY AND CONCLUSIONS

As the demands on gas turbine engines used in high-performance aircraft increase, the ability to understand and predict off-design operation encountered by the compressors of these engines has become very important. Because of the recoverability problems associated with rotating stall, much attention has been given to this area of off-design research.

The majority of models developed to understand rotating stall cells and in-stall characteristics are based on low-speed, low-pressure-rise, 1-to-5-stage compressor experimental data. These models have provided some important insights into rotating stall cells, but have not been able to explain very well the rotating stall operation of high-speed, multistage compressors.

This report has analyzed data from a high-speed, 10-stage compressor in an effort to better understand rotating stall operation in high-speed, multistage compressors. High-response pressure measurements taken at the exit of the CRF compressor in analog form were digitized and calibrated to give the total and static pressures for different discharge throttle and variable vane settings. These pressures were used to calculate and show the axial Mach number distributions associated with rotating stall operation. Observations made from figures showing the axial Mach number distribution at the

compressor exit were then compared with the most recent rotating stall theories; namely, the control volume model [13] and extended starting theory [17].

From the test compressor data analyzed in this report, some interesting and important qualitative insights have been gained about rotating stall cells and in-stall characteristics. Conclusions made from this analysis are presented below.

1. Significant transition zones were found to exist at the exit of the test compressor during rotating stall operation, and these transition zones were related to the in-stall pressure coefficient of the compressor. The change in in-stall characteristic observed by Copenhaver [3] was real and was accompanied by a change T_{TE}/T_{LE} and T_{avg} as defined in Section VIII.

2. The in-stall pressure characteristic was separated into three regions: the reduced throttle region, the negative-sloped hysteresis region, and the positive-sloped recovery region. The rotating stall flow was divided into four zones based on axial Mach number: the reverse flow zone, the fully unstalled zone, and leading and trailing edge transition zones.

The reduced throttle region was characterized by large amounts of reverse flow, and the negative-sloped hysteresis region by a constant reverse flow zone and leading edge

transition zone. The trailing edge transition zone decreased in this region as the flow coefficient increased. In the positive-sloped recovery region, the reverse flow zone disappeared.

3. The control volume model does not appear to apply to the 10th stage of the test compressor. The transition zones of the control volume model were easily defined while those of the test compressor were not. Both T_{TE}/T_{LE} and T_{avg} increased as the pressure coefficient decreased whereas the control volume model predicted T_{avg} to decrease as the pressure coefficient decreased. Furthermore, T_{TE}/T_{LE} and T_{avg} were not constant for a given speedline as assumed in the control volume model, but varied with discharge throttle setting. The control volume model did state the importance of transition zones in determining the in-stall pressure coefficient which was validated from the test compressor data.

4. Results from this report support the extended starting theory. This report suggests that a compressor operating in the extended starting region operates on the negative-sloped hysteresis region of its in-stall characteristic. Furthermore, the smaller the negative-sloped hysteresis region of the in-stall characteristic, the smaller the extended starting region.

5. Results of the CRF test showed that increasing the stagger angle of the variable vanes drove the 10th stage to

lower values of pressure coefficient. For a similar flow coefficient, a decrease in pressure coefficient was accompanied by a increase in T_{TE}/T_{LE} and T_{avg} .

X. RECOMMENDATIONS

From the results and insights gained on rotating stall behavior of the 10th stage of the CRF compressor, the following recommendations are made.

1. To obtain an even more thorough understanding of the trends in axial Mach number distribution along the different in-stall characteristic regions of the 10th stage, additional quasi-steady data points should be digitized. Figure 18 shows that operating points are available that would give additional information at each in-stall pressure characteristic region.

2. Another interesting possibility which was not possible in the CRF test is to obtain data which can be used to show if and how the axial Mach number distribution changes from hub to tip in a high-speed, multistage, axial-flow compressor. Additional insights into the effect of transition zones may be obtained from a spanwise analysis.

3. It is recommended that a study be carried out to investigate any axial variations in the rotating stall cell of the test compressor. When the variable vane stagger angle was increased, the stage-10 in-stall characteristic changed significantly, the stage-9 in-stall characteristic changed only slightly, and stages 4 through 8 in-stall characteristic did not change at all. This suggests that there were axial variations in T_{TE}/T_{LE} and T_{avg} .

4. More high-speed, multistage compressor tests similar to that of the test compressor should be carried out. In addition, to better understand rotating stall flows, intra-stage measurements should be made in these future tests. This would allow general features of rotating stall operation in all high-speed, multistage compressors to be investigated.

5. During other high-speed, multistage compressor tests, variable vanes should be closed as well as opened so that knowledge about variable vane effects on recoverability may be increased.

6. From the results of the CRF compressor test and future tests, a model using the control volume principles based on T_{TE}/T_{LE} and T_{avg} should be developed that attempts predict in-stall characteristics of high-speed, multistage compressors.

REFERENCES

1. Copenhaver, W. W. "Stage Effect on Stalling and Recovery of a Ten-Stage Axial-Flow Compressor." Ph.d. Dissertation, Iowa State University, October 1988.
2. Cohen, H., G.F. Rogers, and H.I. Saravanamuttoo. Gas Turbine Theory, 3rd ed. New York: John Wiley & Sons, 1987.
3. Copenhaver, W. W and T. H. Okiishi. "Rotating Stall and Recoverability of a High-Speed Ten-Stage Axial-Flow Compressor." Presented at the AIAA/SAE/ASME/ASEE 25 Joint Propulsion Conference, AIAA-89-2684, July 1989.
4. Davis, M. W. and W. F. O'Brien. "A Stage-By-Stage Post-Stall Compression System Modeling Technique." Presented at the AIAA/ASME/SAE/ASEE 23 Joint Propulsion Conference, AIAA-87-2088, June 1987.
5. Boyer, K. M. and W. F. O'Brien. "Model Predictions for Improved Recoverability of a Multistage Axial-Flow Compressor." Presented at the AIAA/ASME/SAE/ASEE Joint Propulsion Conference, AIAA-89-2687, July 1989.
6. Emmons, H. W., C. E. Pearson, and H. P. Grant. "Compressor Surge and Stall Propagation." Transactions of the ASME 77 (May 1955): 455-469
7. Stenning, A. H. and A. R. Kriebel. "Stall Propagation in a Cascade of Airfoils." Trans. A. S. M. S., 88 (1958): 777.
8. Fabri, J. "Rotating Stall In Axial-Flow Compressors." Symposium on Turbomachinery, Cambridge, 1967. Published by International Aerodynamics (Turbomachinery), 1970.
9. Day, I. J. and N. A. Cumpsty. "The Measurement and Interpretation of Flow Within Rotating Stall Cells in Axial Compressors". Journal of Mechanical Engineering Science 20, no. 2 (1978): 101-114.
10. Pearson, J. "Wakes in Axial Compressors." Journal of the Royal Aeronautical Society, 63 (July 1963): 415-416.

11. Day, I. J., E. M. Greitzer, and N. A. Cumpsty. "Prediction of Compressor Performance in Rotating Stall." Transactions of the ASME, Journal of Engineering for Power, 100 (January 1978): 1-14.
12. Das, D. K. and H. K. Jaing. "An Experimental Study of Rotating Stall in a Multistage Axial-Flow Compressor." Transactions of the ASME, Journal of Engineering for Power, 106 (July 1984): 542-551.
13. Koff, S. G., R. E. Davis, and E. M. Greitzer. "A Control Volume Model of Rotating Stall in Multistage Axial Compressors." Presented at the AIAA/SAE/ASME/ASEE 23 Joint Propulsion Conference, AIAA-87-2088, June 1987.
14. Small, C. J. and J. T. Lewis. "High Speed Compressor Rig as a Stall Recovery Research Tool." Presented at the AIAA/ASME/SAE/ASEE 21 Joint Propulsion Conference, AIAA-85-1428, June 1985.
15. Johnson, I. A. and R. O. Bullock, ed. Aerodynamic Design of Axial-Flow Compressor. Vol. 13, Compressor Operation with One or More Blade Rows Stalled, by W. A. Benser. Washington: NASA SP-36, 1965.
16. Hosney, W. M. and W. G. Steenken. "Aerodynamic Instability Performance of an Advanced High-Pressure-Ratio Compression Component." Presented at the AIAA/ASME/SAE/ASEE 22 Joint Propulsion Conference, AIAA-86-1619, June 1986.
17. O'Brien, W. F. and K. M. Boyer. "Stall and Recovery in Multistage Axial-Flow Compressors." Presented at the 74 Specialists' Meeting of the Propulsion and Energetics Panel on Unsteady Aerodynamic Phenomena in Turbomachines, AGARD Paper 74 A-26, August 1989.
18. Bendat, J. S. and A. G. Piersol. RANDOM DATA: Analysis and Measurement Procedures. New York: John Wiley & Sons, 1971.
19. Zucrow, M. J. and J. D. Hoffman. Gas Dynamics, Volume 1. New York: John Wiley & Sons, 1976.
20. Na'covska', K. "Temperature Rise in the Multistage Axial Flow Compressor During Rotating Stall and Surge." ASME paper 88-GT-323, 1988.

21. Copenhaver, W. W. and C. J. Worland. "Acquisition of Unsteady Pressure Measurements from a High-Speed Multistage Compressor." ASME paper 88-GT-189, 1989.
22. Abernathy, R. B. and J. W. Thompson Jr. "Handbook Uncertainty in Gas Turbine Measurements." AEDC-TR-73-5, February 1973.

APPENDIX A: COMPRESSOR RESEARCH FACILITY DESCRIPTION

Appendix A presents the buildings and rooms comprising the CRF in Fig. A-1 and the test chamber in Fig. A-2. The operation of the CRF is also explained.

A layout of the buildings and rooms comprising the CRF is provided in Fig. A-1. The test building housed the computer and test article control systems, the operations building contained the test chamber and signal conditioning rooms, and the electrical power conditioning equipment was located in the electrical power conditioning building.

The CRF test was controlled from the facility control room. Commands to carry out the test plan were sent from the control room via a monitor computer to four control computers located in the computer room. The control computers provided input to the electrical power conditioning equipment which operated the drive motors. The control computer also controlled hardware that supported the variable geometry devices of the CRF test compressor.

The CRF compressor was mounted in a 20.0-ft (6.096-m) diameter test chamber as shown in Fig. A-2. Filtered air was drawn from the atmosphere into the test chamber plenum through five inlet control valves. Flow conditioning elements were mounted in the plenum to reduce free stream turbulence intensity to levels below 1 percent. The air was discharged from the test compressor exit throttling valve to the atmosphere through a discharge collector and discharge ducting as shown in Figs. A-1 and A-2.

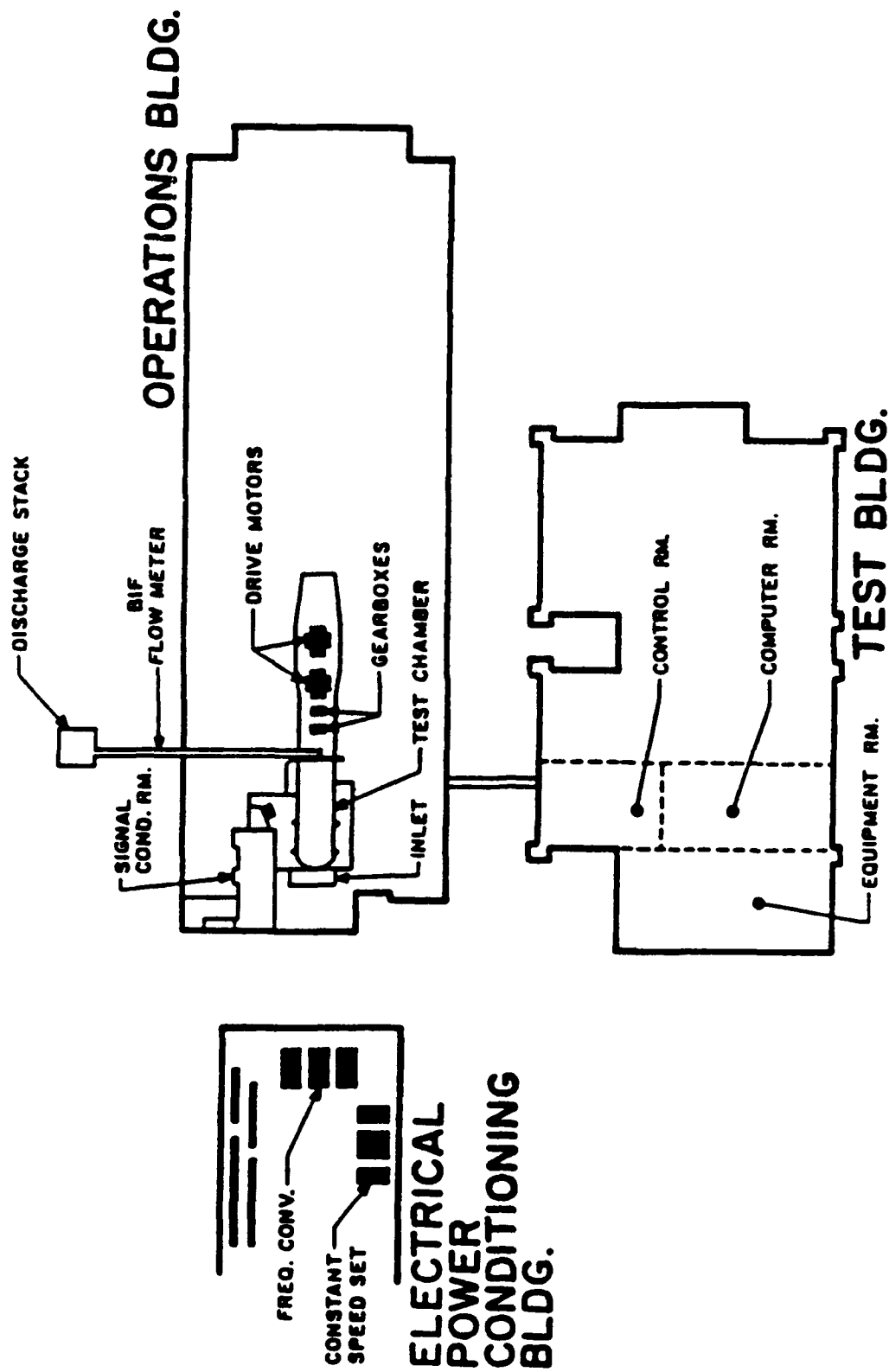


Figure A-1. Compressor Research Facility

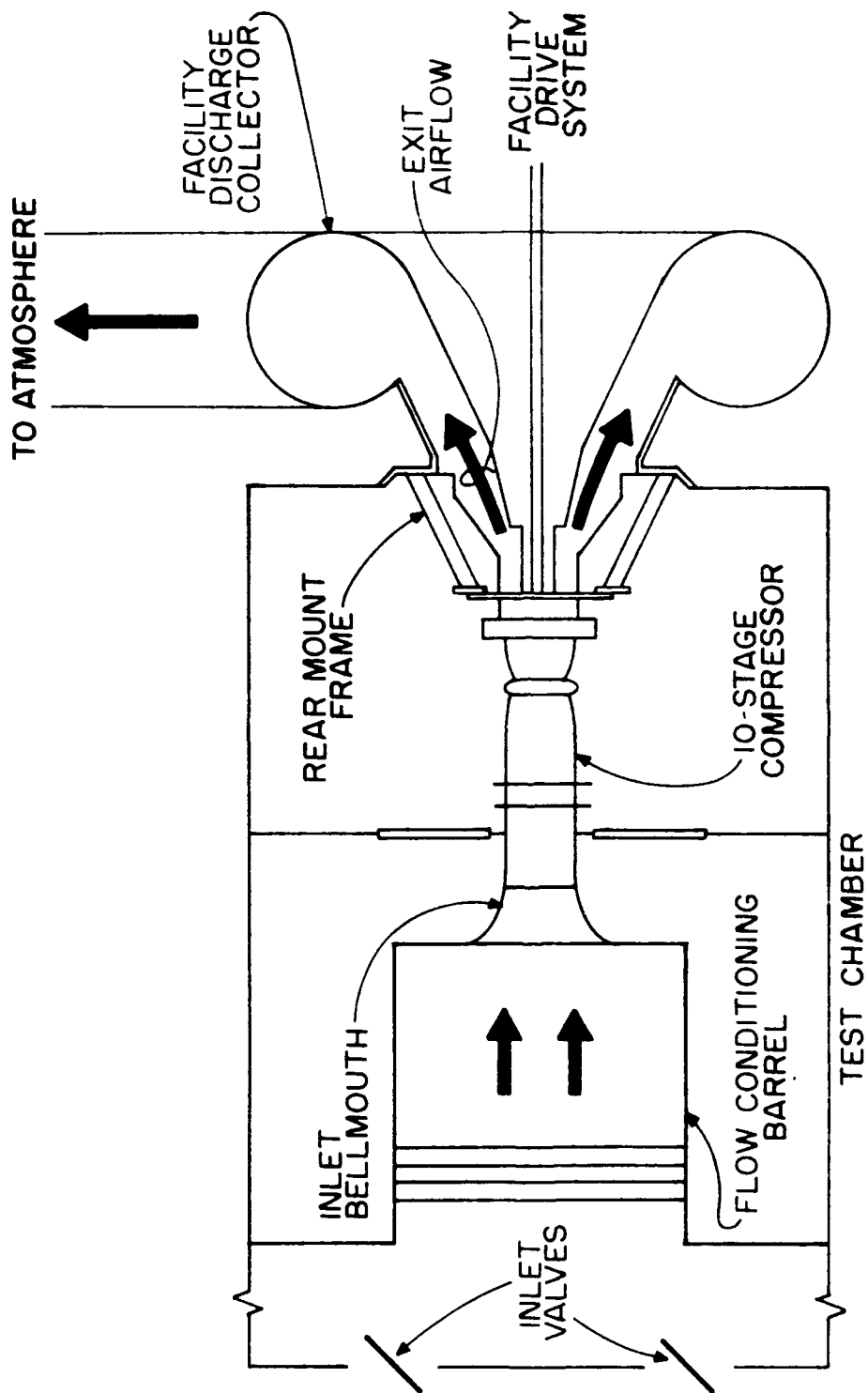


Figure A-2. CRF Test Chamber

APPENDIX B: DATA ACQUISITION METHODS

Details of the high-response and time-averaged data acquisition methods are presented in Appendix B. A schematic of the high-response data acquisition system is provided in Fig. B-1. Measurement uncertainty is also addressed.

Three different data acquisition methods were used to measure performance during the CRF compressor test: high-response, close-coupled, and time-averaged. Data acquired from high-response and time-averaged measurement methods were used in this report and will be described in the present section.

High-Response Pressure Measurements

High-response measurements were used to analyze unsteady pressure variations observed during compressor in-stall operation. These channels had a nominal frequency response of 200 Hz which gave an accurate representation of the in-stall pressure fluctuations.

A schematic of the high-response data acquisition system is provided in Fig. B-1. The high-response data were acquired in analog form and stored on tape through Frequency Modulated (FM) recording of the voltages. Kulite (model XCQ-150) transducers were used to convert the pressures to voltages. These transducers were cooled with a cooling jacket to improve their durability and stability. Because of the high-response transducer sensitivity to temperature changes, special conditioning and recording methods were used to assure data integrity.

The transducer signals were amplified by Pacific (model #8255) signal conditioners. The signal conditioners provided the excitation voltage to the pressure transducers along with

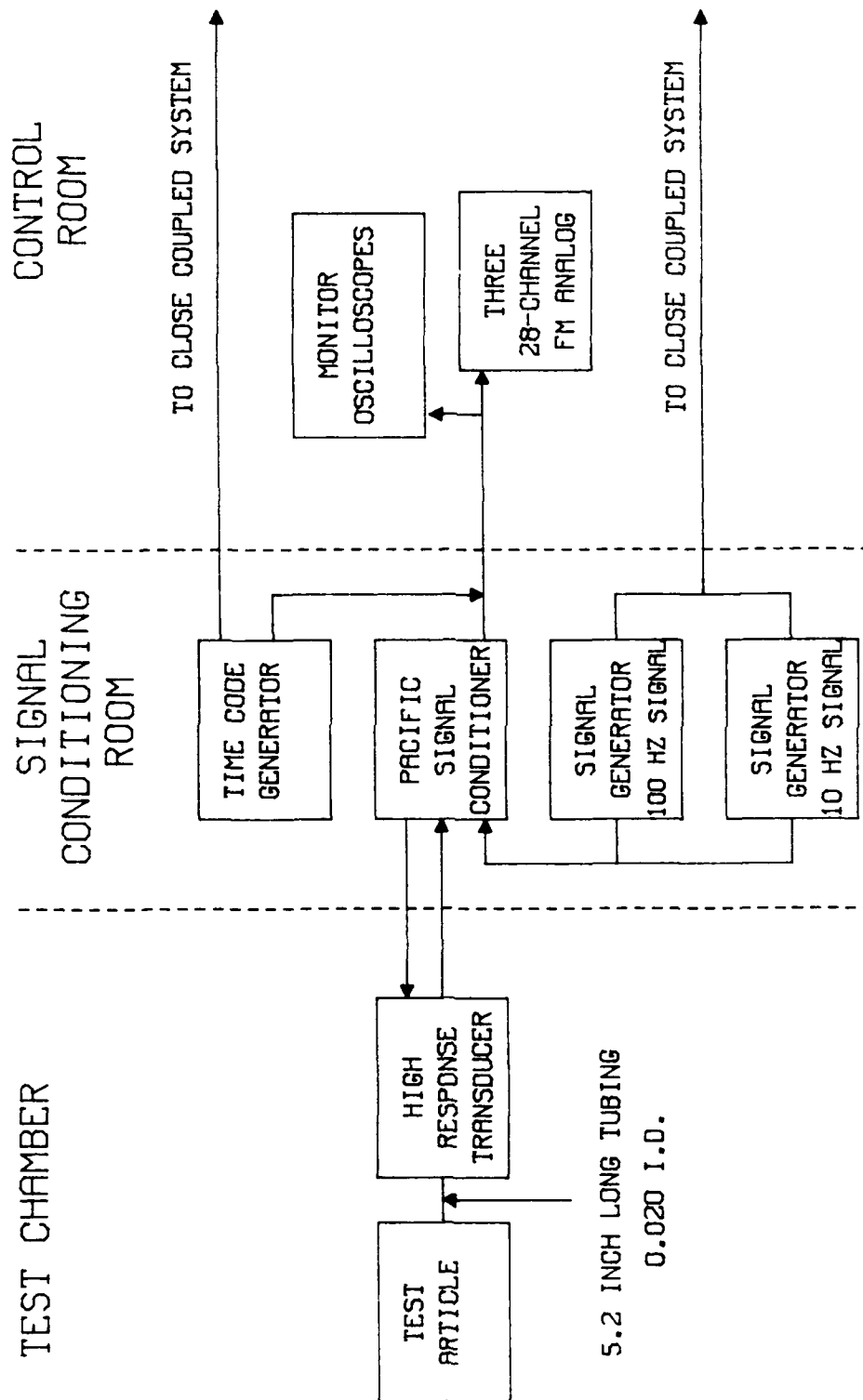


Figure B-1. High-Response Data Acquisition System

output signal filtering and amplification during high-response pressure measurements. The transducer output was filtered by a two-pole Bessel filter with a -3dB attenuation at the cutoff frequency of 1 kHz. This assured that the desired frequency response of 200 Hz was obtained with a minimal attenuation of the high-response channels. Further details concerning the data acquisition system used during the CRF test, as well as a discussion on phase shift were presented by Copenhaver and Worland [21]. The signal conditioners were also DC coupled which allowed the DC component of the pressure measurement to be calibrated with a known steady-state pressure. This method (detailed in Sections VI and VII) was used to obtain absolute transient pressure levels used in the analysis of test results.

The high-response data were recorded on three 28-channel tape recorders (Datatype model #2808). The data were recorded at a center frequency of 75.6 kHz with a deviation adjusted to allow a maximum input signal level of 5 volts. Each high-response channel was assigned to one track of the recorder. When phase correlation was required, data from the necessary channels were placed on the same tape drive head stack.

At startup and shutdown on each test day, the CRF compressor was brought to a fixed speed and pressure ratio. At this checkpoint, the DC output levels of the high-response pressure transducers were recorded and used to monitor the

stability of the transducers. Transducer instability was not found to be a factor during the CRF compressor test. Another reason for daily checking of the transducers was that the transducers required for the higher frequency response were fragile and not best suited for the test environment. The checkpoints allowed faulty transducers to be logged and replaced if possible.

Time-Averaged Pressure Measurements

The time-averaged measurements were used to characterize the steady unstalled and quasi-steady in-stall compressor performance. Time-averaged data were acquired through real-time digitization of measurement voltages and recorded on digital tape. The close-coupled and time-averaged pressure measurements used the same transducers, signal conditioners, and recording techniques. The difference in the two methods was the number of scans taken to make up the measurement and the rate of data acquisition.

The digital data acquisition method used Scanivalve model ZOC-14 (Zero-Operate-Calibrate) pressure transducers. These transducers were maintained at 70° F (21.11° C) with a closed loop cooling system to control calibration, zero offset, and sensitivity stability. The transducers were rugged and well suited for the test environment.

Pressure transducer signals were input to a Preston (model 8300-XWBRC) amplifier in order to increase the ratio of

signal-to-line noise from the amplifiers to the analog-to-digital (A/D) converters. Each amplifier used a three-pole Butterworth-Thomson filter with selectable cutoff frequencies [21]. For time-averaged data, the Butterworth-Thomson filters were set at 10-Hz. The 10-Hz setting was the minimum available and eliminated 60-Hz noise as a possible erroneous signal.

A time-averaged measurement was defined as the average of 30 samples of each channel taken sequentially at the maximum rate possible. The time to obtain these 30 samples was 195 ms. The frequency response of the time-averaged system was limited by the on-line digitizing rate and the tube length between the pressure port and transducer.

Measurement Uncertainty

The method used to determine measurement uncertainties was defined by Abernathy and Thompson [22]. Bias and precision errors were combined using the equation

$$U_m = +(B_m + t_{95}S_m) \quad (5)$$

where

B_m = bias errors base on calibration of time-averaged measurements,

S_m = precision errors associated with the transducer, signal conditioning, and recording devices,

$t_{.95}$ = student T distribution weighting factor based on the number of samples taken to make up a measurement average.

For the 30 samples averaged to make a time-averaged measurement, $t_{.95}$ was set at 2. The resulting time-averaged measurement uncertainties were calculated as ± 0.5 psi for pressure and $\pm 1.0^\circ$ for temperature measurements.

Steady and Quasi-Steady Performance Mapping

The time-averaged performance of the CRF compressor was determined for unstalled (steady) and in-stall (quasi-steady) operating conditions from the time-averaged data acquisition method described in this section. Time averaged measurements were obtained to characterize the test compressor's overall performance as well as the performance of each of its 10 stages at different compressor operating conditions. To assure that the test compressor had reached steady-state or quasi-steady-state equilibrium, a 3-minute delay was imposed after changing the operating condition of the compressor before the time-averaged measurements were taken.

Time-Resolved Performance Data

During the CRF compressor test, high-response measurements were gathered at all times. This was done by

continuously recording the high-response measurements on the analog tape recorders described earlier in this section. The time-resolved data recorded during unstalled compressor operation were used in the high-response measurement calibration procedure defined in Section VII. This allowed calibrated values to be calculated for the high-response measurements taken during in-stall compressor operation.

APPENDIX C: TEST COMPRESSOR PRESSURE CHARACTERISTIC
LEAST-SQUARE CURVE FITS

The plots of nominal and +7 VV pressure characteristic least-square curve fits referenced in Section V and used to calculate Fig. 17 are presented in Figs. C-1 to C-10.

TENTH STAGE PRESSURE CHARACTERISTICS
VARIABLE GEOMETRY EFFECTS, SPEED = 75%

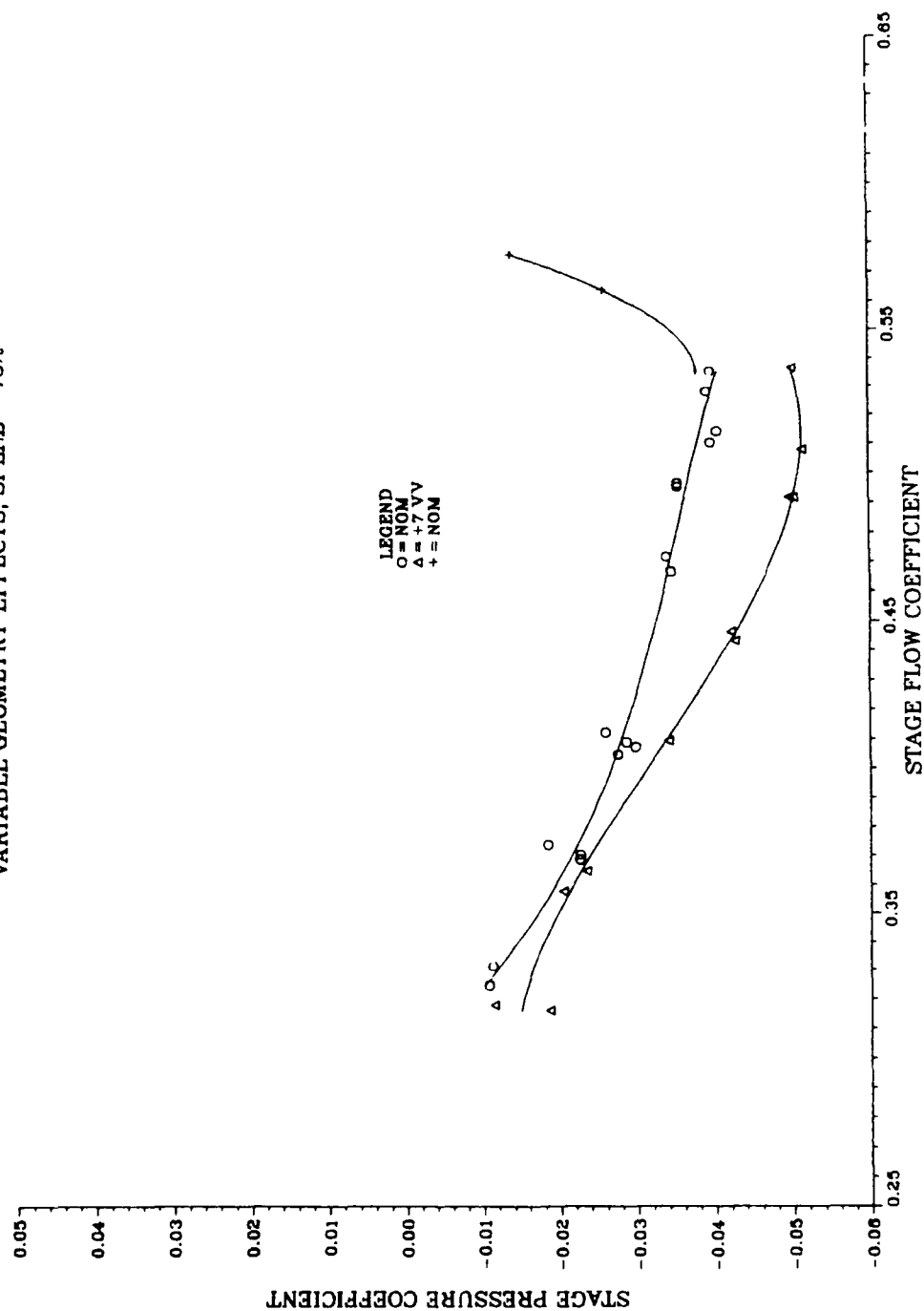


Figure C-1. 10th-Stage Pressure Characteristic Least-Square Curve Fits

NINTH STAGE PRESSURE CHARACTERISTICS
VARIABLE GEOMETRY EFFECTS

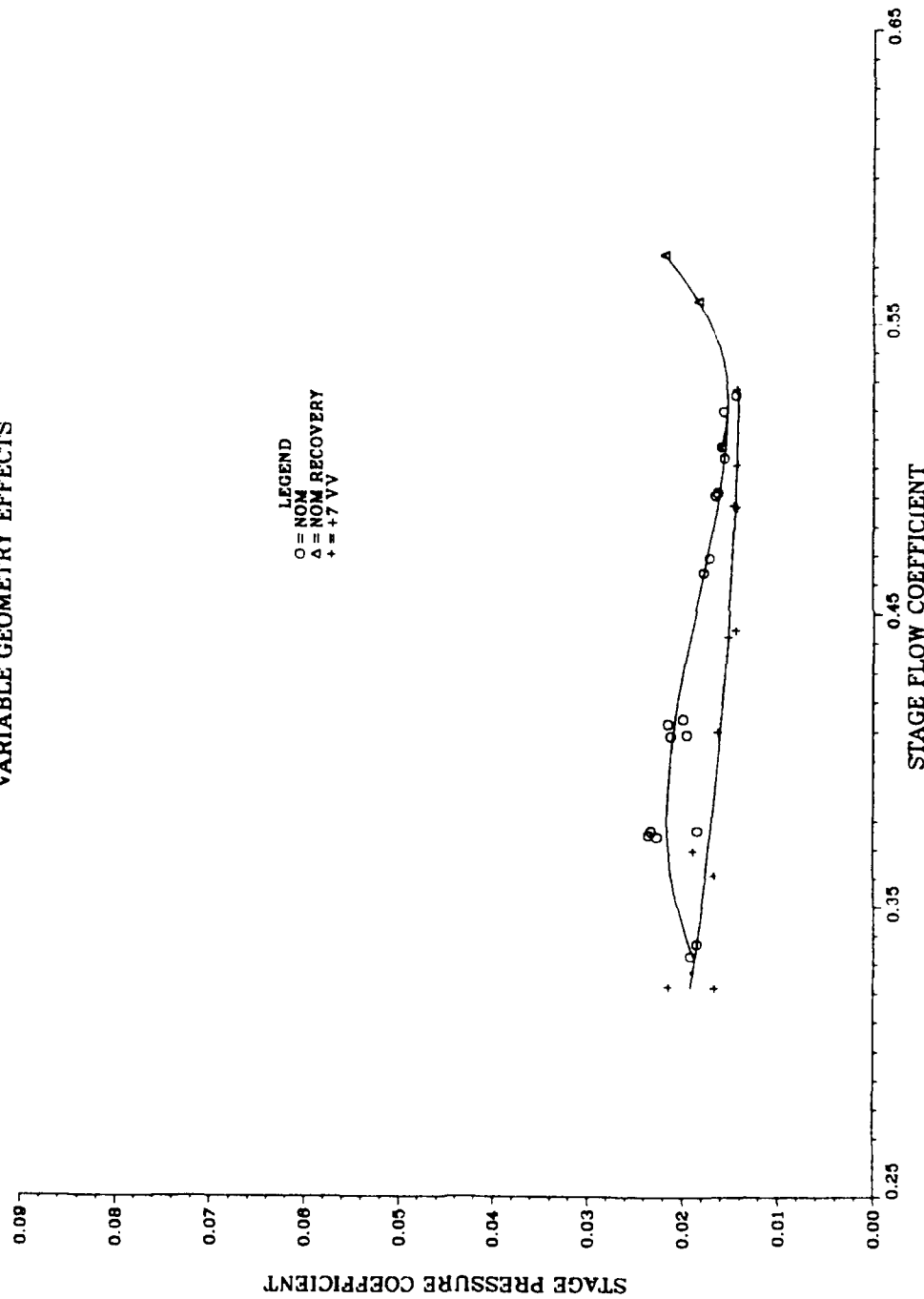


Figure C-2. 9th-Stage Pressure Characteristic Least-Square Curve Fits

EIGHTH STAGE PRESSURE COEFFICIENTS VARIABLE GEOMETRY EFFECTS

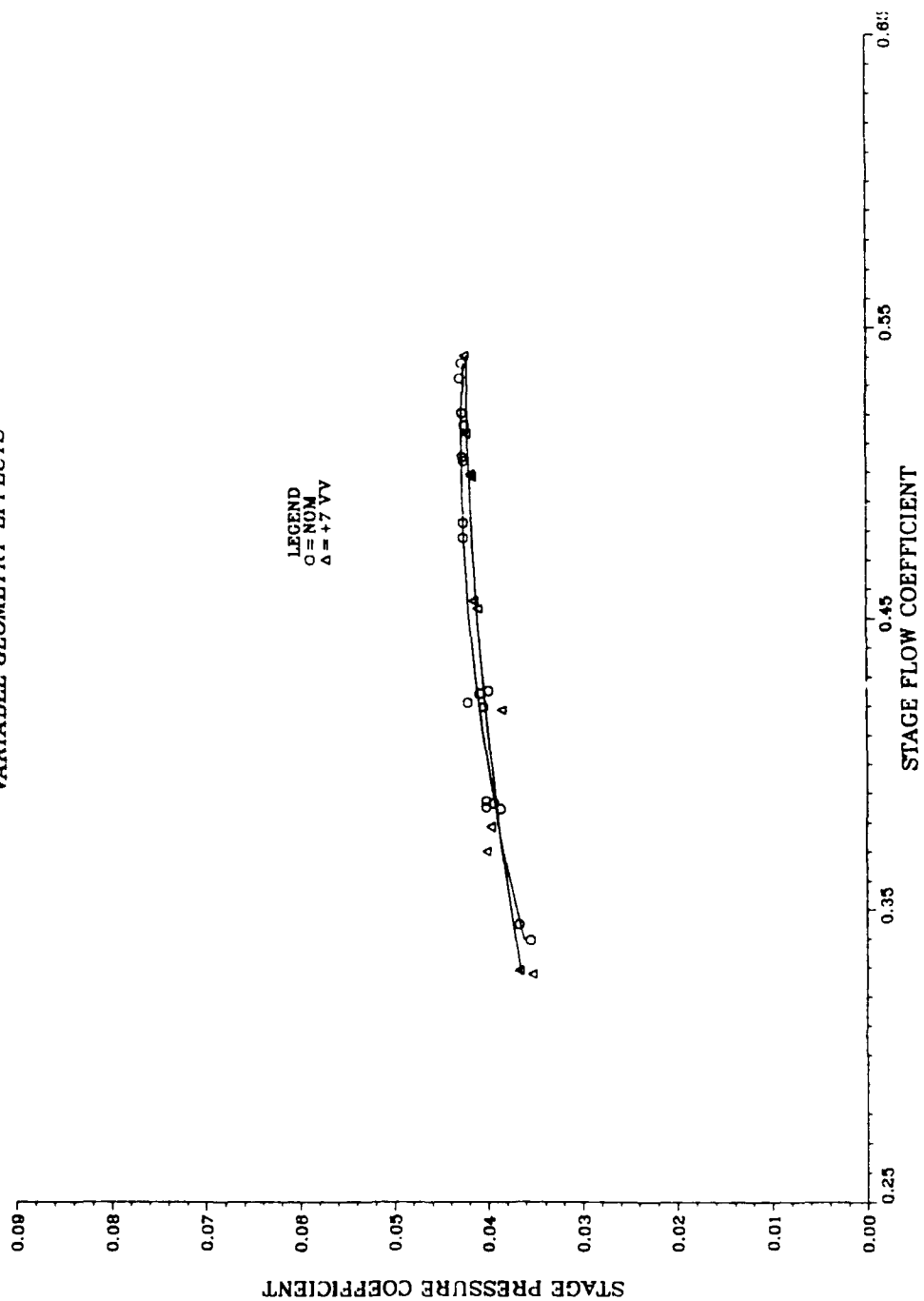


Figure C-3. 8th-Stage Pressure Characteristic Least-Square Curve Fits

SEVENTH STAGE PRESSURE CHARACTERISTICS
VARIABLE GEOMETRY EFFECTS, SPEED = 75%

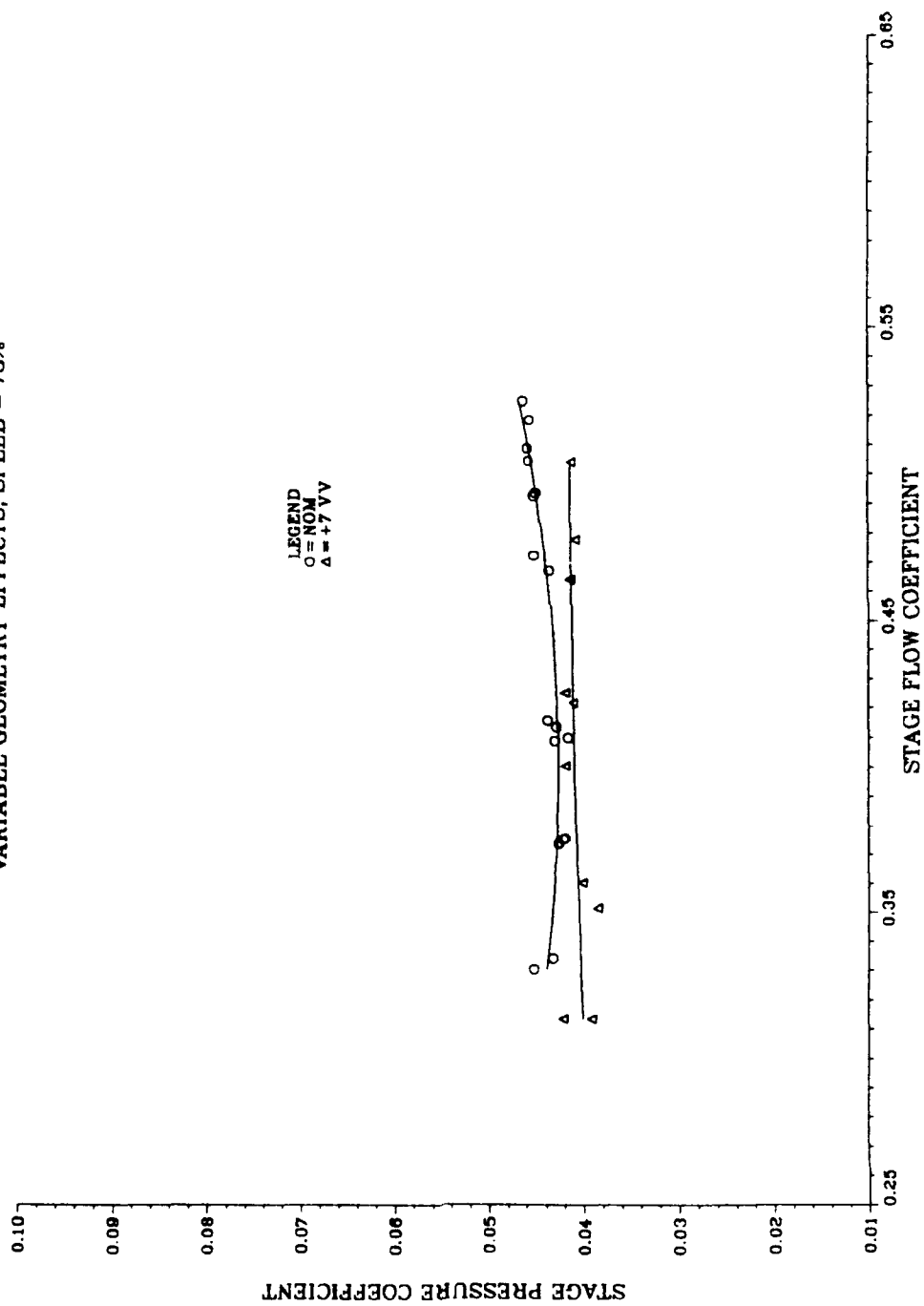


Figure C-4. 7th-Stage Pressure Characteristic Least-Square Curve Fits

SIXTH STAGE PRESSURE CHARACTERISTICS
VARIABLE GEOMETRY EFFECTS, SPEED = 75%

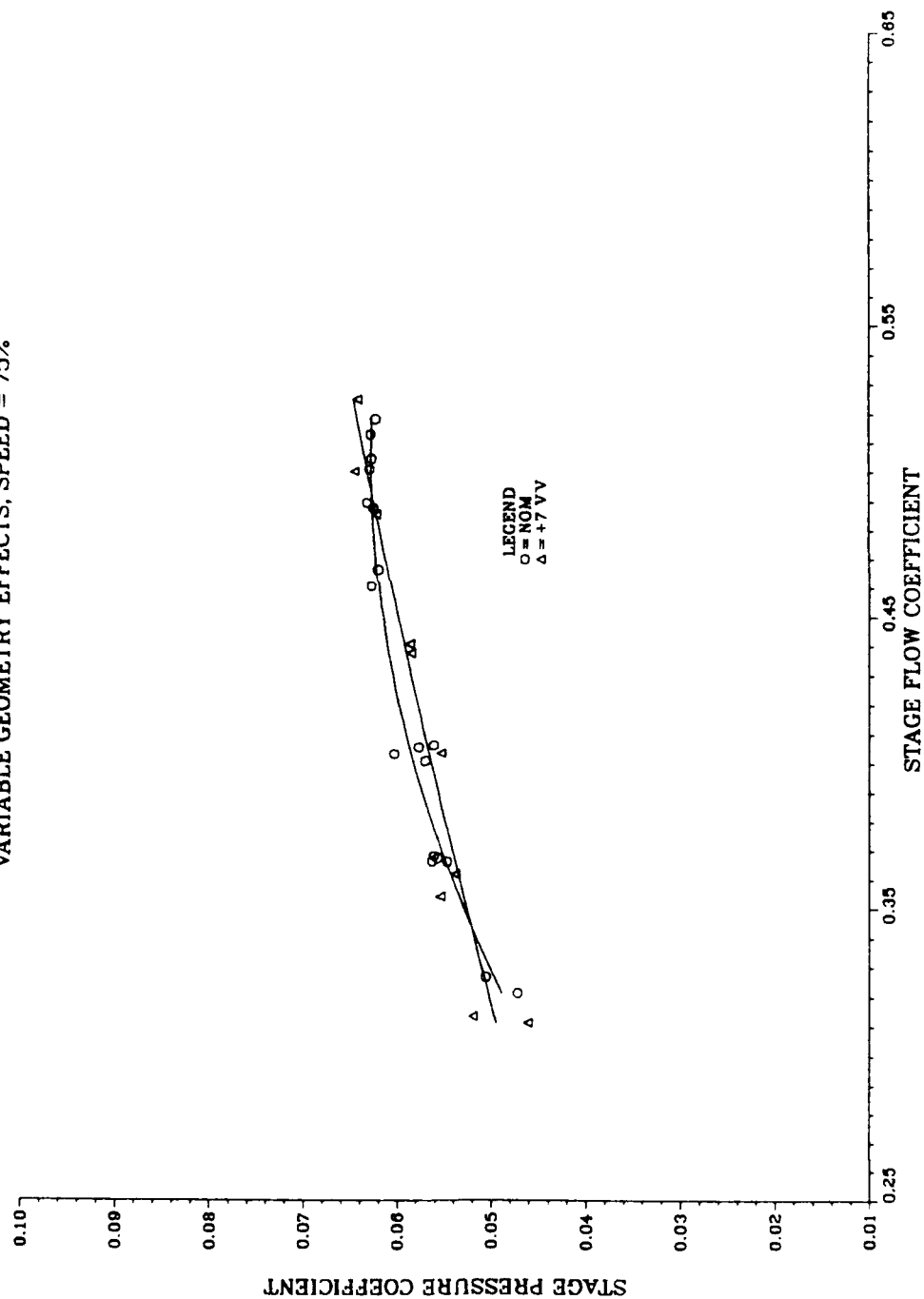


Figure C-5. 6th-Stage Pressure Characteristic Least-Square Curve Fits

FIFTH STAGE PRESSURE CHARACTERISTICS
VARIABLE GEOMETRY EFFECTS, SPEED = 75%

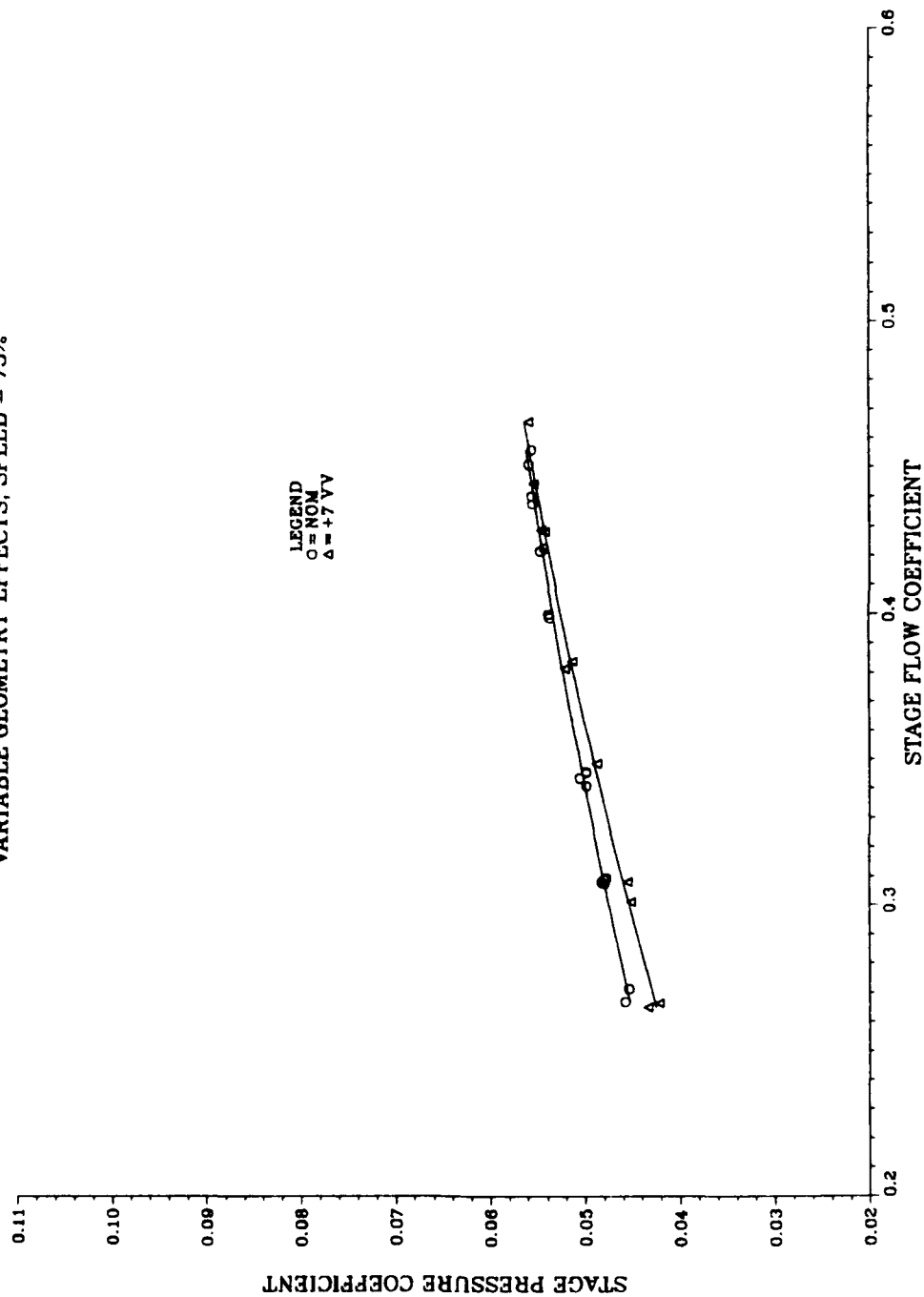


Figure C-6. 5th-Stage Pressure Characteristic Least-Square Curve Fits

FOURTH STAGE PRESSURE CHARACTERISTICS
VARIABLE GEOMETRY EFFECTS, SPEED = 75%

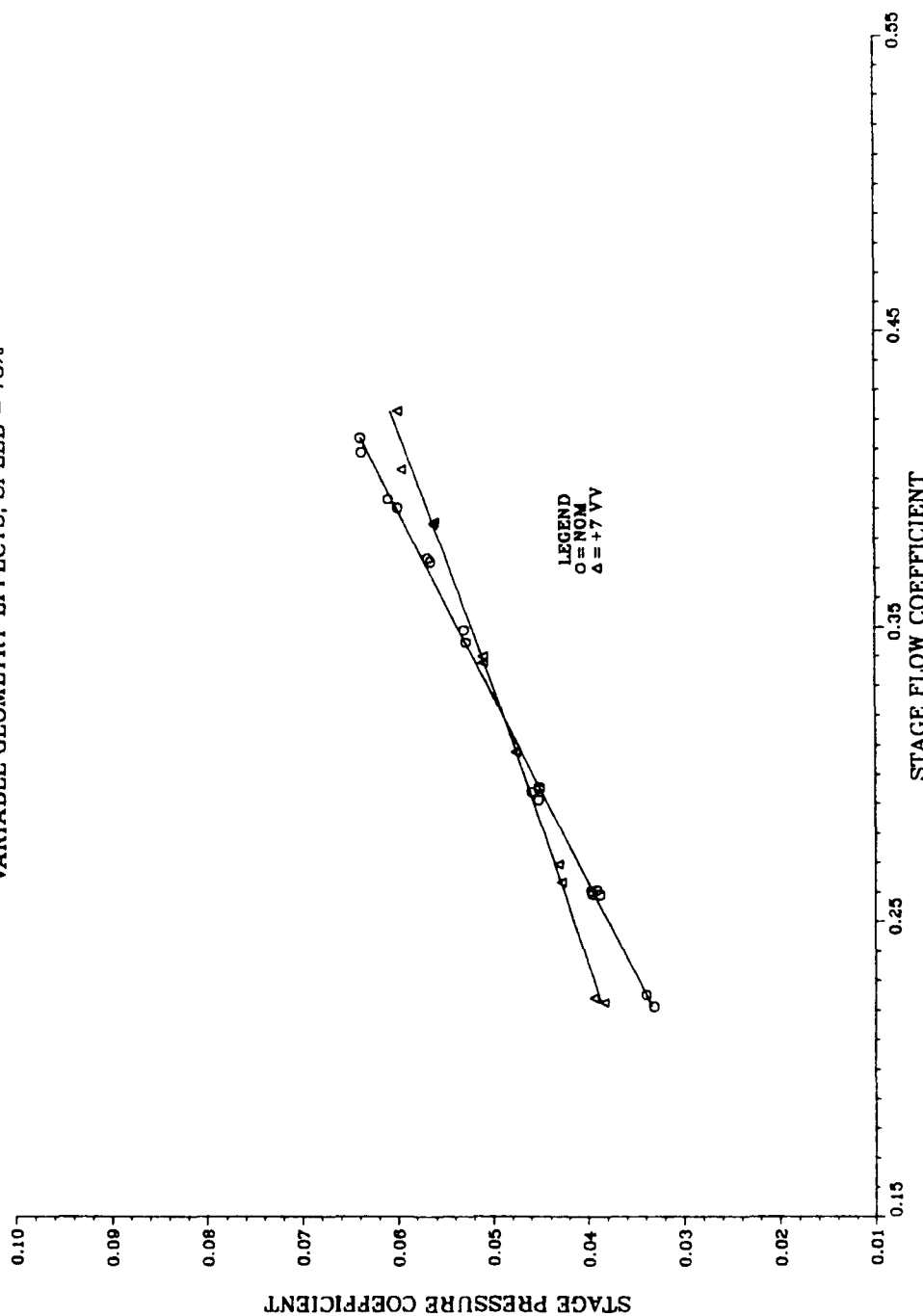


Figure C-7. 4th-Stage Pressure Characteristic Least-Square Curve Fits

THIRD STAGE PRESSURE CHARACTERISTICS
VARIABLE GEOMETRY EFFECTS, SPEED = 75%

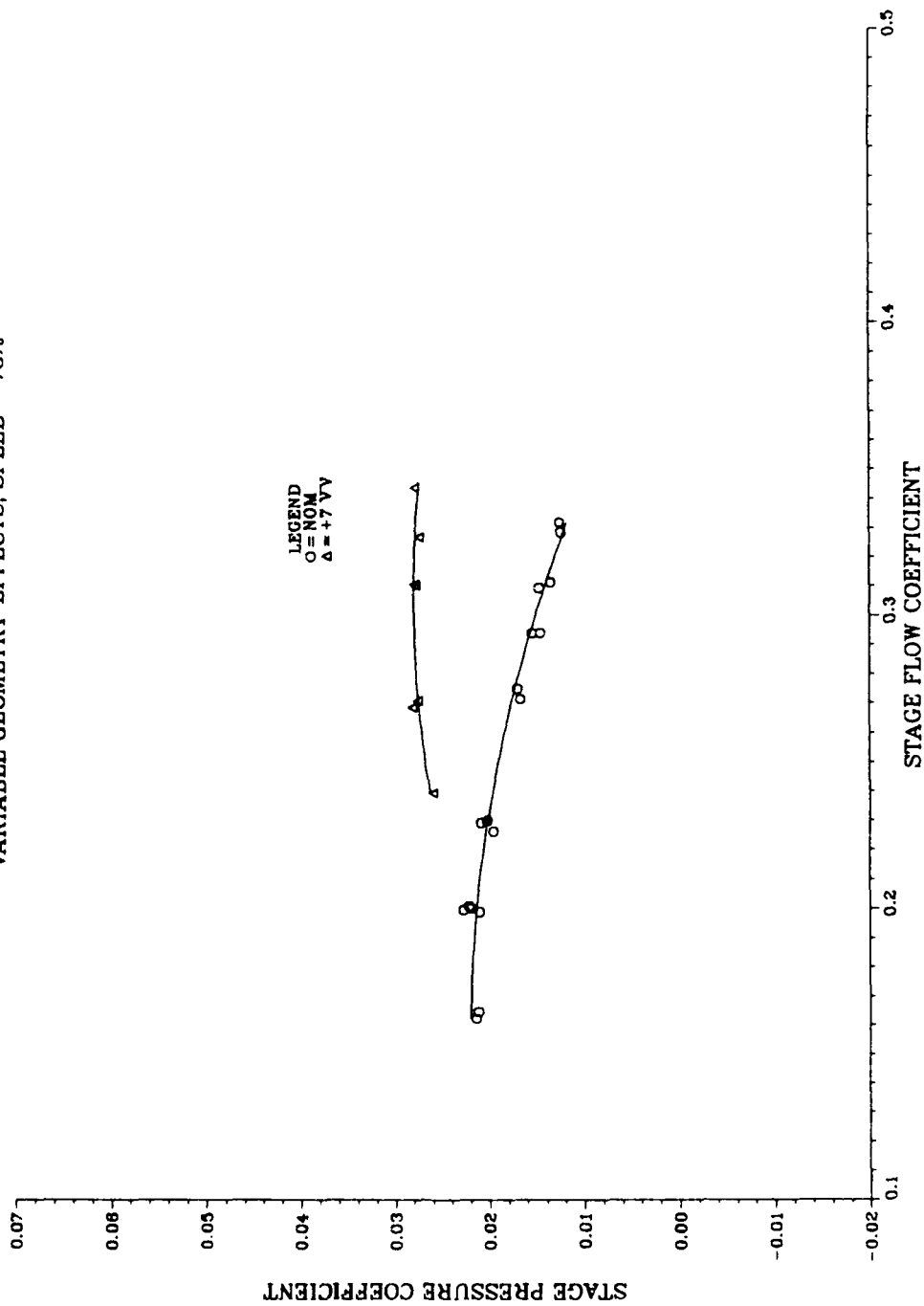


Figure C-8. 3rd-Stage Pressure Characteristic Least-Square Curve Fits

SECOND STAGE PRESSURE CHARACTERISTICS
VARIABLE GEOMETRY EFFECTS, SPEED = 75%

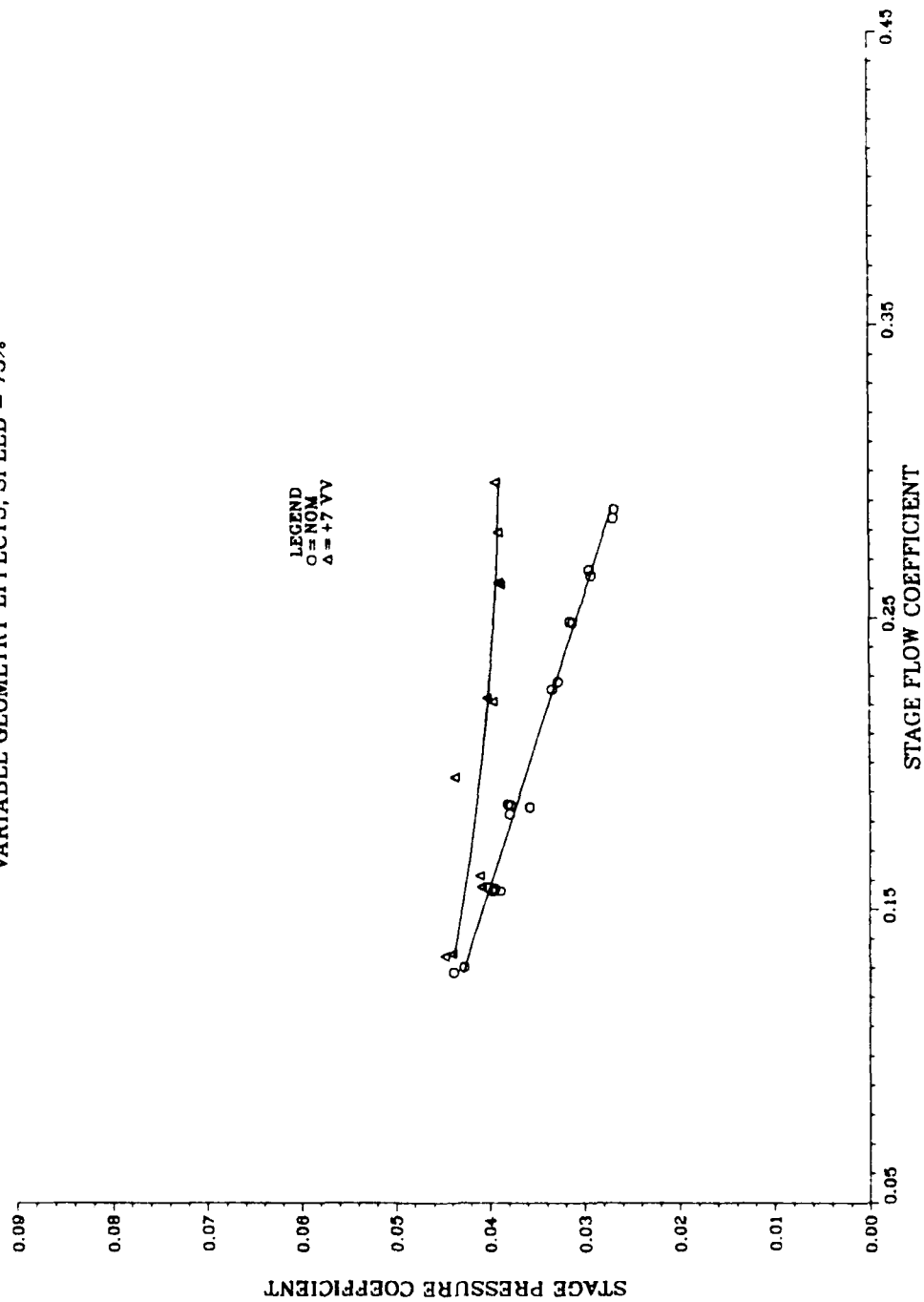


Figure C-9. 2nd-Stage Pressure Characteristic Least-Square Curve Fits

FIRST STAGE PRESSURE CHARACTERISTICS
 VARIABLE GEOMETRY EFFECTS, SPEED = 75%

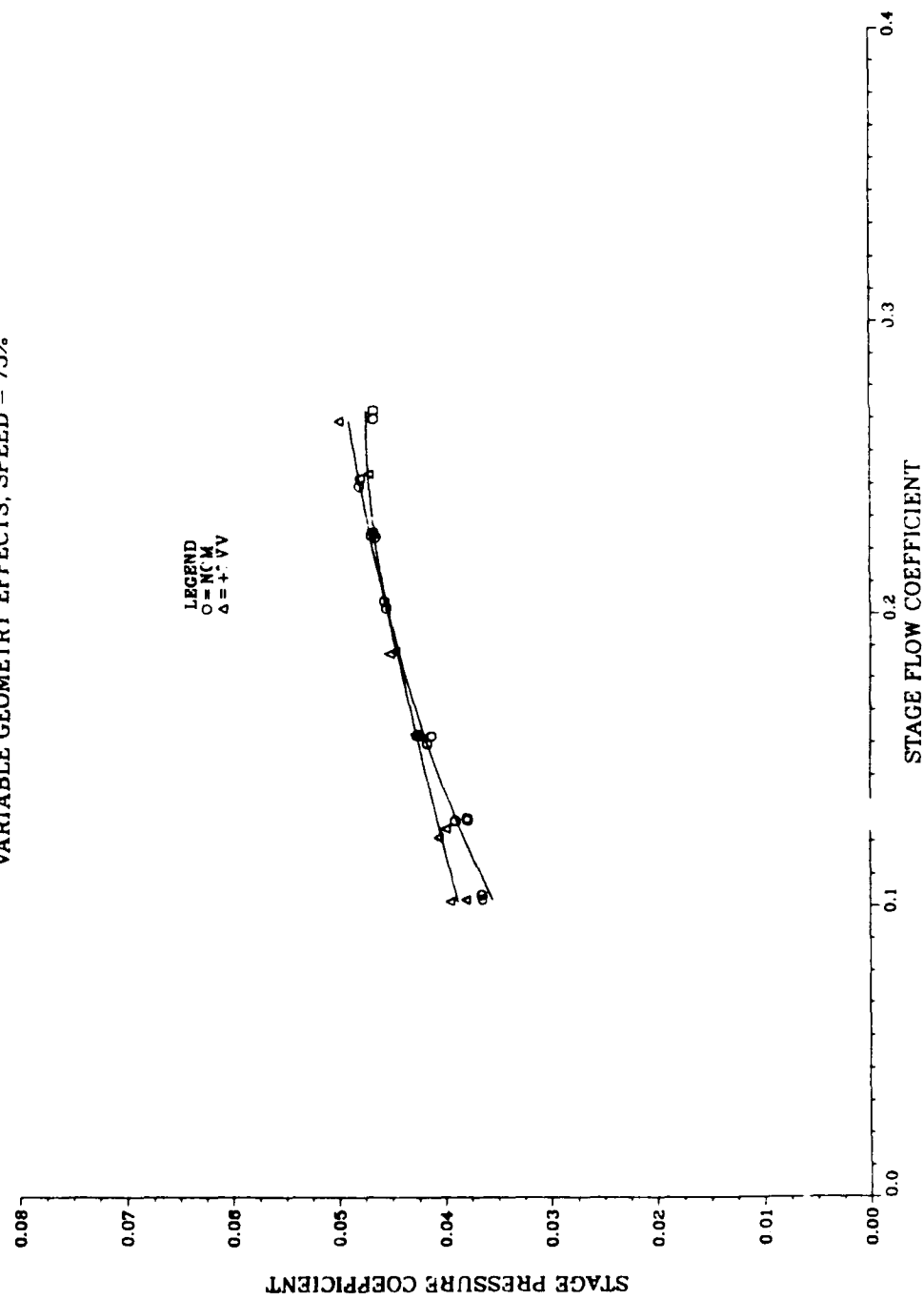


Figure C-10. 1st-Stage Pressure Characteristic Least-Square Curve Fits

APPENDIX D: HIGH-RESPONSE PRESSURE MEASUREMENTS

Ensemble average total and static pressures measured by the Mach probe at station 3.0 of the compressor are given in Figs. D-1 to D-10 of Appendix D.

HIGH RESPONSE PRESSURE MEASUREMENTS ENSEMBLE AVERAGE OF DATA POINT 1267

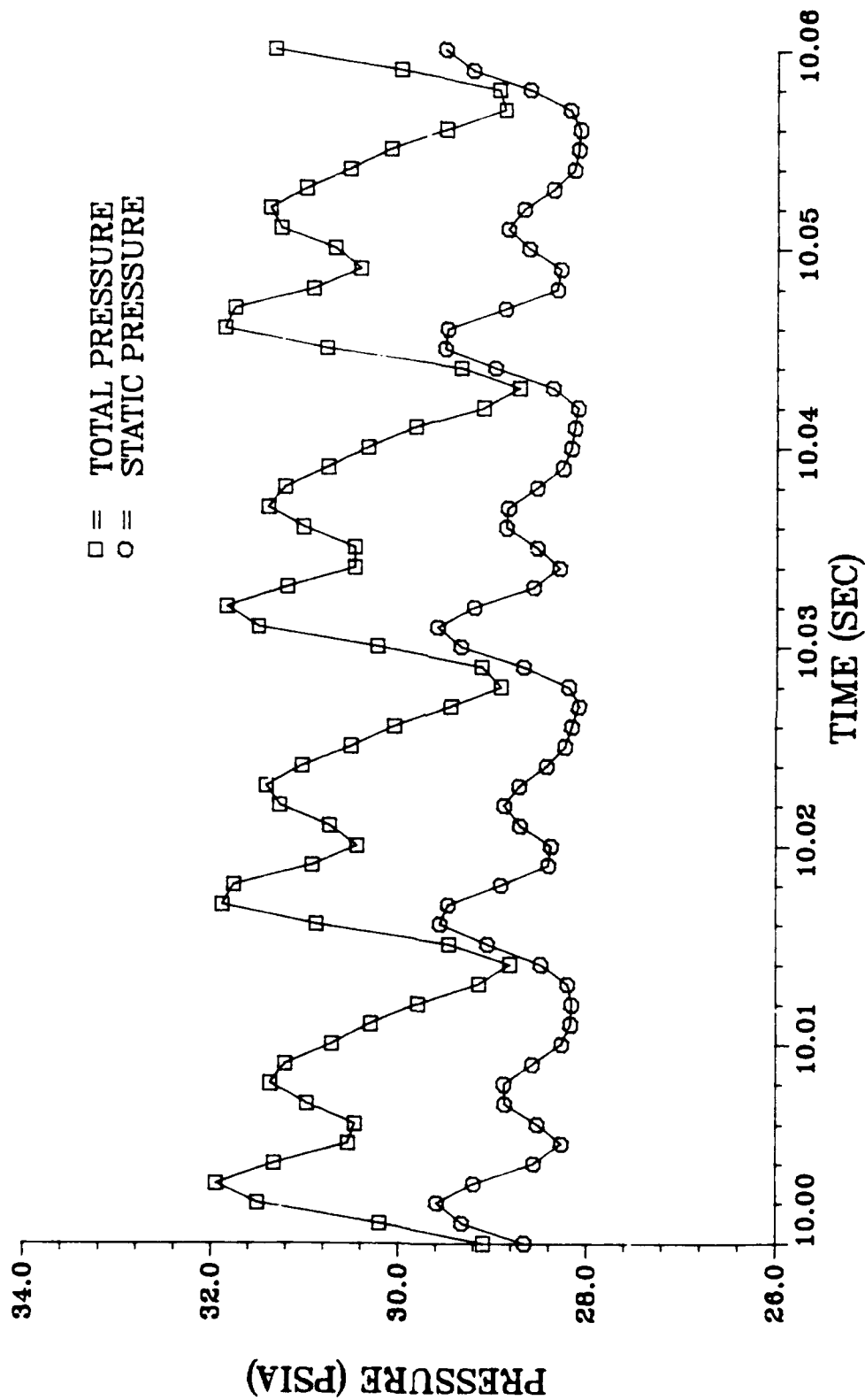


Figure D-1. High-Response Pressure Measurements, Data Point 1267

HIGH RESPONSE PRESSURE MEASUREMENTS ENSEMBLE AVERAGE OF DATA POINT 1195

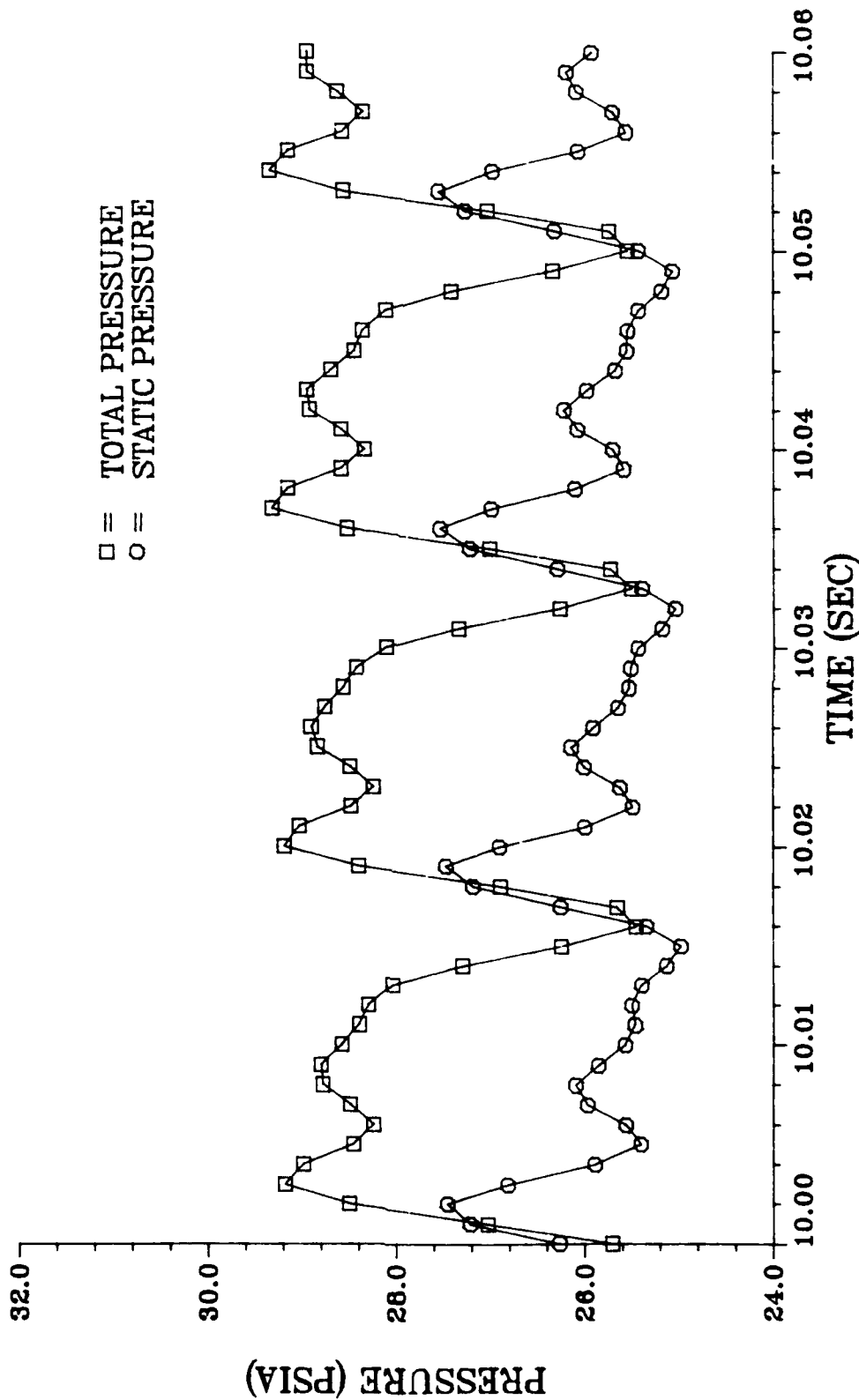


Figure D-2. High-Response Pressure Measurements, Data Point 1195

HIGH RESPONSE PRESSURE MEASUREMENTS ENSEMBLE AVERAGE OF DATA POINT 1193

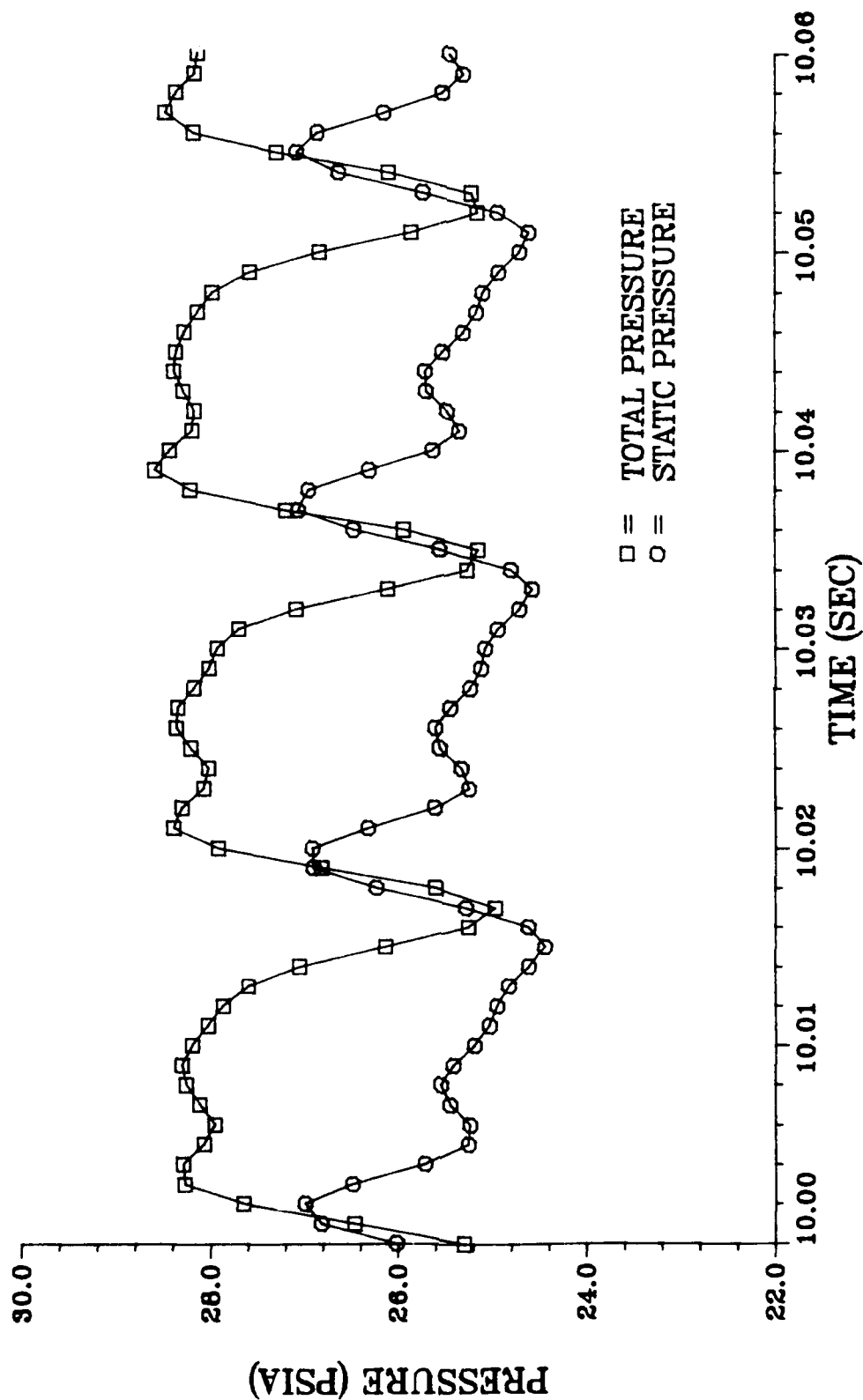


Figure D-3. High-Response Pressure Measurements, Data Point 1193

HIGH RESPONSE PRESSURE MEASUREMENTS ENSEMBLE AVERAGE OF DATA POINT 1259

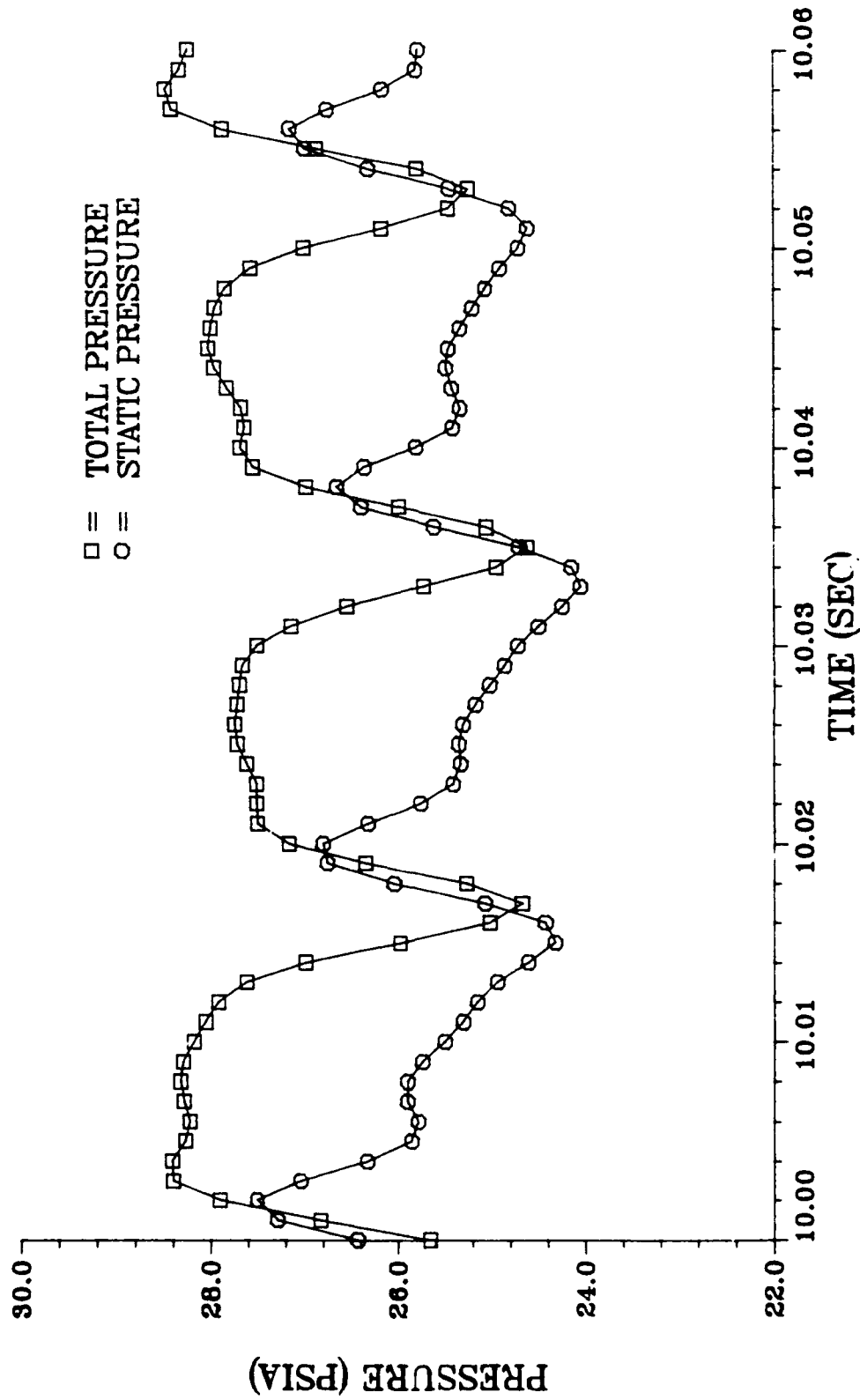


Figure D-4. High-Response Pressure Measurements, Data Point 1259

HIGH RESPONSE PRESSURE MEASUREMENTS ENSEMBLE AVERAGE OF DATA POINT 1227

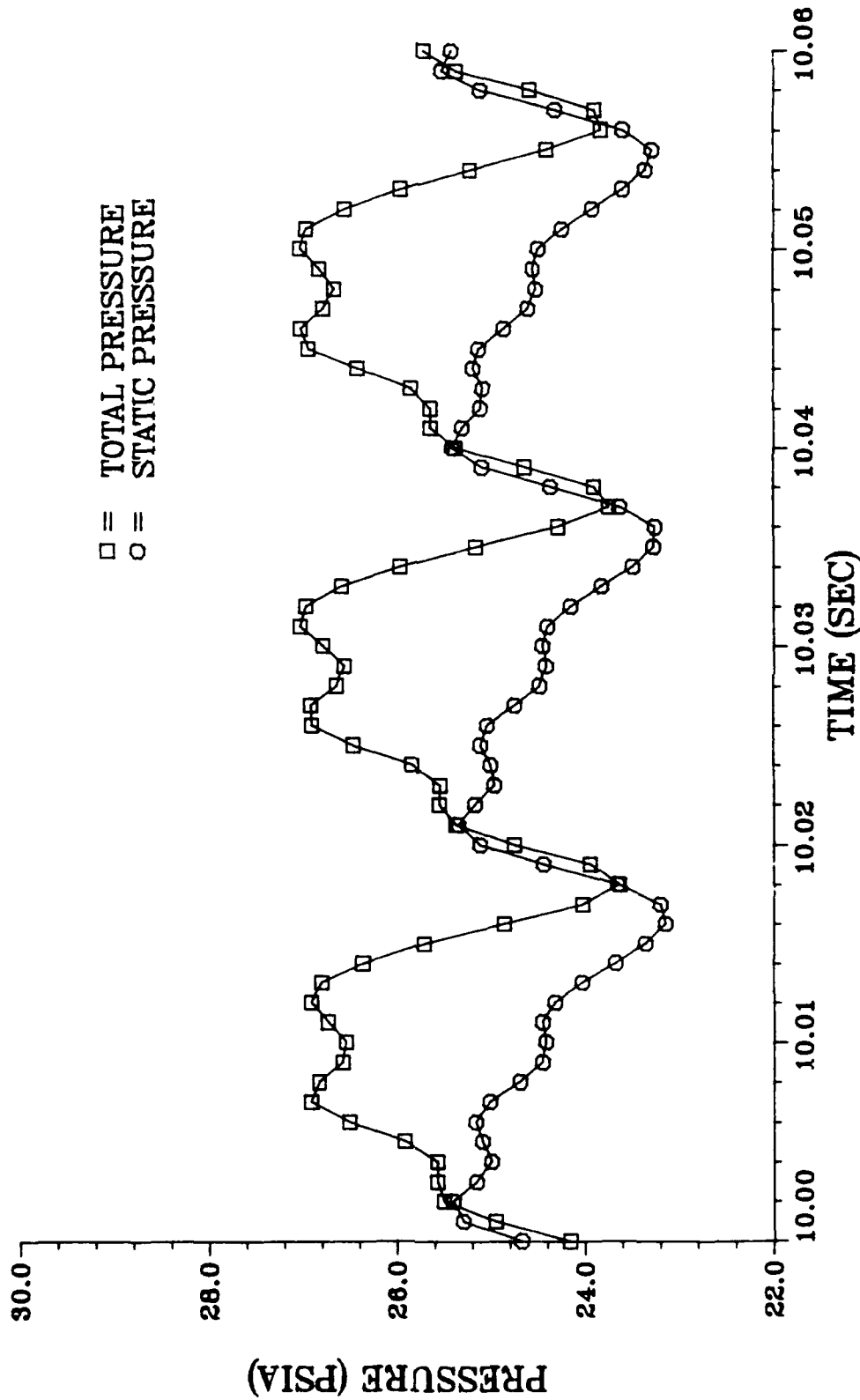


Figure D-5. High-Response Pressure Measurements, Data Point 1227

HIGH RESPONSE PRESSURE MEASUREMENTS ENSEMBLE AVERAGE OF DATA POINT 166

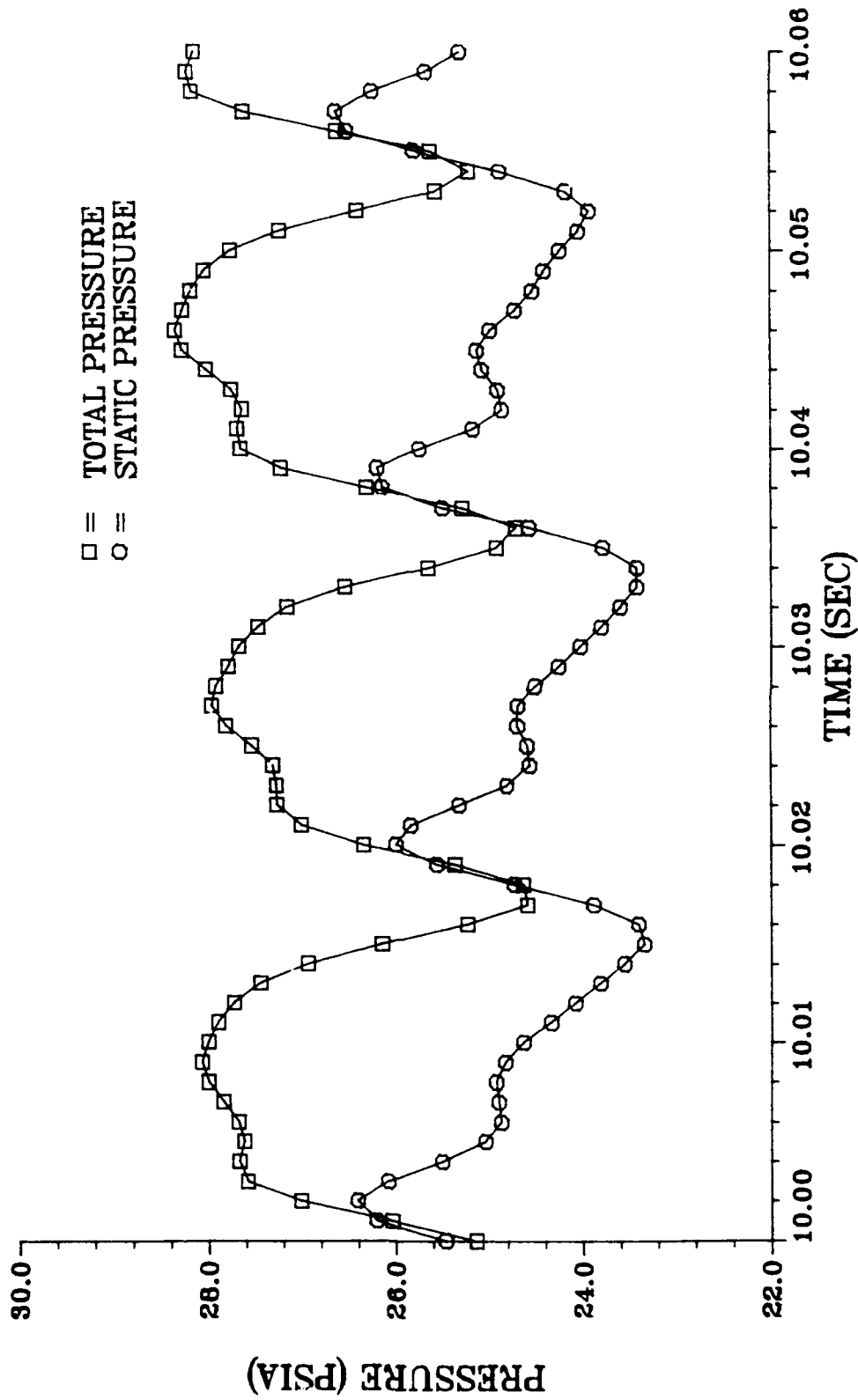


Figure D-6. High-Response Pressure Measurements, Data Point 166

HIGH RESPONSE PRESSURE MEASUREMENTS ENSEMBLE AVERAGE OF DATA POINT 162

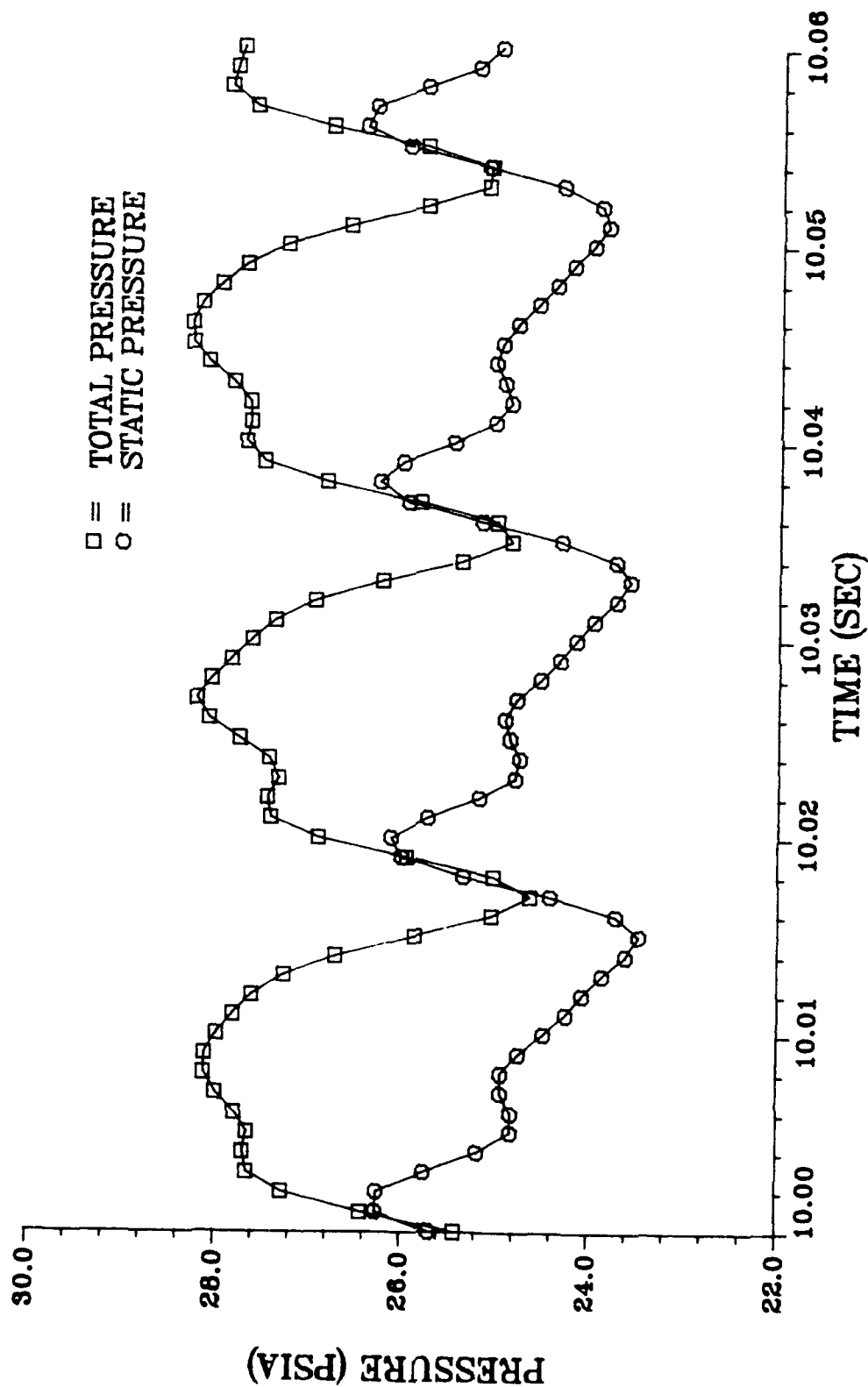


Figure D-7. High-Response Pressure Measurements, Data Point 162

HIGH RESPONSE PRESSURE MEASUREMENTS ENSEMBLE AVERAGE OF DATA POINT 160

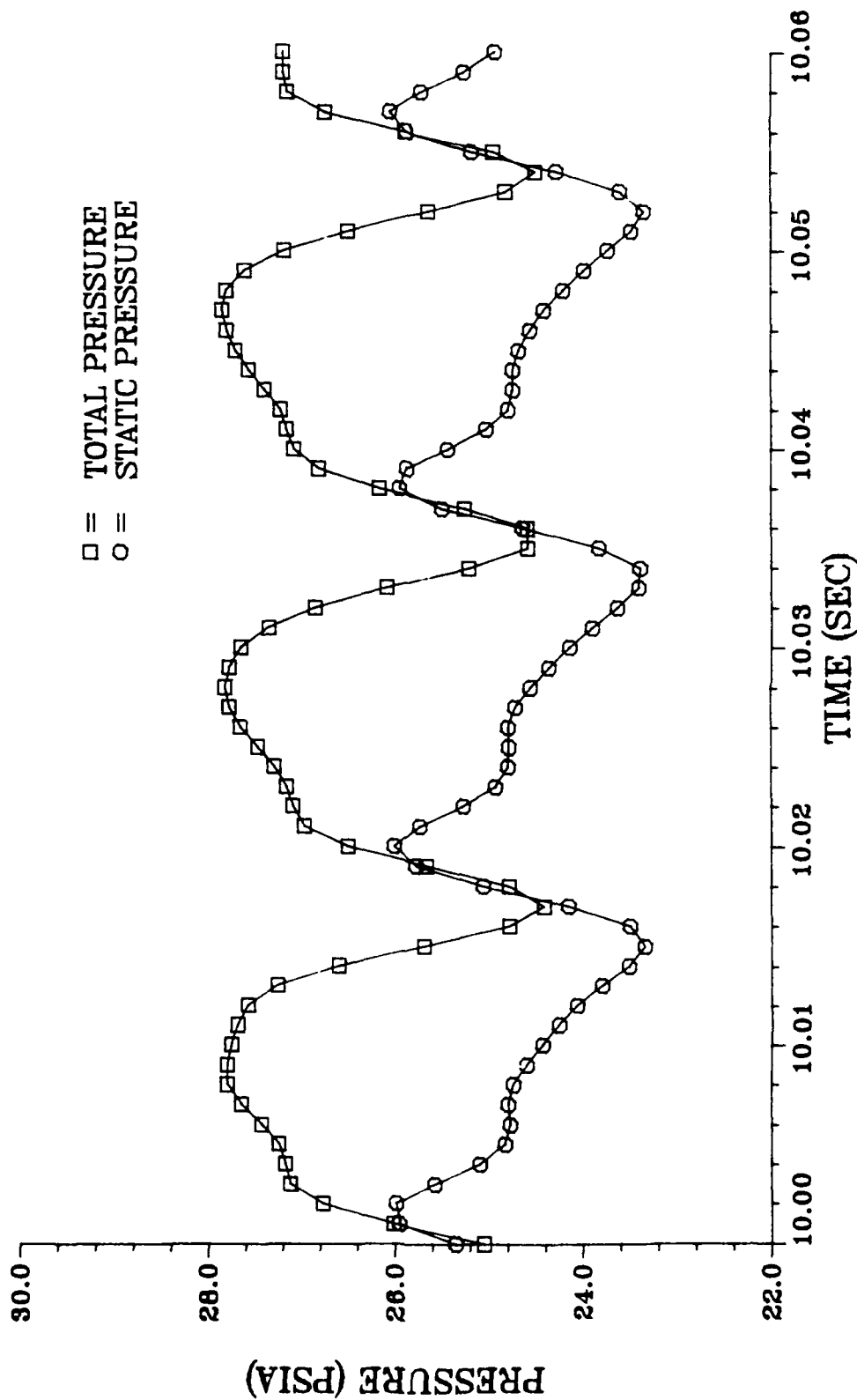


Figure D-8. High-Response Pressure Measurements, Data Point 160

HIGH RESPONSE PRESSURE MEASUREMENTS ENSEMBLE AVERAGE OF DATA POINT 135

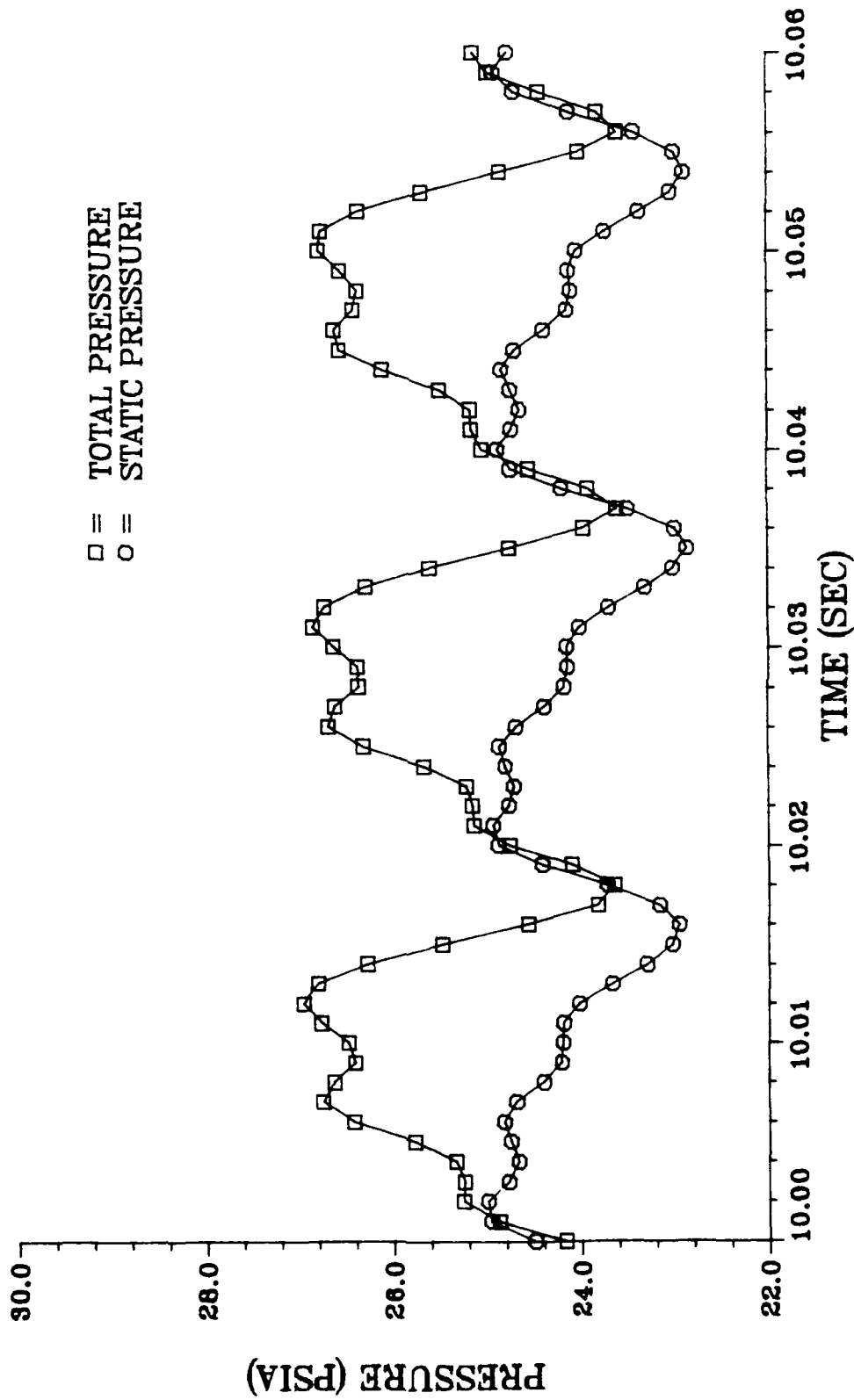


Figure D-9. High-Response Pressure Measurements, Data Point 135

HIGH RESPONSE PRESSURE MEASUREMENTS ENSEMBLE AVERAGE OF DATA POINT 148

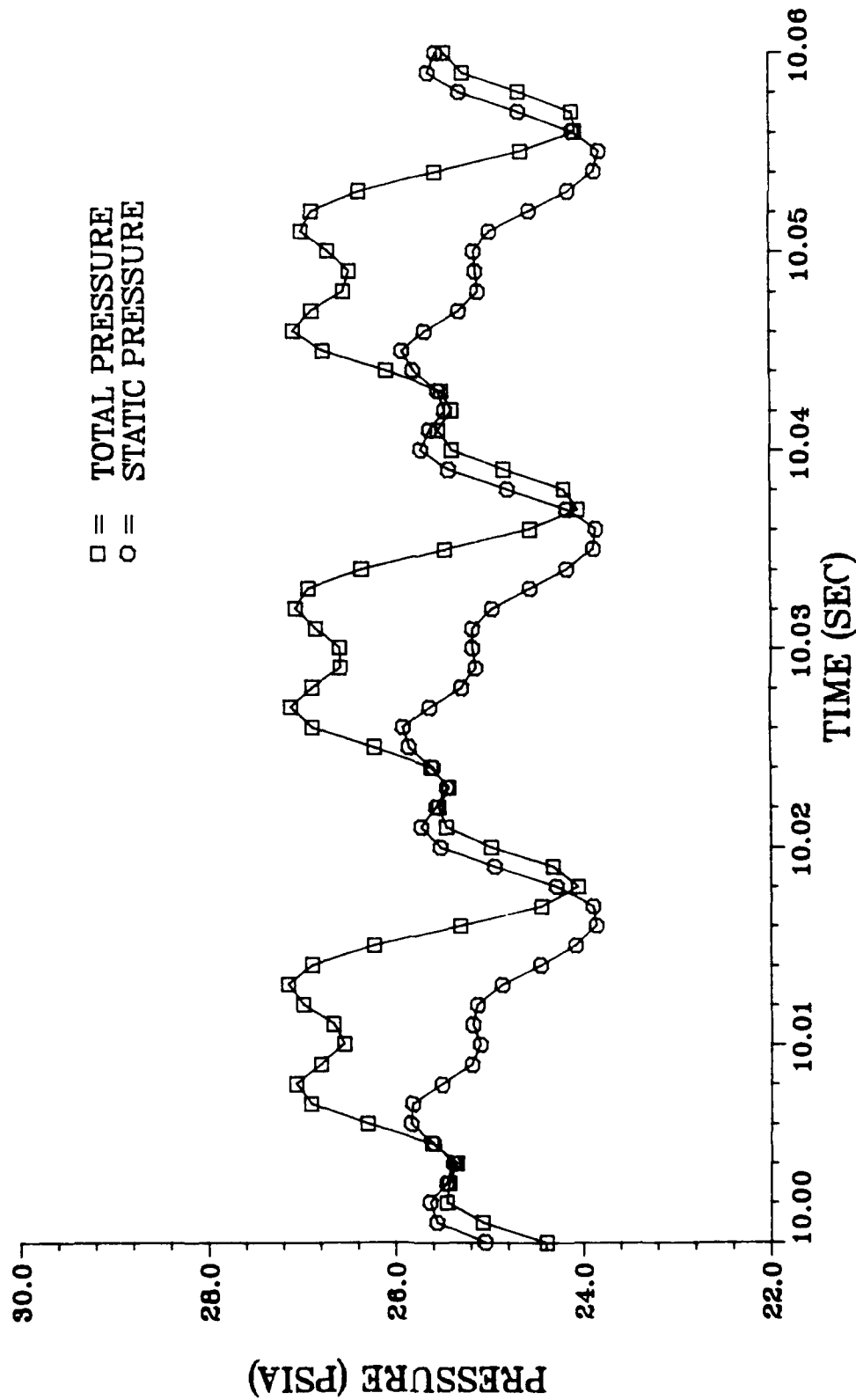


Figure D-10. High-Response Pressure Measurements, Data Point 148